Division of Pharmaceutical Chemistry and Technology
Faculty of Pharmacy, University of Helsinki
Dissertationes Universitatis Helsingiensis
84/2025

Hydrogels and Lipid-based Drug Delivery Systems for Tendon Therapy with Immunomodulatory and Pro-Regenerative Applications

by

Rubén Pareja Tello

ACADEMIC DISSERTATION

To be presented for public examination with the permission of the Faculty of Pharmacy of the University of Helsinki and the Department of Translational Medicine of the University of Salerno, as part of a double doctoral degree, in Suomen Laki Hall, Porthania, on the 12th of April 2025, at 12:15 pm.

Helsinki 2025

© Rubén Pareja Tello 2025

Publisher: Helsingin yliopisto
Series: Dissertationes Universitatis Helsingiensis 84/2025
ISBN 978-952-84-0649-5 (Print)
ISBN 978-952-84-0648-8 (Online)
ISSN 2954-2898 (Print)
ISSN 2954-2952 (Online)

PunaMusta, Joensuu 2025

The Faculty of Pharmacy of the University of Helsinki uses the Ouriginal plagiarism checker to examine all doctoral dissertations.

Main supervisor Professor Dr. Hélder A. Santos
Drug Research Program
Division of Pharmaceutical Chemistry and Technology
Faculty of Pharmacy
and
Department of Biomaterials and Biomedical Technology
University Medical Center Groningen
University of Groningen
The Netherlands

Co-supervisors Professor and Vice-Rector Dr. Jouni Hirvonen
Drug Research Program
Division of Pharmaceutical Chemistry and Technology
Faculty of Pharmacy
University of Helsinki
Finland

Principal Investigator, Docent Dr. Gonçalo Barreto
Clinicum
Faculty of Medicine
University of Helsinki
Finland

Professor Dr. Giovanna Della Porta
Department of Translational Medicine
Faculty of Medicine
Università degli Studi di Salerno
Italy

Reviewers Ana Beloqui García
Université catholique de Louvain
Belgium

Marianna Yanez Arteta
Astrazeneca
Sweden

Opponent Jay Prakash
University of Twente
Netherlands





Hydrogels and Lipid-based Drug Delivery Systems for Tendon Therapy with Immunomodulatory and Pro-Regenerative Applications

PhD thesis

to obtain the degree of PhD of the
University of Helsinki on the authority
of the Dean of the Faculty of Pharmacy,
Professor Jari Yli- Kauhaluoma,
and in accordance with the decision by the
Council of the Faculty of Pharmacy

and

to obtain the degree of PhD of the
University of Salerno on the
authority of the Rector
Vincenzo Loia

Double PhD degree

This thesis will be defended in public
on April 12th 2025 at 12:15 pm

by

Rubén Pareja Tello
born on 27th of January 1997
in Sabadell, Spain

Abstract

Pareja Tello, R., 2025. **Hydrogels and Lipid-based Drug Delivery Systems for Tendon Pathology Treatment with Immunomodulatory and Pro-regenerative Applications**

In the recent years, the pharmaceutical technology field has experienced a remarkable transformation thanks to the development of novel drug delivery systems. The design of innovative formulations, such as hydrogel and nanoparticles (NPs) systems, aims to control drug availability, target specific cells or tissues and prolong the therapeutic effect over time. Furthermore, the production of pioneering drug delivery systems not only follows the need to improve the delivery and bioavailability of highly complex biological cargos, but also aims to ensure their stability and targeting potential. Therefore, the use of innovative delivery systems serves as an alternative to conventional therapeutical approaches, which usually require the use of elevated dosages and high administration frequencies, achieving limited bioavailability, and higher toxicity.

Musculoskeletal diseases are considered an increasing global healthcare problem, with more than 150 distinct pathologies and an estimated incidence of 1.71 billion people worldwide. Specifically, tendinopathies are among the most common musculoskeletal disorders and include a wide and diverse range of disorders that compromise the intrinsic regenerative capabilities of tendon tissue following chronic alteration of the tissue homeostasis. The treatment of tendon-related disorders mainly depends on the specifically affected tendon and the type of injury, with surgical interventions and physiotherapy-based activities considered as common therapeutical approaches in combination with administration of therapeutics used for the symptomatic relief of pain and inflammatory symptomatology. Therefore, there is an increasing need for the development of novel therapeutical tools capable of mediating the inflammatory state, support the regeneration process and improve the restitution of the original tissue matrix and mechanical properties. The implementation of novel drug delivery-based technologies, such as hydrogels and nanoparticles, remains a highly promising opportunity to design alternative drug formulations for the delivery of biological cargos, such as nucleic acids, growth factors or stem cells-derived conditioned media, aiming to support the regeneration of the affected tissue and improve the recovery process.

In this thesis, different hydrogel and NPs-based formulations were developed as drug delivery systems for the delivery of biologically complex cargos and the treatment of tendinopathy-derived conditions. First, *in-situ* gellable inverse electron demand Diels-Alder (iEDDA)-crosslinked poly(ethylene glycol) (PEG) hydrogel microspheres (MPs) were developed *via* water-in-oil emulsification as a potential protein delivery system. The developed hydrogel MPs production was optimized, and the produced MPs were characterized in terms of physicochemical and morphological properties, rheological and swelling behavior. The system showed a high protein encapsulation efficiency and cell biocompatibility, demonstrating its potential use as drug vehicle. Second, a hyaluronic acid (HA) and PEG *in-situ* gellable iEDDA-crosslinked and heparin-functionalized hydrogel formulation was produced for the encapsulation of amniotic epithelial stem cells (AEC)-derived conditioned media (CM). The system was also studied in terms of physicochemical, morphological, and rheological characteristics, displaying fast crosslinking kinetics. Heparin-functionalized hydrogels allowed the sustained release of predominant growth factors from AEC-CM over 14 days. *In vitro* studies in peripheral blood mononuclear cells (PBMCs) showed an enhanced suppression

efficacy and a significant shift towards M2 macrophage phenotype in comparison with non-encapsulated AEC-CM, proving its potential as an alternative immunomodulatory therapeutic tool. Third, mesenchymal stem cells (MSC)-derived extracellular vesicles (EVs) were used to produce lipidic hybrid NPs by microfluidic-sonication for collagen type I (COL1A1) mRNA encapsulation and delivery in tendon progenitor stem cells (TSPCs). The formulation was optimized and characterized in terms of physicochemical properties, proving that MSC-Hyb NPs encapsulated mRNA and included EVs-derived surface proteins. Moreover, MSC-Hyb NPs remained highly biocompatible with TSPCs and proved to be functional mRNA delivery agents with certain limitations in comparison with lipid nanoparticles (LNPs). Overall, this dissertation presented diverse innovative alternatives for the design of hydrogel and NPs-based drug delivery systems for the treatment of tendinopathic-derived conditions, demonstrating the significant role and potential of drug delivery for advanced regenerative medicine applications.

Acknowledgements

Ten years ago, a high school teacher gifted me with a handwritten bookmark with a dried flower and a message:

"Com l'insecte i l'orquídia, així ha estat la nostra relació. Recorda-la per sempre"
- Àngela Torreguitart, Juny 2015

"Like the insect and the orchid, that's how our relationship was. Always remember it"
- Àngela Torreguitart, June 2015

Àngela was a remarkable scientist with an admirable passion for teaching and a fascinating personality, who brought joy and contagiously shared her passion during each biology lecture that I followed during the years prior to my university studies. I was lucky enough to simultaneously become a pupil for multiple other brilliant professors like her, who vividly shared their passion for disciplines such as chemistry, physics and mathematics with me. Therefore, my first acknowledgement goes to her and all the extraordinary professors who shared their love for science and taught me how to question everything. Moltes gràcies per tot, no ho oblidaré mai.

...

In 2021, I was offered the opportunity to conduct a PhD as a Marie Skłodowska-Curie PhD fellow under the supervision of Professor Dr. Hélder A. Santos at the University of Helsinki. The idea seemed quite dauting, especially considering the complexity and the requirements associated with an opportunity like that. However, my previous experience in another nordic country had been extremely positive and my motivation to explore new horizons pushed me to accept the challenge and embrace this life-changing opportunity. Three years later I can definitely affirm that I made the right decision.

A PhD is a formidable journey through science where every single step becomes a personal lesson. During these years, I have had the opportunity to learn from many outstanding scientists, acquire multiple technical skills, further develop my critical thinking skills and professionally grow as an early stage researcher in the field of drug delivery, nanomedicine and pharmaceutical technology. This journey has been characterized by specially challenging situations, where uncertainty, anxiety and stress inevitably raised after every single obstacle that appeared along the way. However, this experience has taught me that every difficulty can be solved with perseverance, maturity, self-determination and persistence, among other fundamental tools. This journey has also highlighted the importance of being surrounded by highly professional and empathic people, who offered their support and assistance in multiple occasions, regardless of the distance between us and even with larger or slighter awareness of it. Therefore, I would like to personally thank all of those who helped me to conduct the scientific work described in this dissertation.

Firstly, I would like to express my gratitude to Professor Dr. Hélder A. Santos, who three years ago selected me to participate in this life changing opportunity as a Marie Skłodowska-Curie PhD candidate. Thank you for offering me the opportunity to learn and conduct research in your research group, it has truly been a crucial experience in my short professional career. Thank you for the supervision, guidance and support provided during this journey, regardless of the distance or the obstacles. It has been truly inspiring to witness your predisposition and motivation to question everything, share your advice, welcome any kind of idea and support me with any issue that I may have faced. Your hardworking commitment and enthusiasm for

research are truly admirable and I am genuinely thankful for this experience and everything I have learned under your supervision. Obrigado.

I would also like to express my gratitude to my co-supervisors, Principal Investigator Dr. Gonçalo Barreto, Professor and Vice-Rector Dr. Jouni Hirvonen and Professor Dr. Giovanna Della Porta. Gonçalo, thank you for your support and assistance during these years, your contributions in innumerable discussions, your highly appreciated suggestions following your expertise in the biology of musculoskeletal diseases and your help regarding the possibility to collaborate with clinicians. Moreover, thank you for allowing me to continue performing research shortly after the conclusion of my doctoral studies. I really appreciate it and I am really thankful for the opportunity. Professor Jouni, thank you for your support and your feedback to my research, manuscripts and my thesis. Professor Giovanna Della Porta, my co-supervisor from the University of Salerno, thank you for your hospitality, your assistance, your availability and the multiple discussions we maintained during my secondment in Salerno.

Moreover, I would like to thank the pre-examiners of this doctoral dissertation, Dr. Ana Beloqui García and Dr. Marianna Yanez Arteta, for providing their helpful feedback, which remained a fundamental tool to improve the quality of this work. I am also extremely thankful to Professor Dr. Jay Prakash for accepting the invitation as opponent of this doctoral dissertation; it is an honor and an unique opportunity to be able to discuss this thesis with you. I would also like to thank Professor Dr. Tapio Kotiaho for accepting the invitation to be part of the Grading Committee for this dissertation.

Secondly, I would like to thank all the co-authors and collaborators who have contributed to the publications included in this doctoral dissertation. Thank you for your cooperation and proficiency, your suggestions and your critical eye for research. I would like to thank the members from the P4FIT consortium for their help, feedback and advice during these years. Particularly, I would like to thank Pauliina Hallikas for all the support and help you provided during these years, your willingness to listen and all the moments we shared during the course of the project.

This journey would not have been possible without two fundamental figures and colleagues who not only supported and helped me in uncountable occasions, but also became true friends and my PhD companions: Giuseppina and Sandra.

Giuseppina, *amo*, I don't think I could express with words how thankful I am for everything you have done for me during these years. I am so lucky to have met such a genuine and true friend who also turned out to be my PhD colleague. I cannot thank you enough for the countless laughs in the lab, the never-ending conversations, gossip sessions, dinners, trips, concerts and all the experiences I had the privilege to share with you. *Please, do not be alarmed, remain calm*, I am not going to start enumerating each and single one of them, simply because if I did so, this thesis would not have an end. We have supported each other when the struggle was real and I would not change a single thing of this journey (even when *trying explosions* was the most tempting thing to do). *Girl, it's so confusing sometimes to be a PhD student*, we know it, but I am so happy to have lived this confusing experience next to you. I am proud of us for not allowing that anything could *break our soul* and I cannot wait to continue living many more experiences next to you. Como narra Rosalía, *A de alfa, altura, alien y, sobretodo, de amiga.*

Sandra, I will never forget the moment I got off the bus in Vuolukiventie and met you for the first time. Since my first day in Finland, I was extremely lucky to experience innumerable moments with you, including surprising visits to the laundry room from Vuolukiventie and countless situations in which we would start to laugh by just looking at each other (without saying a single word) even though it was not the most appropriate thing to do. Thank you for all the laughs in the lab, the gossip sessions, all the times we complained about microfluidics

and the manufacturing of those chips, las meriendas a base de Fasupala de plátano and all the special moments we experienced together (including our video riding Taiga in Linnanmäki). I could not thank you enough for your support during the most difficult situations and your friendship. I am truly honored to have been able to meet you and live this experience with both of you.

The P4FIT consortium has also allowed me to meet and collaborate with incredibly talented young researchers that have had a remarkable impact in this experience, including Francesco Iorio, Adrián Cerveró Varona, Marta Clerici, Melisa Faydaver, Veronica Pinnaro and Arlette Haidar Montes. Francesco, thank you so much for being such a great friend and PhD colleague, this journey would not have been the same without you, your podcast-like long audio messages and all the trips together (San Francisco and Berlin remain some of the best I have ever experienced). Adrián, thank you so much for your friendship and being such an incredibly smart and hard-working collaborator. Thank you for all the moments and laughs we shared, your ability to remain calm even under the most stressful situations and all the work you did in Helsinki while I simultaneously had to conduct my own secondment (those phone calls were authentic voice-narrated polymer functionalization protocols). Marta, thank you so much for all your support and for warmly welcoming me in Salerno, I really appreciate it. Thank you for all the laughs, the *'nciuci e ciacchiere* sessions, for listening to me in countless occasions, for all your help and for all the fond memories I keep from our time in Salerno. Melisa, thank you so much for all the laughs and memories in Helsinki and in every P4FIT event, your musical sessions in the lab with Bad Bunny and your friendship. Veronica and Arlette, thank you so much for the moments and laughs we shared in Helsinki and in every P4FIT event.

Subsequently, I would like to thank Principal Investigator Dr. Shiqi Wang and Dr. Flavia Fontana, who offered their support as senior post-doc supervisors since the moment I started my doctoral studies. Shiqi, thank you so much for the guidance, the assistance and your advice since the beginning of this journey, you really had a fundamental impact during the initial stages of my doctoral studies. Flavia, thank you so much for your guidance, support and advice during these years, your support also had a fundamental impact at the beginning of this journey. I could not be more thankful for the expertise, critical thinking skills and creativity that both of you irradiated and shared with me since the beginning. I would also like to extend my deepest gratitude to Alexandra Correia, co-author in almost all the publications listed in this doctoral dissertation. Thank you so much for all your assistance, advice, kindness, willingness to teach and help, patience and commitment in the lab. Your support has played an essential role during my doctoral studies and I could not imagine a day in Viikki without stepping into the lab and hearing an early *Bom dia* or the innumerable conversations during lunch time. I would also like to thank Professor Dr. Sami Hietala, for his support in multiple publications and allowing me to use essential instrumentation for the rheological characterization of hydrogel formulations.

Moreover, I would like to acknowledge my colleagues from Santos' lab for welcoming me in the group, participating in multiple scientific discussions and sharing their expertise, either during the initial phases of the doctoral studies or subsequently during the final stages. Particularly, I would like to thank Dr. Antti Rahikkala, Dr. Carmine d'Amico, Dr. Christos Tapeinos, Dr. Giulia Torrieri, Dr. João P. Martins, Khalil Elbadri, Dr. Pei Zhang and Dr. Voitto Känkänen. I would also like to acknowledge Rasmus Enno, who I had the privilege to supervise during the last months of my PhD and thanks to whom I was able to learn so much following our discussions and his inspiring passion for research.

Subsequently, I would like to acknowledge my colleagues from UNISA for also welcoming me in the group, sharing their knowledge and expertise, helping me with many

experiments and participating in numerous scientific discussions during my stay in Salerno. Particularly, I would like to thank Dr. Erwin Pavel Lamparelli, Dr. Maria Camilla Ciardulli, Dr. Pasqualina Scala and Dr. Valentina Giudice. Moreover, I would like to specially extend my gratitude to another talented young researcher, Giacomo Cortella, who was a fundamental support during part of this journey. Giacomo, thank so much for your friendship, for being such a kind and encouraging colleague, for all the moments and laughs we shared and for the endless conversations. Those gym sessions, overcrowded bus rides and weekend dinners will be unforgettable. Furthermore, I would also like to extend my gratitude to all of those who accompanied me during my experience in Salerno, welcomed me with open arms, shared many moments and laughs, and insistently brightened my days and made me smile. Specially, I would like to thank Anna Lisa Cammarota, Assunta Manna, Biagio Santella, Dr. Domenico Rocco, Gaia Scoppetta, Gennaro Rocco, Luigi Fortino and Marianna Marino.

...

This doctoral dissertation would not have been either possible without the unconditional support I have continuously received from numerous friends. Firstly, I would like to thank to the incredible friends who made Helsinki my new home and the best place where I could have experienced this adventure. During these years, I have had the pleasure of sharing my journey in Finland with really special friends: Alessia, Anisa, Giuseppina, João, Katia, Matej, Sandra and Sanjana. Alessia, *amo*, thank you so much for constantly being next to me during these years, all the laughs, the gossip sessions around the iconic round table and the fun nights. Either dancing at the first row under the stage with Kaytranada or spending the evening in the most demure way, thank you so much for allowing me to share so many *unique* moments with you during this journey. Anisa, thank you so much for all the dinners, the laughs and the endless conversations reflecting about our PhD journeys. João, *amigue*, thank you so much for all the hysterical laughs and for always being there listening, understanding and advising, I have felt strongly inspired by your professional journey since the day we met in the lab. Thank you for all the fun moments and the *tea* sessions, for always making me smile and for having such an excellent musical taste, and by *excellent* I mean similar to mine. Katia, *gioia*, thank you so much for being such a caring and kind friend, for all the laughs, for bringing the most crazy energy to the group, for always listening and for all the moments we shared. I can always count on you whenever I want to order some extra food even though I feel I may be the only one craving for something else. Matej, thank you so much for being my Michelin star-awarded caring friend, for also listening, understanding and advising so wisely, and for serving as such an inspirational friend during this doctoral journey. Thank you for literally having such a demure personality, an outstanding talent for the cuisine and also an extremely good taste for music. Sanjana, who would have thought that we would become such good friends after the first time we met at 7 AM at the gym. I am so thankful to have met such a genuinely kind friend like you, who has listened to me religiously every morning and has supported me regardless of the distance. Thank you so much for all the hysterical laughs, for the bubble tea sessions, for the endless conversations and all the videophone calls. I still vividly remember all the walks and conversations we had during the hardest moments and I cannot thank you enough for that. I really cherish our friendship and I feel blessed to have found my Katia. With love, your Trixie.

I would also like to thank all those who I met in Helsinki and were part of this experience: David, Diana, Elena, Filippo, Gabriella, Gianni, Giulia, Inés, Jacopo, Kari, Laura, Loïc, Marco, Martino, Matilde, Matteo, Salvatore, Simon, Waltteri and Yvonne.

I would also like to thank my friends from Sabadell, who have constantly been by my side during these years, despite the distance and the limited occasions I had to see them. I would like to thank Maria, who has been a fundamental friend since my childhood and has continued

enlightening my life for more than 20 years. I would also like to thank Marina for her essential friendship and her support for so many years, including our time at the university as pharmacy students. I could not be prouder of both of you and I am so lucky to have you both in my life. I would also like to thank Alba, Bernat, Carla, Carlos, Jose Luis, Marina, Neus, Nicole and Pau. Thank you all so much for your love and support during all these years. I feel so fortunate to have friends like you and I could not thank you enough for your support.

To Jesús Alejandro Vega, for his true and indispensable friendship and his support during the most uncertain and stressful moments. I know it has not been easy to get to know me during such a bizarre and dynamic experience like this, especially considering all the times I had to move from one country to another. Our friendship has truly kept me afloat in countless situations and your kindness, patience, consideration and support have truly made a mark on me. No tengo palabras para agradecerte lo importante que has sido en todo este viaje, muchísimas gracias por estar a mi lado a pesar de los quilómetros de distancia.

Finally, I would like to express my deepest gratitude to my family. Aquesta tesi no hauria sigut possible sense el suport i l'amor incondicional de la meva família, que constantment s'ha sacrificat i m'ha ajudat en tot el possible per poder tenir una vida millor i aconseguir tot allò que em proposava. A mis abuelos, Antonia, Concha, Juan Francisco y Vicente, por criarme y guiarme desde pequeño, a pesar de que ya no estén. Os echo de menos y sé que estaríais orgullosos. A tots els meus tiets i cosins per la seva estima i el seu suport, tot i la distància i les limitades ocasions que tenim per veure'ns. Als meus tiets Josep i Oriol i al meu cosí Mer, per tot el suport incondicional, la seva ajuda i per ser uns grans referents a nivell personal i acadèmic. Finalment, als meus pares i a la meva germana. Neus, moltíssimes gràcies per ser la persona més especial i intel·ligent amb qui he tingut la sort de compartir aquesta vida. Per tot el teu amor, les trucades en els moments difícils, les teves visites a Helsinki i a Salerno (i la teva passió pel fred finès) i totes les sessions de risoteràpia cada cop que parlem per videotrucada o torno a casa per vacances. Moltíssimes gràcies per ser el millor suport que he tingut mai i la millor germana possible. A mi madre y a mi padre, que siempre se han esforzado todo lo posible e incluso mucho más para hacer posible que yo y mi hermana pudiéramos estudiar y perseguir la carrera que queríamos. Por su constante amor incondicional, aceptación y por siempre animarme a tirarme a la piscina y cumplir mis metas, aunque sean a más de 2500 km de distancia. Por su constante apoyo durante estos tres años, independientemente de la distancia, y por su ayuda y su sabiduría en los momentos más duros. Por su paciencia y su energía incluso para visitarme, independientemente del destino. Esta tesis doctoral no hubiera sido posible sin las incontables conversaciones telefónicas a diario y su amor infinito. Esta tesis es especialmente para vosotros.

“Science and everyday life cannot and should not be separated.”

- Rosalind Franklin

“Vindran les flors, pensava, i els dies blaus amb llargs crepuscles rosa.”

- Mercè Rodoreda

Table of contents

Abstract ..... **i**

Acknowledgements ..... **iii**

Table of contents ..... **ix**

List of original publications ..... **xi**

List of additional publications ..... **xii**

Abbreviations ..... **xiii**

1 Introduction **1**

2 Literature overview **3**

2.1 Polymer-based hydrogels for controlled drug delivery 3
2.1.1 Hydrogel classification and crosslinking methods 5
2.1.2 Nano/micro-scale hydrogels as drug delivery systems 13
2.1.3 Microfluidics-assisted production of hydrogel MPs 15

2.2 Extracellular vesicles (EVs) as drug delivery systems 17
2.2.1 Extracellular vesicles (EVs) engineering 19
2.2.2 Extracellular vesicles-derived hybrid nanoparticles 20

2.3 Local administration route for drug delivery 23

2.4 Tendon-related disorders 25
2.4.1 Tendon structure and physiology 26
2.4.2 Tenocytes and tendon progenitor stem cells 27
2.4.3 Spectrum of tendon pathologies 29
2.4.4 Tendon healing and remodelling 30
2.4.5 Traditional therapeutical tools and current hydrogel and nanotechnology-based approaches for local tendon delivery 32

3 Aims of the study **37**

4 Experimental **38**

4.1 Hydrogels and nanoparticles production 38
4.1.1 Polymers functionalization and hydrogel formation (I-II) 38
4.1.2 Hydrogel microspheres production (I) 39
4.1.3 Hybrid nanoparticles production (III) 40

4.2 Physicochemical characterization 40
4.2.1 Morphological and physicochemical evaluation: Scanning electron microscopy (SEM) and Fourier-transform infrared spectroscopy (FTIR) (I-II) 40
4.2.2 Rheological studies (I-II) 40
4.2.3 Swelling studies (I-II) 41
4.2.4 Dynamic light scattering (DLS), electrophoretic light scattering (ELS) and nanoparticle tracking analysis (NTA) (III) 41
4.2.5 Cryo-transmission electron microscopy (Cryo-TEM) (III) 41
4.2.6 Hybridization studies: Fluorescence resonance energy transfer (FRET) and surface markers analysis (III) 41

4.3 Drug loading and *in vitro* drug release studies 42
4.3.1 Drug loading degree in hydrogel systems (I-II) 42
4.3.2 In vitro drug release (I-II) 43
4.3.3 mRNA loading and quantification assay in hybrid nanoparticles (III) 43

4.4 *In vitro* cell studies 44

4.4.1 Cell lines and culture conditions (I-III)....44
4.4.2 Cell-cytocompatibility studies (I-III)....44
4.4.3 PBMCs activation and macrophages polarization studies (II)....45
4.4.4 Cellular uptake of rhodamine-labelled hybrid nanoparticles (III)....45
4.4.5 Transfection efficiency with eGFP mRNA model-loaded hybrid nanoparticles(III)....46
4.4.6 Efficacy studies with collagen I mRNA-loaded hybrid nanoparticles (III)....46
4.5 Ethical permits (I-III)....47
4.6 Statistical analysis....47
5 Results and Discussion....48
5.1 Physicochemical characterization of bulk hydrogels and hydrogel microspheres 48
5.1.1 Precursor polymers functionalization and hydrogels fabrication (I-II)....48
5.1.2 Morphological and physiochemical evaluation: SEM and FTIR analyses (I-II) 50
5.1.3 Rheological characterization (I-II)....51
5.1.4 Swelling studies (I-II)....53
5.2 Physicochemical characterization of hybrid nanoparticles (III)....55
5.2.1 Dynamic light scattering (size, PDI and ζ-potential) and nanoparticle tracking analysis (III) 55
5.2.2 Morphological evaluation (Cryo-TEM) and hybridization studies: FRET and surface markers analysis (III)....56
5.3 Drug loading and *in vitro* drug release studies (I-III)....58
5.4 Cytocompatibility studies (I-III)....60
5.5 PBMCs activation and macrophages polarization studies (II)....62
5.6 Cell–nanoparticles interactions: Quantitative cell uptake studies (III)....64
5.7 Quantification of the transfection efficiency of the hybrid nanoparticles (III)....64
5.8 *In vitro* efficacy studies with COL1A1 mRNA-loaded hybrid nanoparticles(III) .66
6 Conclusions....69
References....72

List of original publications

This thesis is based on the following publications, which are referred to in the text by their respective roman numerals (**I-III**).

I **Pareja Tello, R.**, Wang, S., Fontana, F., Correia, A., Molinaro, G., López Cerdà, S., Hietala, S., Hirvonen, J., Barreto, G., Santos, H. A. Fabrication of hydrogel microspheres via microfluidics using inverse electron demand Diels–Alder click chemistry-based tetrazine-norbornene for drug delivery and cell encapsulation applications. Biomaterials Science, 11(14), 4972–4984, 2023.

II **Pareja Tello, R.**†, Cerveró-Varona, A.†, Prencipe, G., Molinaro, G., Pinnarò, V., Haidar-Montes, A. A., Correia, A., Hietala, S., Stöckl, J., Hirvonen, J., Barreto, G., Russo, V., Barboni, B., Santos, H. A. Development of amniotic epithelial stem cells secretome-loaded in situ inverse electron demand Diels-Alder-crosslinked hydrogel as a potential immunomodulatory therapeutical tool. ACS Applied Materials & Interfaces 2025 17 (2), 2977-2990.

III **Pareja Tello, R.**, Pavel Lamparelli, E., Ciarduli, M. C., Hirvonen, J., Barreto, G., Mafulli, N., Della Porta, G., Santos, H. A. Hybrid lipid nanoparticles derived from human mesenchymal stem cell extracellular vesicles by microfluidic-sonication for collagen I mRNA delivery to human tendon progenitor stem cells. Biomaterials Science, 2025, Advance Article.

The publications are referred to in the text by their respective roman numerals (**I-III**). The papers are reprinted with kind permission from Royal Society of Chemistry (**I, III**) and American Chemical Society (**II**).

In publication **II**, the first authorship is shared with the authors marked with †.

Publication **II** will be defended in the doctoral thesis of the co-shared author Adrian Cerveró Varona.

List of additional publications

The list below presents additional manuscripts published during the doctoral studies, which are not included in the experimental section of this thesis:

I López Cerdá, S.[†]; Molinaro, G.[†]; **Pareja Tello, R**.; Correia, A.; Waris, E.; Hirvonen, J.; Barreto, G.; & Santos, H. A. Antifibrotic and Pro-regenerative Effects of SMAD3 siRNA and Collagen I mRNA-Loaded Lipid Nanoparticles in Human Tenocytes. ACS Applied Nano Materials, 7, 2024, 17736-17747.

II Molinaro, G.; Fontana, F.; **Pareja Tello, R**.; Wang, S.; López Cerdá, S.; Torrieri, G.; Correia, A.; Waris, E.; Hirvonen, J. T.; Barreto, G.; Santos, H A. In Vitro Study of the Anti-inflammatory and Antifibrotic Activity of Tannic Acid-Coated Curcumin-Loaded Nanoparticles in Human Tenocytes. ACS Applied Materials & Interfaces, 2023, 15 (19), 23012-23023.

III López-Cerdá, S.; Molinaro, G.; **Pareja Tello, R.**; Correia, A.; Künig, S.; Steinberger, P.; Jeltsch, M.; Hirvonen, J. T.; Barreto, G.; Stöckl, J.; Santos, H. A. Study of the Synergistic Immunomodulatory and Antifibrotic Effects of Dual-Loaded Budesonide and Serpine1 siRNA Lipid–Polymer Nanoparticles Targeting Macrophage Dysregulation in Tendinopathy. ACS Applied Materials & Interfaces, 2024, 16 (15), 18643-18657.

IV Fontana, F. [†]; Molinaro, G. [†]; Moroni, S. †; Pallozzi, G. †; P. A., Ferreira, M.; **Pareja Tello, R**.; Elbadri, K.; Torrieri, G.; Correia, A.; Kemell, M.; Casettari, L.; Celia, C.; Santos, H. A. Biomimetic Platelet-Cloaked Nanoparticles for the Delivery of Anti-inflammatory Curcumin in the Treatment of Atherosclerosis. Advanced Healthcare Materials, 2024, 2302074.

V López Cerdá, S.; Fontana, F.; Wang, S.; Correia, A.; Molinaro, G.; **Pareja Tello, R**.; Hirvonen, J.; Celia, C.; Barreto, G.; Santos, H. A. Development of siRNA and Budesonide Dual-Loaded Hybrid Lipid–Polymer Nanoparticles by Microfluidics Technology as a Platform for Dual Drug Delivery to Macrophages: An In Vitro Mechanistic Study. Advanced Therapeutics, 2023, 6, 2300048.

Abbreviations

AECs	Amniotic epithelial stem cells (AECs)
ADSCs	Adipose-derived mesenchymal stem cells
α-MEM	Alpha minimum essential medium
AM	Amniotic membrane
AREG	Amphiregulin
BFGF	Basic fibroblast growth factor
BSA	Bovine serum albumin
BGN	Biglycan
BMSCs	Bone marrow-derived mesenchymal stem cells
CA	Carbic anhydride
CO_2	Carbon dioxide
CS	Chondroitin sulfate
Cu	Cooper
CuAAC	Copper catalyzed azide-alkene cycloaddition
CTGF	Connective tissue growth factor
DBCO	Diphenylcyclooctyne
DLS	Dynamic light scattering
DMEM	Dulbecco's Modified Eagle's Medium
DMF	Dimethylformamide
DMSO	Dimethyl sulfoxide-d_6
ECL	Enhanced chemiluminescence assay
EDC	1-Ethyl-3-(3-dimethylaminopropyl)carbodiimide
EDTA	Ethylenediamine tetraacetic acid
EE	Entrapment efficiency
ELS	Electrophoretic light scattering
EVs	Extracellular vesicles
EtOH	Ethanol
F-12	Nutrient mixture F-12
FBS	Fetal bovine serum
FDA	Food and Drug Administration
FMOD	Fibromodulin
FTIR	Fourier-transform infrared
GDF5	Growth differentiation factor 5
GM-CSF	Granulocyte-macrophage colony stimulating factor
HAM	Ham's nutrient mixture
HA-PEG	Hyaluronic acid and poly(ethylene glycol) hydrogel
HA-PEG-HEP	Hyaluronic acid and heparin-functionalized poly(ethylene glycol) hydrogel
HBSS	Hanks' balanced salt solution
HBTU	N,N,N',N'-tetramethyl-O-(1H-benzotriazol-1-yl)uranium
HEDSCs	Human exfoliated deciduous teeth stem cells
HEPES	4-(2-Hydroxyethyl)-1-piperazineethanesulfonic acid
HGF	Hepatocyte growth factor
hMSCs	Human mesenchymal stem cells
^{1}H-NMR	Proton nuclear magnetic resonance
ICE	Indocyanine green
IEDDA	Inverse electron demand Diels-Alder

IFN-γ	Interferon gamma
IGF1	Insulin-like growth factor
IL	Interleukin
LD	Loading degree
LNPs	Lipid nanoparticles
MP	Microsphere
MPEG-CL	Methoxy polyethylene glycol-*b*-polycaprolactone
MSC-Hyb	hMSC-EVs derived hybrid lipid nanoparticles
NBD-PS	18:1 1,2-Dioleoyl-sn-glycero-3-phospho-L-serine-N-(7-nitro-2-1,3-benzoxadiazol-4-yl) ammonium salt
NEAA	Non-essential amino acids
NaOH	Sodium hydroxide
NHS	*N*-Hydroxysuccinimide
NIR	Near infrared radiation
NMP	N-methyl-2-pyrrolidinone
NPs	Nanoparticles
NSAIDs	Non-steroidal anti-inflammatory drugs
NTA	Nanoparticle tracking analysis
PAMAM	Poly(amidoamine)
PBMC	Peripheral blood mononuclear cells
PBS	Phosphate buffered saline
PDGFBB	Platelet-derived growth factor
PDI	Polydispersity index
PDMS	Polydimethylsiloxane
PEG	Poly(ethylene glycol)
PEST	Penicillin and streptomycin
PFA	Paraformaldehyde
PHEMA	Poly(2-hydroxyehtyl methacrylate)
PLA	Poly(lactic acid)
PLGA	Poly(lactic-co-glycolic acid)
PNIPAAm	Poly(N-isopropylacrylamide)
P(NIPA-co-AA)	Poly(N-isopropylacrylamide-co-acrylic acid)
PPZ	Poly(organophosphazene)
PRP	Platelet-rich plasma
PVA	Poly(vinyl alcohol)
PVP	Poly(viniylpyrrolidone)
Rhodamine-PE	18:1 1,2-Dioleoyl-sn-glycero-3-phosphoethanolamine-N-(lissamine rhodamine B sulfonyl) ammonium salt
ROS	Reactive oxygen species
RPMI	Roswell Park Memorial Institute
RT	Room temperature
SFM	Macrophage serum free media
SPAAC	Strain-promoted azide-alkyne cycloaddition
SPANC	Strain-promoted nitrone-alkyne cycloaddition
TEM	Transmission electron microscopy
TGF-β1	Transforming growth factor beta 1
TNF-α	Tumour necrosis factor-alpha
TSPCs	Tendon stem/progenitor cells

UV	Ultraviolet
VEGF	Vascular endothelial growth factor
W/O	Water in oil emulsion

1 Introduction

In the recent years, the pharmaceutical technology field has experienced a remarkable transformation thanks to the development of novel drug delivery systems. The design of innovative formulations, such as hydrogel and nanoparticles (NPs) systems, aims to control drug availability, target specific cells or tissues and prolong the therapeutic effect over time[1,2]. Furthermore, the production of pioneering drug delivery systems not only follows the need to improve the delivery, pharmacokinetics and bioavailability of conventional small molecules, but also aims to encapsulate highly complex biological cargos, including proteins and nucleic acids, and ensure their stability and targeting potential, as well as reducing the toxicity and necessary doses[3–5]. Therefore, the use of innovative delivery systems serves as an alternative to conventional therapeutical approaches, which require to frequently administer elevated dosages achieving limited bioavailability and higher toxicity[6].

Musculoskeletal diseases are considered an increasing global healthcare problem, with more than 150 distinct pathologies and an estimated incidence of 1.71 billion people worldwide[7]. Specifically, tendinopathies are among the most common musculoskeletal disorders and include a wide and diverse range of disorders that compromise the intrinsic regenerative capabilities of tendon tissue following chronic alteration of the tissue homeostasis[8]. While the prevalence of tendon-related disorders differs between different regions, high-income countries are estimated to be the most affected nations. For example, recent studies conducted in the central European area and the UK concluded that the average incidence of Achilles tendon rupture was between 7 and 8 per 100,000 person-years, with most injuries predominantly caused by performing sport activities[9,10].

The treatment of tendon-related disorders mainly depends on the specifically affected tendon and the type of injury, with surgical interventions and physiotherapy-based activities considered as two highly common therapeutical approaches in combination with oral administration of non-steroidal anti-inflammatory drugs (NSAIDs) or other therapeutics used for the symptomatic relief of pain and inflammatory symptomatology[11,12]. Therefore, there is an increasing need for the development of novel therapeutical tools capable of mediating the inflammatory state and supporting the regeneration process to allow the restitution of the original tissue matrix and mechanical properties.

The implementation of novel drug delivery-based technologies remains a highly promising opportunity to design alternative drug formulations for the delivery of biological cargos, such as nucleic acids, growth factors or stem cells-derived conditioned media, aiming to support the regeneration of the affected tissue and improve the recovery process. Particularly, hydrogels and NPs remain optimal drug delivery systems for the encapsulation of biological cargos and their controlled release after direct administration into the affected tissue, enhancing the therapeutical efficacy and reducing the administration frequency.

In this thesis, different hydrogel and NPs-based formulations were developed as drug delivery systems for the delivery of biologically complex cargos and the treatment of tendinopathy-derived conditions. Firstly, in **publication I**, *in-situ* gellable inverse electron demand Diels-Alder (iEDDA)-crosslinked poly(ethylene glycol) (PEG) hydrogel microspheres (MPs) were developed *via* water-in-oil (W/O) emulsification as a potential protein delivery system. The developed hydrogel MPs production was optimized and the produced MPs were characterized in terms of physicochemical and morphological properties, rheological and swelling behaviour, protein encapsulation and cargo release potential, as well as cell biocompatibility in primary human tenocytes.

Subsequently, in **publication II**, a hyaluronic acid (HA) and PEG *in-situ* gellable iEDDA-crosslinked and heparin-functionalized hydrogel formulation was produced for the encapsulation of amniotic epithelial stem cells (AEC)-derived conditioned media (CM). The system was also studied in terms of physicochemical and morphological characteristics, as well as rheological and swelling properties. The release profile of the encapsulated AEC-CM was evaluated from heparin-functionalized hydrogels to assess the potential utility of the system for the prolonged release of the encapsulated CM. Moreover, the immunomodulatory potential of the system was investigated by studying the proliferation of peripheral blood mononuclear cells (PBMC) and the macrophages phenotypic polarization.
Finally, in **publication III**, mesenchymal stem cells (MSC)-derived extracellular vesicles (EVs) were used for the production of lipidic hybrid NPs by microfluidic-sonication for collagen type I (COL1A1) mRNA encapsulation and delivery in tendon progenitor stem cells (TSPCs). The formulation was optimized and characterized in terms of physicochemical properties, hybridization studies and mRNA encapsulation efficiency. The *in vitro* biocompatibility, cell-uptake and transfection efficiency studies were performed in TSPCs with eGFP mRNA-loaded NPs. Moreover, *in vitro* studies in TSPCs with COL1A1 mRNA-loaded NPs were conducted and protein production was studied by Western Blot and immunofluorescence staining of collagen type I.

2 Literature overview

2.1 Polymer-based hydrogels for controlled drug delivery

During the recent decades, the development of controlled drug delivery systems has revolutionized the pharmaceutical technology field[13,14]. Conventional drug administration methods have generally been correlated with several drawbacks, including administration of high dosages and administration frequencies, reduced drug bioavailability, considerable toxicity and numerous side effects[1,15,16]. Therefore, huge efforts have been made to design and produce drug delivery systems capable of addressing these challenges. Drug delivery systems are designed to control drug availability in a specific space, the target cells or tissues of interest, over a concrete period of time[17–19]. From the delivery of small-molecule drugs, initially considered the predominant therapeutic class, to more recently developed therapeutic tools, such as proteins, peptides, nucleic acids or monoclonal antibodies; the drug delivery field has faced several challenges, depending on the typology of cargo[6,20,21]. Delivery of small molecules requires to extensively study the physicochemical properties of each specific compound and design strategies to improve key factors such as solubility, pharmacokinetics and bioavailability[22,23]. In stark contrast, delivery of biological cargos presents different critical aspects, such as the need to intracellularly deliver the cargo of interest or its stability[24–26]. Conception of drug delivery systems, such as NPs, liposomes, hydrogels and implants aims to enhance the efficacy, improve the targeting, increase the biological barriers permeability and reduce the toxicity and dose of therapeutics[27,28].

Among the several systems developed during the past decades, hydrogels remain a highly popular system[29]. The term dates back to the end of the 19th century, when hydrogels were firstly described as colloidal gels based on inorganic salts[30,31]. However, the current interpretation of the concept was firstly developed in 1949 under the trade name of Ivalon®, a poly(vinyl alcohol) (PVA) biomedical implant[32]. Subsequently, Wichterle and Lim developed the first poly(2-hydroxyehtyl methacrylate) (PHEMA) hydrogel for ophthalmic application[33]. During the following decades, research on hydrogel formulations grew exponentially following the advances achieved in the polymer chemistry field. The concept of hydrogel was defined as a three-dimensional (3D) polymer-based structure with the ability to own large amounts of water in aqueous media[34–36].

Their predominant characteristic remains their ability to absorb and retain water within their network of polymer chains crosslinked, in a lower or higher degree, with each other[37,38]. The level of crosslinking between the polymeric structure defines the mesh size of the matrix network, which can vary up to 100 nm[39]. Moreover, their structure can either be classified based on the presence or absence of microscopic pores (**Figure 1**), differentiating between nonporous hydrogels, microporous (<100 nm pores) , macroporous (< 1 μm) and superporous hydrogels (>100 μm)[40]. Therefore, the structural characteristics of the matrix define the rheological and mechanical properties of the hydrogel, allowing to produce structure with stiffness values among 0.5 kPa and 5 Pa[41–43]. Moreover, the ratio between the hydrophilic and hydrophobic functional groups that constitute each polymer chain defines their water absorbing ability[44]. The highly hydrophilic nature of their structure contributes to their use as extracellular matrix-mimicking constructs and the encapsulation of hydrophilic cargos[45,46]. In fact, the crosslinked network of the structure remains crucial for the encapsulation of biological therapeutics, since the control of the polymer network mesh size is responsible for the retention and immobilization of the loaded cargos, as well as avoiding the penetration of external agents that may play a role in the degradation of the cargo[47–49]. Hydrogels can also be described

based on other features, such as their macroscopic design (**Figure 1**), mechanical properties, biodegradability or adhesivity to biological tissues, among others[50,51]. Moreover, other approaches have focused on the development of stimuli-responsive hydrogels, capable of detecting a specific physical or chemical stimulus, including pH, temperature or the presence of specific metabolites, and trigger a specific effect, such as the release of the encapsulated cargo or the degradation of the polymer chains[49,52,53].

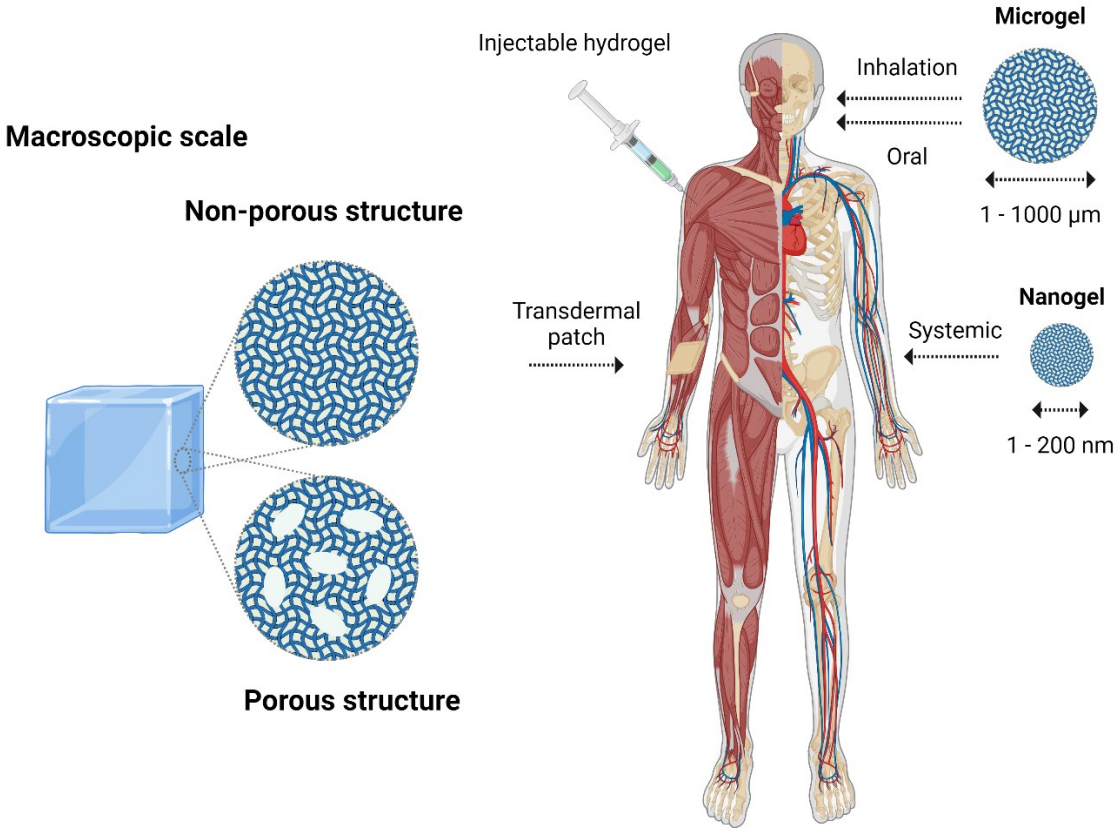


Figure 1. Multiscale structure and macroscopic design of hydrogels. Hydrogels can be macroscopically designed based on the characteristics of their polymer network, including the mesh size, and the presence of microscopic pores. Based on their nanometric structure and their physicochemical properties, hydrogels can be formulated for transdermal delivery *via* polymeric patches, local administration by *in situ* forming hydrogels, oral or inhalation administration as microgels and systemic administration as nanogels. Adapted with Biorender.com with permission from ref. [54]; Copyright © (2016) Springer Group.

Recently, more advanced hydrogel designs were developed using stereoregular polymers, which can stereoselectively interact and form structures with different physicochemical properties[55], or even non-polymeric materials, such as metal-ligand complexation or peptide-interaction systems[56,57]. Despite the different nature of each hydrogel design, the development of any hydrogel formulation must ensure the non crossreactivity with the encapsulated cargo and its stability and protection against external agents[58,59]. The release of the loaded cargo must respond to the specifications of the desired therapeutic effect, the target tissue, the drug availability time and the release profile, which remain specific for each application[60–62]. After the complete release of the cargo, the system should be designed to degrade without causing any toxicity, considering the specific physiological characteristics of the tissue of implantation[63,64]. Design of advanced hydrogel systems has continued evolving alongside

simultaneous advances in other intercorrelated fields. Studies indicate that more than 100 hydrogel-based products have been approved by different regulatory agencies and more than 210 clinical trials have been conducted[65,66]. Their wide applicability for all types of biomedical applications and the constant evolution of the clinical landscape remain clear indicators of the value and importance that these systems play in the medical field[67,68].

2.1.1 Hydrogel classification and crosslinking methods

Hydrogels can be widely classified according to several parameters, including the origin and nature of the used precursor polymers, the type of crosslinking between the precursor polymers, the method of synthesis, the ionic charge of the polymer chains or the physical structure of the matrix[69,70], among other modalities exemplified in **Figure 2** .

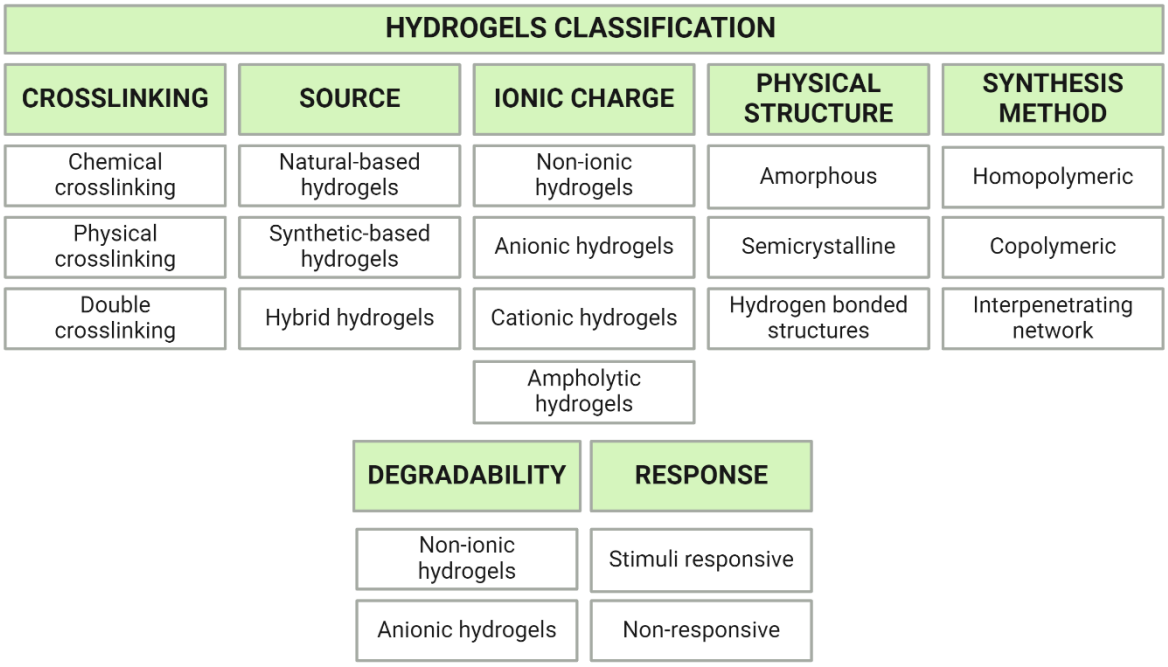


Figure 2. Hydrogels classification methods according to their physicochemical properties. Table created with Biorender.com.

2.1.1.1 Polymer origin

Based on the nature of the used precursor polymers, hydrogels can be classified as natural-based, synthetic-based or hybrid structures. **Table 1** provides a brief summary of the polymers used in this work, including their main characteristics and possible crosslinking methods for their use as precursor polymers.

Natural-derived polymers used for the production of hydrogels include polysaccharides and proteins, which can be produced by a wide variety of living organisms[71,72]. Polysaccharides are the main source of natural polymers used for the development of hydrogels and are formed by a series of monosaccharide units linked to each other by glycosidic linkages, which are differently organized forming homo- or hetero-polysaccharides[73,74]. Widely used polysaccharide precursors include hyaluronan, alginate, guar gum, gellan gum, dextran, poly-γ-glutamic acid, polyesters and polyamines, among others[75]. Proteins can also be used as hydrogel precursors due to their amino acid-based structure linked *via* peptide bonds. Commonly used protein precursors remain high molecular weight proteins such as collagen and gelatin[76–78].

Table 1. Summary of the main characteristics and possible crosslinking strategies of the used polymers, classified according to their origin.

Type of polymer	Composition	Properties	Crosslinking	Ref.
Natural polymers				
Hyaluronan	Non-sulphated polysaccharide based on β-1,4-D-glucuronic acid and β-1,3-N-acetyl-D-glycosamine units	▪ Highly hydrophilic ▪ Anionic charge ▪ Water-retention properties ▪ Biodegradability by specific enzymes ▪ Intrinsic biological properties based on the molecular weight ▪ Possible functionalization *via* carboxy and hydroxyl groups	▪ Chemical crosslinking, including modification with specific moieties ▪ Enzymatic crosslinking ▪ Photo-crosslinking after functionalization	79,80
Collagen	Amino acid-specific sequence highly rich in glycine-proline-X and glycine-hydroxyproline-X motifs, with X as different amino acids. The amino acid sequence is organized as different types of triple-helices, structured as fibrils	▪ Hydrophilic ▪ Highly biocompatible and non-toxic ▪ Low immunogenicity ▪ Intrinsic biological activity as cell adhesion and signalling agent ▪ Biodegradability by specific enzymes ▪ Possible functionalization at mild conditions	▪ Chemical crosslinking ▪ Temperature-responsive gelation ▪ Photo-crosslinking after functionalization	81,82
Synthetic polymers				
Poly(ethylene glycol)	Ethylene oxide repeating units-based chains. Synthesis is achieved by alkaline catalysis using a highly nucleophilic alkali metal and a proton donator such as polar and aprotic solvents	▪ Hydrophilic ▪ Soluble in specific organic solvents (chloroform, benzene) ▪ Biocompatible and non-toxic ▪ Mono and polydisperse, depending on the synthesis ▪ Multiple shapes, including linear, branched or star ▪ Inert and non-volatile ▪ Odourless	▪ Chemical crosslinking, since it can be anchored with multiple functionalization groups ▪ Photo-crosslinking after functionalization	83,84

Naturally-derived polymers have been widely used due to their advantageous properties, including their highly hydrophilicity, non-toxicity and biodegradability[85,86]. Moreover, some of

the used natural polymers are indeed produced as extracellular matrix (ECM) components, a highly beneficial aspect for the design of novel drug delivery formulations[87]. However, their application remains limited due to their lack of production homogeneity, since polymers can easily differ from batch-to-batch, own limited mechanical strength, and induce potential antigenicity[88,89].

Synthetic polymers are petroleum oil-derived products made up of monomeric units, such as PVA, poly(ethylene glycol) (PEG), poly(viniylpyrrolidone) (PVP) and poly(N-isopropylacrylamide) (PNIPAAm), among others[90,91]. Their use has been widely spread due to their high purity, batch-to-batch uniformity, tuneable mechanical properties and non-immunogenicity[92]. However, several drawbacks, such as limited biodegradability, lack of biological moieties and possible toxicity remain limiting aspects worth to consider[93,94]. Despite some polymers may have been designed to contain degradable linkages in their structure, such as poly-(lactic-co-glycolic acid) (PLGA), many others are considered chemically inert and own a considerable hydrophobic nature, which limits their degradability[95]. Moreover, synthetic polymers are difficult to dispose, a highly-cost and time-consuming process that can lead to environmental contamination[96].

More recent approaches have focused on the development of hybrid hydrogels based on the use of both natural and synthetic polymers, combining the properties of both types of polymers.

2.1.1.2 Crosslinking method

A different classification method is based on the type of crosslinking between the precursor polymers (**Figure 3**). Physically crosslinked hydrogels are formed based on intermolecular reversible interactions, including electrostatic and ionic interactions, hydrogen bonds, hydrophobic interactions, metal coordination, crystallization or stereo-complex establishment, among others[86,97]. Physical crosslinking has been generally correlated with higher biocompatibility profiles due to the absence of chemical crosslinking moieties, which could remain unreacted and cause certain cytotoxicity[98,99]. Moreover, most of the used strategies allow to develop stimuli-responsive hydrogels that can respond to environmental changes, such as pH, temperature, ionic strength, light emission, electric and magnetic fields, pressure, oxygen concentration or presence of certain metabolites[100]. The main advantages of physical crosslinking include its reversible nature, reactivity in mild and even physiological conditions, as well as its generally high biocompatibility. However, physical crosslinking still owns significant drawbacks, including poor mechanical and rheological properties and susceptibility to changes in the environmental changes[101,102].

Chemical crosslinking is based on the formation of chemically covalent bonds between the used precursor polymers, which are permanent and irreversible[99,103]. Covalent crosslinking is generally correlated with higher stability under physiological conditions and enhanced mechanical properties[104]. Moreover, degradability of the formed bonds can be controlled by multi-functionalizing precursor polymers[105]. Reported chemical crosslinking strategies include free radical polymerization induced reaction, several types of click chemistry, Michael type-addition, Schiff base formation or even hydrogel formation *via* addition of external crosslinkers[106]. Several studies have reported the use of chemical crosslinkers, such as glutaraldehyde or 1-ethyl-3-(3-dimethylaminopropyl)carbodiimide (EDC), as well as naturally-derived crosslinkers, such as genipin or even enzymes[107]. Specific covalent unions can also be established under mild reaction conditions *via* enzymatic crosslinking based on the specific enzyme type[108].

Studies have also reported the possibility to form double network hydrogels, which can be crosslinked following a combination of different methods[109,110]. The formed hydrogels have

been described to amplify the properties of the obtained structure, overcoming the limitations of single crosslinking methods and combining the benefits of each one. The designed hydrogels still own a robust structure integrity provided by the covalent binding, combined with a reversibly-crosslinked matrix[111–113].

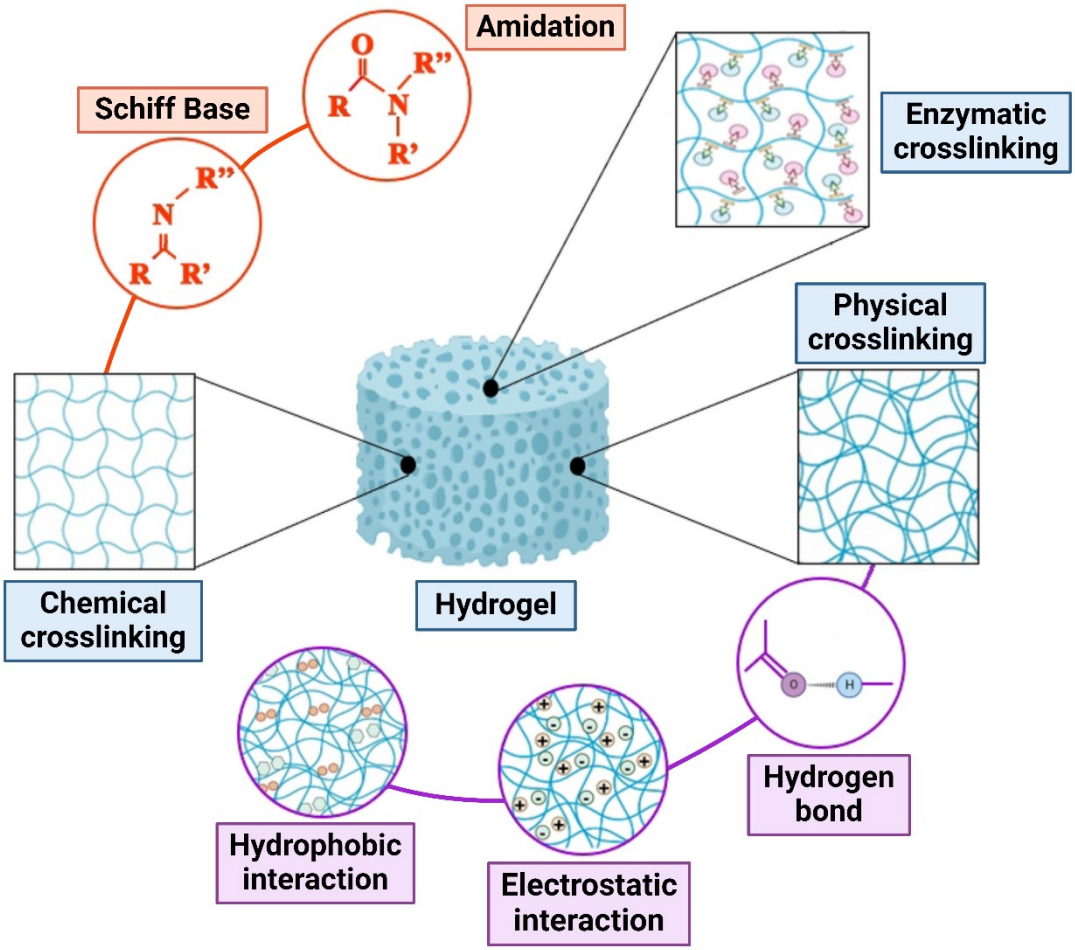


Figure 3. Classification of crosslinking methods. Schematic representation crosslinking types based on their nature. Adapted with Biorender.com with permission from ref [114]; Copyright © (2023) Springer Group.

2.1.1.2.1 Inverse Electron Demand Diels-Alder click chemistry

The term "click chemistry" was introduced in 2001 by Sharpless *et al.* as a novel approach based on the principle of developing new molecules by assembling small units with each other, easing the applicability into several fields[115,116]. Click chemistry has been defined as a modular and broad in scope range of reactions with high reactivity, specificity and high yield under mild conditions[117,118]. Moreover, click chemistry-based reactions are characterized by the formation of nontoxic byproducts, the use of benign solvents and the stereospecificity of the reactive moieties[119]. Click reactions have commonly been described as bioorthogonal due to their high compatibility with proteins, metabolites and even living cells, since they do not interfere with biological processes[120,121]. Click chemistry has traditionally been divided into three types of reactions, including copper (Cu) catalysed azide-alkyne cycloaddition (CuAAC), Cu-free click reactions and alternative click reactions. Representative reaction examples are illustrated in **Figure 4**.

CuAAC was firstly reported by Sharpless and Meldal in 2002 and was characterized by its high efficiency, bioorthogonality, regiospecificity and fast kinetics[122,123]. Both reactive moieties,

alkynes and azides, can react under physiological conditions within minutes without interference with biomolecules such as proteins or living cells, since alkynes and azides are not part of living organisms[124,125].

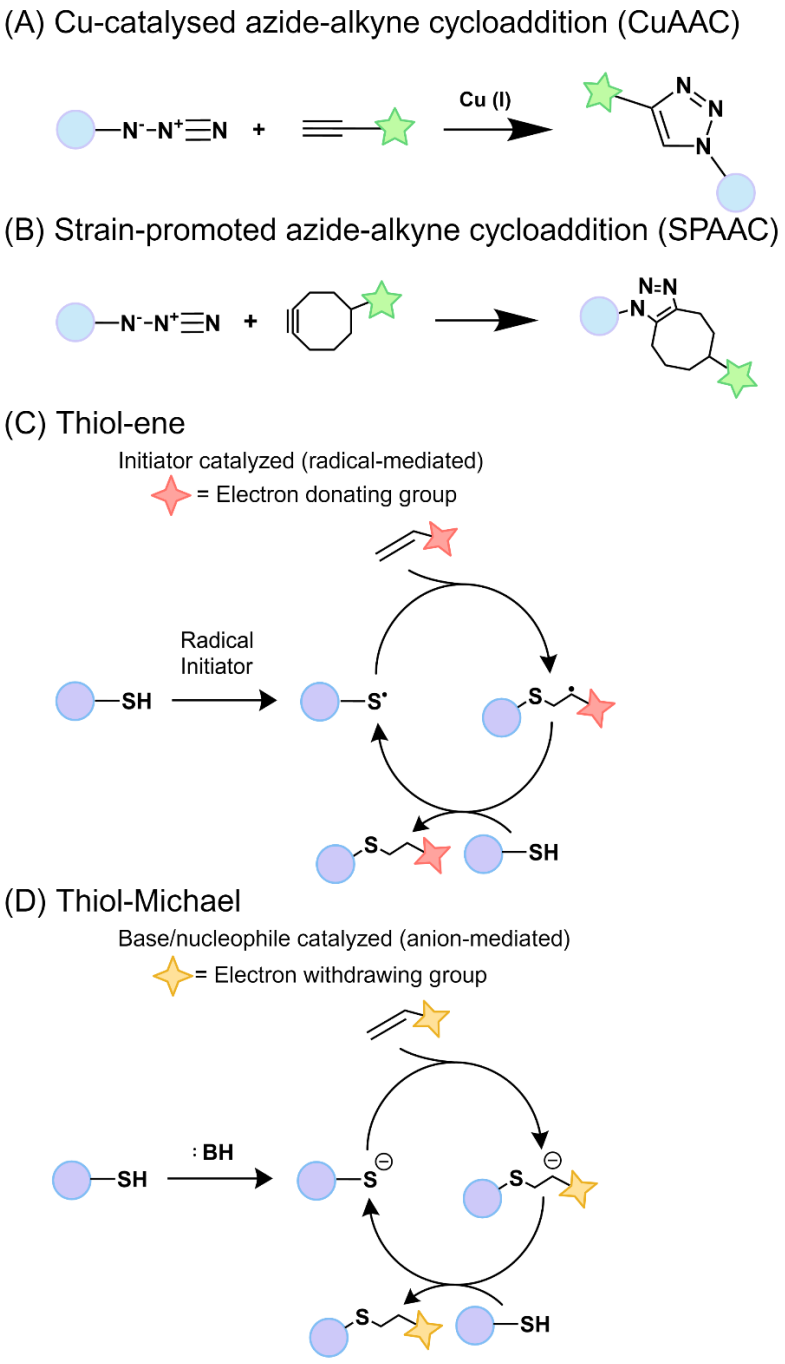


Figure 4. Representative click and alternative click reactions. (A) Cu-catalysed azide-alkyne cycloaddition (CuAAC); (B) Strain-promoted azide-alkyne cycloaddition (SPAAC); (C) Thiol-ene reaction; (D) Thiol-Michael reaction. Blue and purple circles and green stars correspond to the different substitute groups of click and alternative click reactions. Red stars correspond to the electron donating groups of the thiol-ene reaction and yellows stars correspond to the electron withdrawing groups of the thiol-Michael reaction. Adapted with Biorender.com with permission from ref [126,127], Copyright © (2024) Springer Group and Copyright © (2021) Royal Society of Chemistry.

Despite the bioorthogonal nature of the reaction, CuAAC faces a critical limitation due to the presence of Cu (I) ions and the correlated cytotoxicity. Presence of residual Cu (I) may be

responsible for the production of reactive oxygen species (ROS), which can affect the structural integrity of possible biological cargos such as proteins, lipids or nucleic acids[128,129]. Therefore, alternative Cu-free approaches were developed with the aim to avoid the use of any cytotoxic catalyst. Among the different Cu-free reactions, approaches like strain-promoted azide-alkyne cycloaddition (SPAAC) can be highlighted based on the use of cyclooctyne moieties capable of reacting with azides without additional catalyst[130,131]. Despite its promising potential, this approach has still not been fully explored in the drug delivery field mainly due to the high cost and synthetic complexity cyclooctyne moieties, which are produced following intricate synthesis routes[132]. Other approaches have focused on the development of alternative click reactions with high efficiency, mild reaction conditions and high yield, such as thiol-ene chemistry, which can be characterized by free radical-mediated addition of thiol groups to electron-rich double bonds (*e.g.*, vinyl ether or allyl ether[133,134]) under the application of UV light radiation[135,136]. This allows to achieve spatiotemporal control of the reaction, as well as appropriate gelation kinetics. However, the major drawbacks include the possible crossreactivity between thiol groups and other biomolecules, as well as the potential cytotoxicity associated with possible radicals derived from the photo-induced reaction[137,138]. Another type of thiol reaction remains catalysed thiol-Michael addition between a thiol group and an electron-poor vinyl group *via* basic-mediated or nucleophile-mediated catalysis[139,140]. This reaction has been widely used thanks to its fast kinetics, high coupling efficiency and easiness to develop precursors with both thiol and ene functionalization[135]. Other significant approaches include the aldehyde-hydrazide reaction, which has been described to be highly versatile, accessible and biocompatible[141]. The main disadvantage of the different alternative click reactions remains their limited orthogonality, since reactions can either occur with other biomolecules in *in vitro* or *in vivo* conditions[142].

Inverse electron demand Diels-Alder (IEDDA) chemistry was initially reported in 2008 as an alternative bioorthogonal Diels-Alder [4+2] cycloaddition reaction between an electron-rich dienophile, including alkenes or alkynes, and an electron-poor diene, such as tetrazines, forming a six-membered ring[143,144]. This differs from previously developed Diels-Alder reaction approaches, in which a highly electron-rich diene reacts with electron-poor dienophiles. The reaction is performable in aqueous solutions under mild and physiological pH conditions, owns high selectivity and remarkable fast kinetics[145,146]. The reaction is exemplified in **Figure 5** and occurs *via* the 1,4-cycloaddition of the -C=N-N=C- diene from a tetrazine and a corresponding alkene, *via* a bicyclic intermediate, followed by the release of 1 equivalent of nitrogen and a retro-Diels-Alder reaction, forming a 4,5-dihydropyridazine. The obtained dihydropyridazine, which can be found as two different isomers, is subsequently oxidized and a final pyridazine product is obtained[143]. IEDDA has been proposed as a promising crosslinking approach for the development of novel hydrogel formulations. In this context, numerous IEDDA-crosslinked hydrogel formulations have been designed and developed as potential drug carrier systems as well as novel therapeutical tools for tissue engineering[147]. For example, Anseth *et al.* initially developed a IEDDA-crosslinked hydrogel based on tetrazine-functionalized 4-arm PEG and dinorbornene peptide with fast gelation kinetics[148]. The biocompatibility of the system was studied *via* the encapsulation of hMSCs, which showed excellent viability rates between 90 and 80% after 24 and 72 h[148].

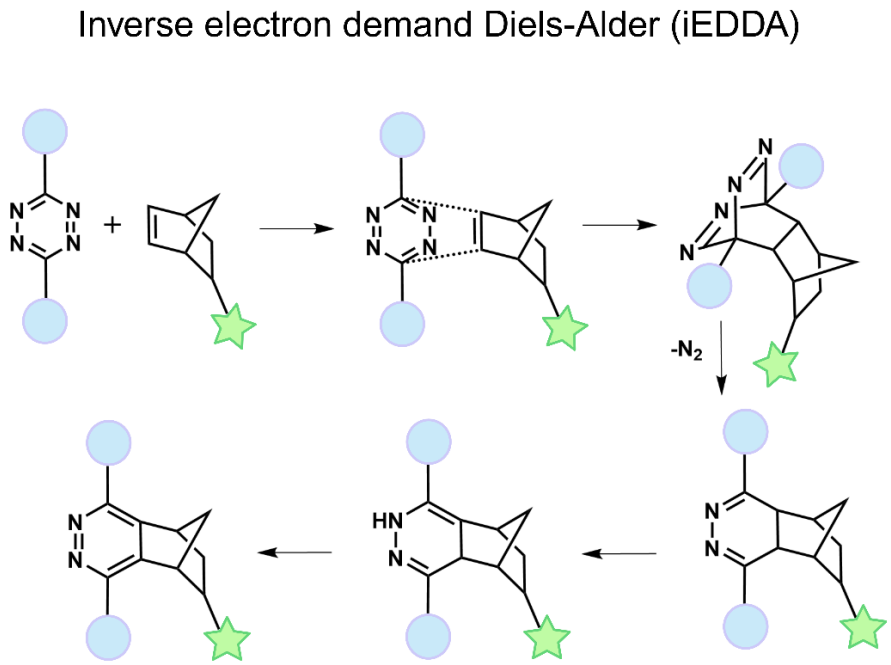


Figure 5. Mechanism of IEDDA reaction. Reaction representation of the reaction between a dienophile and a diene. Blue circles and green stars correspond to the different substitute groups of the reaction. Adapted with Biorender.com with permission from ref. [143]; Copyright © (2017) Royal Society of Chemistry.

Lim *et al.* successfully modified alginate incorporating norbornene moieties and developed an injectable doxorubicin-loaded hydrogel in combination with a tetrazine-modified reduction-responsive PEG-based disulfide crosslinker[149]. The produced hydrogel owned high swelling properties and high drug entrapment efficiency (EE), with stimulus-mediated release of the encapsulated doxorubicin after exposing the formulation to glutathione concentrations of 10 mM. Specifically, less than the 25% of the encapsulated doxorubicin was released after 11 days in contrast to more than the 90% after the stimulus-induced release[149]. A similar approach was used for the development of redox-responsive hydrogels based on norbornene-functionalized gelatin and a tetrazine and diselenide-functionalized crosslinker[150]. The system was similarly loaded with doxorubicin and allowed a stimulus-mediated release of more of the 90% of the loaded drug under reducing conditions. Indocyanine green (ICG) was additionally co-loaded and allowed a near infrared radiation (NIR)-stimulated release[150].

Shoichet *et al.* developed IEDDA crosslinked hyaluronic acid (HA) hydrogels with regulable gelation kinetics and low swelling behaviour as ECM-mimicking 3D cell culture matrices and retinal explant imaging systems[151]. The developed hydrogels were highly biocompatible with primary photoreceptors and allowed multiphoton imaging of retinal explants for more than 30 h, significantly increasing the imaging time in comparison with other hydrogel systems[151]. Overall, all the previously described click chemistry approaches have been extensively used for the development of covalently-crosslinked hydrogels as drug delivery and cell encapsulation systems. A summary of previously developed hydrogel formulations for each type of crosslinking-reaction, types of precursors and application is presented in **Table 2**.

Table 2. Summary of click chemistry-crosslinked hydrogel formulations classified according to the reaction type, precursors and application.

Type of system	Properties	Applicability	Biological studies	Ref.
Copper catalysed azide-alkene cycloaddition (CuAAC)				
Synthetic precursors	▪ High crosslinking efficiency ▪ Tuneable swelling and storage modulus	▪ Development of standardized hydrogel systems for cell adhesion	▪ Fibroblast adhesion in cell adherent regions	152–154
Natural precursors	▪ Fast gelation rate ▪ High swelling behaviour ▪ Elastomer-like mechanical properties	▪ Cartilage tissue regeneration	▪ Chondrocytes adhesion and proliferation enhancement in *In vitro* studies	155,156
Hybrid precursors	▪ Fast gelation rate ▪ Tunability of physicochemical properties ▪ Tuneable degradability	▪ Small molecules delivery system (Doxorubicin, etc) ▪ Cell-based wound healing	▪ Improved cell attachment and cell proliferation rate ▪ Temperature-dependent release of doxorubicin	157–160
Strain-promoted azide-alkyne cycloaddition (SPAAC)				
Synthetic precursors	▪ Fast kinetics ▪ pH dependent hydrolysis ▪ Fast degradability ▪ High biocompatibility	▪ Wound healing biomaterial or embolic agent ▪ Human mesenchymal stem cells (hMSCs) encapsulation system	▪ Tissue adhesion and temporary blockage of blood vessel after auricular injection ▪ Successful encapsulation of cells and high viability percentage	161–163
Hybrid precursors	▪ Rapid kinetics ▪ Slow degradation ▪ Reduced storage modulus	▪ Cell encapsulation platform ▪ Development of filling materials for surgery	▪ Osteogenic differentiation of BMSCs ▪ Cell delivery	164,165
Thiol-ene click addition				
Synthetic precursors	▪ Reduced swelling degree ▪ High mechanical energy storage efficiency	▪ Development of highly resilient hydrogels ▪ Protein delivery ▪ Encapsulation and controlled release of small molecules (Paclitaxel, etc)	▪ The system showcased resilience values comparable to natural resilin ▪ Sustained release of small molecules and protein cargos	166–168

Hybrid precursors	▪ High swelling ▪ Fast kinetics	▪ hMSCs cell encapsulation, culture, differentiation and migration ▪ Growth factor delivery for tissue regeneration (bone, etc)	▪ High viability, strong cell adhesion, variable migration based on the crosslinking degree ▪ Controlled release of growth factors and osteogenic differentiation	169–171
Inverse electron demand Diels-Alder (IEDDA)				
Synthetic precursors	▪ Tuneable gelation time ▪ Tuneable degradation	▪ Protein encapsulation and sustained release ▪ Cell delivery	▪ Prolonged release of protein cargo ▪ Fast degradation after injection in *in vivo* models.	172,173
Hybrid precursors	▪ High swelling ▪ Tuneable gelation kinetics ▪ High porosity	▪ Encapsulation and controlled release of small molecules ▪ 3D culture differentiation of stem cells	▪ Stimuli-induced release of cargos ▪ Trilineage differentiation of encapsulated stem cells	174–176

2.1.1.3 Preparation method and physical structure

Hydrogels can alternatively be classified based on the method used for their development, including homopolymer, copolymer or interpenetrating matrix-based methods[177]. Homopolymer hydrogels are formed by one type of hydrophilic monomer unit, meanwhile copolymer formulations combine two types of monomer units with different properties, with at least one of them owning a highly hydrophilic nature[178]. Interpenetrating matrix hydrogels are formed by the combination of not monomers but two polymers that crosslink after the exposition to each other, combining both polymer structures. Another classification method is based on the physical structure of hydrogels based on their amorphous, semicrystalline or hydrogen-bonded structure[179].

2.1.2 Nano/micro-scale hydrogels as drug delivery systems

Reduction of hydrogel structures to the colloidal regime has allowed to develop alternative hydrogel forms, such as nano- and micro-scale hydrogels. Nanogels are described as polymeric hydrogel particles with sizes varying from 1 to 200 nm, whereas microgels correspond to polymer particles with diameters between 1 and 1000 μm[180,181]. Both types of concepts are known as colloidal systems and own remarkable potential for drug delivery and tissue engineering applications. Microgels are usually developed as hydrogel microspheres (MPs) with average sizes varying from 100 to 300 μm, which allows their injectability through different types of needles and catheters[182]. MPs can be either functionalized to improve the controlled release of loaded cargos, including small compounds or biological therapeutics[183,184], as well as targeting their delivery thanks to the addition of specific biomolecules, such as antibodies on their surface[185]. MPs can also be designed to allow cellular adhesion and serve as 3D cell culture systems as well as cell delivery formulations[186–189]. As opposed to MPs, nanogels own smaller particle size and a larger specific surface area in comparison with the particle volume [190,191]. Nanogels can cross different types of physiological barriers, travel through systemic circulation with higher bioavailability and penetrate certain tissues[192]. Their

nanoscale size allows them to not only interact with cells but also experience internalization, allowing to intracellularly deliver specific cargos[193,194]. Both types of formulations can be produced by different methods following different fabrication techniques. Microgels can be produced by techniques, such as microfluidics, spray drying, electrohydrodynamic spraying or 3D-bioprinting, meanwhile nanogels have been described to be produced by microemulsion, physical self-assembly, dispersion and precipitation polymerization or supramolecular interactions[195–197].

Spray drying uses an atomizer instrument, which atomizes polymer solutions and suspensions with the desired drug cargos and forms micrometric-size droplets[198], which are exposed to hot air to rapidly evaporate the solvent while simultaneously both precursor polymers crosslink with each other, obtaining MPs with different sizes between 1 and 10 μm[199–201]. Despite its widely-spread use, spray drying faces some limitations, such as low efficiency and low production yield[202,203]. Albertsson *et al.* reported the production of stimuli-responsive hemicellulose microgels with fast gelation kinetics at high temperatures *via* spray drying, with average diameter sizes between 1 and 4 μm and high biocompatibility properties[204]. The produced microgels were loaded with different stimuli-responsive components, such as poly(acrylic acid), aniline pentamer or iron to confer pH, electrochemical or magnetic stimuli-responsive properties[204]. Blanco *et al.* similarly described the production of PNIPAAm and Poly(N-isopropylacrylamide-co-acrylic acid) (P(NIPA-co-AA)) for the encapsulation of 5-aminolevulinic acid *via* spray-drying as a potential transdermal delivery system[205]. The obtained microgels owned entrapment efficiency (EE) values between 60 and 75%, with encapsulated drug amounts between 250 and 300 μg of drug per mg of microgel. The system showcased improved transdermal permeation and efficiently delivered the cargo[205].

Electrospraying can also be applied for the production of microgels with some limitations. Microgels are formed by liquid atomization of the precursor polymers thanks to extrusion through a metal needle with high voltage followed by the application of a high electric field, which surpasses the surface tension of the precursor solutions[206,207]. Therefore, the obtained polymer droplets require fast crosslinking kinetics to obtain MPs. Despite its great potential, previous studies have suggested that the technique can only be applied for the encapsulation of limited cargos due to the harsh conditions that precursor solutions have to go through[208,209]. Ng *et al.* reported the fabrication of chitosan-coated native Konjac glucomannan microgels *via* electrospray technique for the encapsulation of quercetin as a potential colon-delivery system [210]. The system owned high EE values superior to 75% and *in vitro* sequential oral-gastric-intestinal digestion studies confirmed the retarded release of the coated formulations[210].

Another promising fabrication method remains 3D-bioprinting[211], which requires a computational-guided modelling of the desired 3D structure, followed by mixing of precursor polymers forming a pre-gel solution, which is sheared, forming a layer-by-layer structure[211]. The technique allows to use several crosslinking strategies, especially stimuli-induced gelation by application of UV light radiation or temperature changes[212]. This approach allows to obtain MPs with high precision and efficiency, mainly for the controlled deposition of cargos or even cells[213], despite some limitations, including the limited production yield, the associated high cost or the possible damage to the loaded cargos or cells due to the applied pressure and, in some cases, temperature conditions that pre-gel mixtures go through[214]. Dong *et al.* optimized a dynamic crosslinking microgel bioink with high printability and biocompatibility properties thanks to dynamic covalent intermicrogel interactions [215]. Microgels were prepared with methacrylate and phenylboric acid-modified HA and methacrylated gelatin and, subsequently, MPs were assembled as bioink *via* dopamine-modified HA as dynamic crosslinker. The printed

constructs owned high shape fidelity and high cell biocompatibility, as well as remarkable tissue adhesion and self-healing properties[215].
Nanogels can easily be produced by microemulsion, a highly common technique based on the use of different immiscible phases together with specific surfactants and co-surfactants[197]. The technique allows to obtain nanogel suspensions with particle sizes ranging from 10 to 100 nm based on the used parameters and the emulsification method, which can differ between techniques, such as mechanical stirring or ultrasound sonication[216]. Nanogels can be formed by polymer crosslinking of both precursors or initiator-induced polymerization after the application of UV light or chemical stimuli[217,218]. The work performed by Dai *et al.* showcased the fabrication of chondroitin sulphate-based nanogels produced by inverse microemulsion polymerization loaded with doxorubicin [219]. The obtained nanogel formulations, which owned controllable particle sizes between 145 and 340 nm, showcased high biocompatibility, prolonged stability, and high drug EE, with efficient pH-stimuli responsive doxorubicin release[219]. Similarly, Jiang *et al.* designed glutathione-responsive poly-*α,β*-polyasparthydrazide and 3,3'-dithiodipropionic acid-base nanogels loaded with 5-fluorouridine, which owned excellent redox-responsive release sensitivity and significant anti-tumor therapeutic efficacy[220]. Other described methods for the production of nanogels include physical self-assembly of different precursor polymers *via* electrostatic interactions, hydrogen bonds or hydrophobic interactions[221,222]; as well as dispersion and precipitation polymerization. Dispersion and precipitation polymerization are based on the initiator-mediated monomer polymerization, forming polymer chains which subsequently grow until the insoluble chain length is achieved[223,224]. The obtained polymer chains aggregate and form colloidal polymer particles with relatively uniform sizes, based on the applied reaction conditions[225].
Overall, despite the advantages and simplicity of most of the common fabrication techniques for the preparation of micro and nanogels, some challenges still need to be addressed, such as batch-to-batch variability, scalability issues or limited control of the formulation parameters. During the previous decade, microfluidics has emerged as a promising alternative fabrication technique with potential to ease and facilitate the production of nano and micro-scale hydrogels[226].

2.1.3 Microfluidics-assisted production of hydrogel MPs

Microfluidics constitutes a multidisciplinary field focused on the study, control and manipulation of fluids in nanolitre and microlitre volumetric scales *via* their integration in micrometric channels[227,228]. The used channels own diameter sizes that vary from tens to hundreds micrometres and are geometrically aligned following specifically designed conformations[229]. Despite being originally conceived for other applications, microfluidics has become a highly significant technique with a significant impact on the development of novel nano and micro-scale drug delivery systems[230]. Microfluidics remains a high-throughput, reproducible and low-cost alternative for the design, production, screening and optimization of drug delivery formulations in comparison with other conventional bulk methods[231,232]. As a result of the rapid mixing of different fluids within microchannels, highly monodisperse and homogeneous colloids can be produced with tuneable sizes and morphologies using a wide variety of materials and requiring a reduced volume amount of precursor reagents[233]. In comparison with other techniques, microfluidics allows for a rapid and more precise control of the mixing rates between the different preliminary phases, which contributes to obtain higher encapsulation efficiencies of a large variety of cargos[234]. Injection of fluids into microfluidics channels with precise laminar flows requires a precise control of parameters, such as the Reynolds number,

which refers to the ratio between inertial and viscous forces, the flow ratio between the different phases injected into the system, or the capillary number, which refers to the ratio between viscous forces and surface tensions between fluids[235].

Microfluidic devices can be manufactured based on different materials, including glass, poly(dimethylsiloxane), poly(methylmethacrylate) and other polymeric materials, silicon and fused silica or ceramics, among others[236]. Despite the recent advances in novel materials, glass remains a highly appropriate and convenient option due to its innate advantages compared to other polymeric or inorganic substrates[237]. Most of its advantageous properties include its chemically inert nature, which allows to use organic solvents, smooth surface, low conductivity, compatibility with high temperatures and appropriate optical characteristics[238]. Moreover, the inner surface of glass capillaries can be chemically modified to optimize the hydrophilicity or hydrophobicity nature of the system. Glass microfluidic devices are prepared by heating and pulling of circular glass capillaries, which are shaped based on the desired tip geometries and orifice diameters[239]. Capillaries are inserted and coaxially aligned with secondary capillaries with wider diameter sizes and different morphologies and attached to glass slides to form the final microfluidic device[240]. Glass microfluidics allows to develop systems suitable for the production of different types of formulations based on the specific geometry design of the device (**Figure 6**)[228]. Single emulsion microgels can be produced following three main geometries: flow focusing, co-flow and T-junction[229]. Different types of geometries can be combined in a single microfluidic device for the development of double or multiple emulsion formulations, as well as other types of systems such as Janus microparticles, which require the confluency of two different streams within a single channel to obtain two-sided microgels with different composition and properties in each side[229]. While different publications focus on the study of the wide range of geometries used for the production of different types of microgels, this literature review will focus on co-flow microfluidics production of single-component microgels since it remains a commonly used glass microfluidics setup.

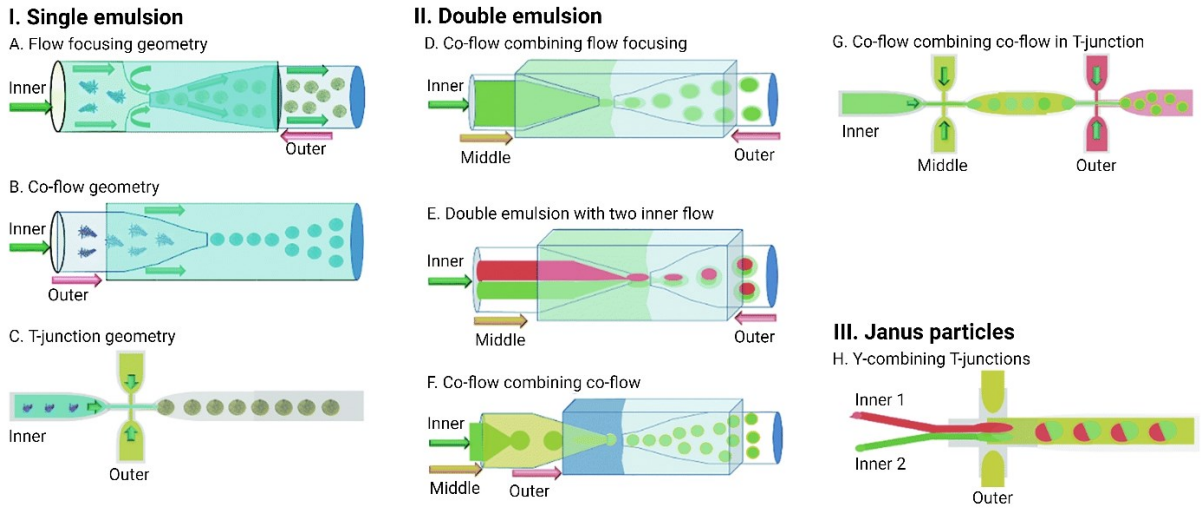


Figure 6. Microfluidic device geometries. Single emulsions can be produced using (A) flow-focusing, (B) co-flow and (C) T-junction geometries. Double and multiple emulsions can be produced following geometries combinations, including the combination of co-flow and flow focusing with (D) one inner fluid and (E) two inner fluids, (F) sequential co-flow and (G) sequential T-junction. (H) Janus particles can be produced by combining two parallel T junctions. Adapted with Biorender.com from ref. [228]. Copyright © (2017) Royal Society of Chemistry.

Co-flow geometry microfluidic devices are formed by the alignment of an inner cylindrical capillary coaxially inserted into an outer capillary, so that both fluid phases flow in parallel. The relationship between both types of flows plays an important role on the type of produced formulation, specifically on the diameter size of the produced particles[241]. Dripping flow regime is achieved when the inner capillary fluid forms individual droplets at the tip of the inner capillary until the shearing force exerted by the coaxial flow at the extreme of the capillary exceeds the interfacial tension of the inner fluid and droplet-based microgels are produced[242]. This setup requires both precursor solutions to be pumped at relatively low rates and allows to produce single emulsion droplet-based microgels. Contrary to the previous phenomenon, jetting flow regime is reached when the inner fluid is ejected as a continuous stream and eventually is reduced to smaller droplets further downstream in the outer flow[243]. This regime is used to produce nanoscale particles by injection of both precursor fluids at high rates and with a lower concentration of particle precursors[244]. Optimization of microfluidic parameters and precursor polymers concentrations are responsible for the production of different types of formulations with variable homogeneity.

2.2 Extracellular vesicles (EVs) as drug delivery systems

At the end of the 20th century, nanotechnology was postulated as a highly promising revolutionary field with extensive applicability in the development of novel drug delivery systems[245]. During the 21st century, nanomedicine has transformed the drug delivery field with the development of innovative nanosystems capable of efficiently deliver and control the release of specific cargos, target particular cells and even allow imaging and facilitate diagnostic techniques[246]. Among the different types of drug delivery systems that have been studied, NPs have emerged as the main exponent of this discipline thanks to their advantages over conventional drug delivery systems[247]. Different types of NPs can be classified according to their physicochemical properties and origin between organic nanoparticles, which include lipid-based NPs, polymeric NPs, and inorganic NPs. The use of NPs has been extensively correlated with prolonged release rate, increased drug solubility, specific targeted delivery and enhanced therapeutic efficacy[248]. Despite the fundamental barriers that still difficult the clinical translation of nanosystems[249], a recent and highly significative example remains the success of lipid nanoparticles (LNPs)-based COVID-19 vaccines, which allowed to successfully encapsulate and intracellularly deliver mRNA to target cells, avoiding its degradation from external agents[250]. Therefore, by intracellular delivery of nucleic acids, host cells could translate the mRNA into viral proteins and induce an effective immune response against the SARS-CoV-2 virus[251].

Despite their potential and numerous advantages, NPs still face several challenges, including potential long term toxicity and adverse immunological effects[252]. Considering its potential limitations, the field of nanomedicine has continued evolving towards new endeavours aiming to improve the current approaches. In fact, during the previous decade, research has focused on the design of biomimetic nanosystems with improved targeting properties and increased permeability through physiological obstacles[253,254]. The use of cell-derived material has shown to be a promising rationale for the design of biomimetic nanosystems, which have proved to own improved biocompatibility profiles, superior target specificity, reduced toxicity, higher circulation half-life and improved biological barriers-crossing capabilities in comparison with other synthetic NPs[255–257]. Considering the previously mentioned benefits, the field has focused on the use of cell-derived structures, such as EVs for the design of alternative nanosystems.

EVs are multivesicular bodies-derived lipidic bilayer vesicles that can be classified based on their diameter, origin or generation mechanism[258]. EVs can be detected in many body fluids, including blood, urine, bronchoalveolar lavage fluid and cerebrospinal fluid[259]. EVs are formed by a lipidic bilayer with a considerably complex composition based on different types of glycerophospholipids and sphingolipids, as well as cholesterol[260]. The lipid distribution between both bilayers remains asymmetric, since it has been described that the outer section is mainly formed by sphingolipids and phosphatidylcholine, whereas the cytosolic section is predominantly formed by other glycerophospholipids, such as phosphatidylserine and phosphatidylethanolamine, among others[261]. Moreover, the distribution of other lipids, such as cholesterol or intracellular lipids, has been extensively discussed and is still being investigated, proving that EVs own a highly intricate structure[262]. The lipidic bilayer additionally owns a wide variety of membrane proteins, including glycoproteins, tetraspanins or signalling receptors[263]. Moreover, EVs contain a bast repertoire of biomolecules, including proteins, lipids and coding and non-coding nucleic acids such as mRNA, miRNAs and even DNA[264]. Traditionally, EVs have been considered as a cellular waste disposal system, useful for the secretion of toxic substances and waste residues[265]. However, successive studies observed that EVs can act as intercellular communication agents and tissue homeostasis regulators, with the ability to model several physiological processes and even promote tissue repair[266]. Consequently, EVs own an extensive variety of roles as trafficking agents and mediator carriers due to their combination of intrinsic bioactive cargos and surface moieties[267]. Their potential as drug delivery agents resides on their ability to encapsulate cell-produced cargos, transport them through biological media and even biological barriers such as the brain-blood barrier, and protect the encapsulated cargos from degradation[268]. Therefore, the use of EVs as highly biocompatible nanosystems for intracellular delivery of therapeutics is a promising alternative to other nanoformulations.

EVs can be classified according to their size and mechanism of formation, since they can be categorized as exosomes, microvesicles or apoptotic bodies. Exosomes are described as the smallest form of EVs, with reported diameter sizes between 30 and 150 nm, and are originated from multivesicular bodies within the endosomal system[269]. Endosomes originate from an initial endocytosis phenomena, which result in early endosomes[270]. This primitive form of endosomes follows a maturation process, in which the inner membrane of these multivesicular bodies is drawn towards the inner side of the structure[271]. This invagination allows to incorporate cytosolic biomolecular cargos such as proteins, nucleic acids or lipids within intraluminal vesicles located inside multivesicular bodies[272]. These structures can fuse with the lipidic bilayer and release the intraluminal vesicles as exosomes into the extracellular space or interact with the lysosome and be degraded[272]. In contrast, microvesicles are described as larger structures, with diameters between 100 and 1000 nm[273]. Microvesicles are directly released from the plasma membrane by budding and fission. Apoptotic bodies are considered the largest form of EVs, with reported diameters between 1 and 5 µm, and are originated from apoptosis phenomena[273].

The applicability of exosomes as drug delivery systems depends, among different factors, on their potential to interact with other cells [274]. Exosomes can selectively target specific cells based on the specificity of the molecules located on their surface, despite the exact mechanisms remain unclear [275]. However, studies have extensively observed that exosomes can be internalized by specific recipient cells by different mechanisms, such as endocytosis or specific cell-surface receptors interactions[276,277]. Endocytosis is described as the complete engulfment of the exosome structure *via* different types of mechanisms, such as clathrin-mediated endocytosis, caveolin-mediated endocytosis, micropinocytosis and phagocytosis[278–

[280]. Following endocytosis, exosomes fuse their structure with the endosome membrane, releasing the exosome cargos within the endosome[267]. This phenomena remains a considerable challenge, since the therapeutic effect will not be achieved unless the incorporated biomolecules are released from the endosomal structure, following a process commonly known as endosomal scape [281]. This highly limiting factor is avoided during another type of internalization mechanism such as the direct fusion of the exosome structure with the plasma membrane of the cell[282]. This process is way less frequent than endocytosis and is characterized by the direct release of the exosome cargos into the cytoplasm. Moreover, another possible endocytosis mechanism is based on specific interactions between specific proteins located on the surface of exosomes and specific receptors on the surface of receptors cells[267].

2.2.1 Extracellular vesicles (EVs) engineering

Following their innate biological properties, EVs have been used as drug delivery agents thanks to the loading of additional therapeutic agents, including proteins, nucleic acids or small drug molecules[268,283]. The different loading methods can be classified between pre-isolation and post-isolation methods, since the additional cargos can be loaded directly into the source cells before the EVs are isolated or directly into the EVs after their isolation from the source cells[284]. Among each classification, the addition of external cargos can be performed following passive loading or active loading [284]. Passive loading is performed by incubating the specific therapeutic cargo with the isolated EVs or by culturing the cargo with the specific source cells responsible for the production of EVs[285]. Despite its apparent simplicity, it is highly correlated with low loading efficiencies due to the lack of control of the process. Moreover, it requires that the therapeutic molecule remains hydrophilic and capable of crossing both cells and EVs membranes, which limits the applicability of this technique to certain molecules[286]. Another approach focuses on the genetic modification of the source cells with the objective to express proteins or nucleic acids and their encapsulation within the EVs produced by the source cells[287,288]. This technique is usually performed for the encapsulation of specific proteins or nucleic acids, since it requires to produce a specific plasmid including the sequence of interest, followed by its packaging in a virus, which will be used to infect the host cells[289]. This approach is considerably more complex, time consuming and not suitable for all types of loading cargos. In stark contrast, active loading is mostly performed after the isolation of EVs and is based on the application of external stimulus capable of increasing the permeability of the membrane[290]. Cargos can be actively loaded by using specific techniques, such as ultrasonication, extrusion, electroporation, freeze thaw cycles or the incubation with specific agents such as detergents[285,291]. These methods are generally correlated with higher EE values and a more precise control of the process and the amount of loaded cargo. Ultrasonication remains a commonly used technique for the encapsulation of external cargos in EVs, since it allows to obtain remarkable EE thanks to the temporary and reversible disruption of the EVs lipid structure under low power and cold temperature conditions[292,293]. Freeze thawing has been described as another efficient technique that requires special attention, since EVs can be loaded *via* partial disarranging of the lipid membrane caused by the application of consecutive cycles of freezing and thawing[294]. Therefore, it is important to highlight that each method may affect EVs differently, since passive methods are correlated with low EE values and active methods may significantly improve the EE and affect the stability of EVs.

2.2.2 Extracellular vesicles-derived hybrid nanoparticles

A more recently described approach focuses on the production of hybrid NPs derived from EVs and synthetic NPs with the objective to combine the advantageous properties of both types of systems within a single nanocarrier[295] (**Figure 7**). Hybrid NPs have been described to be prepared by the fusion of both MSC-EVs and NPs precursors by different bulk methodologies, including extrusion, sonication, freeze-thaw, microfluidics in combination of sonication or chemically-induced membrane fusion[296,297]. Moreover, different studies indicate that hybrid NPs can be constructed from different materials, including LNPs and polymeric NPs[298]. Generally, hybrid NPs are manufactured following physicochemical alteration of both precursor particles, which are exposed to a series of electrostatic and hydrophobic interactions following the disruption and permeabilization of the lipid membrane from the EVs, which subsequently reassembles forming a hybrid structure in combination with the added synthetic NPs[299]. The different methodologies used for the prepared hybrid NPs can be divided between physical induction strategies and chemical induction strategies. Physical induction strategies include passive hybridization and transitory opening of lipid membrane[300]. Moreover, chemical induction strategies include fusion of lipid membranes[301].

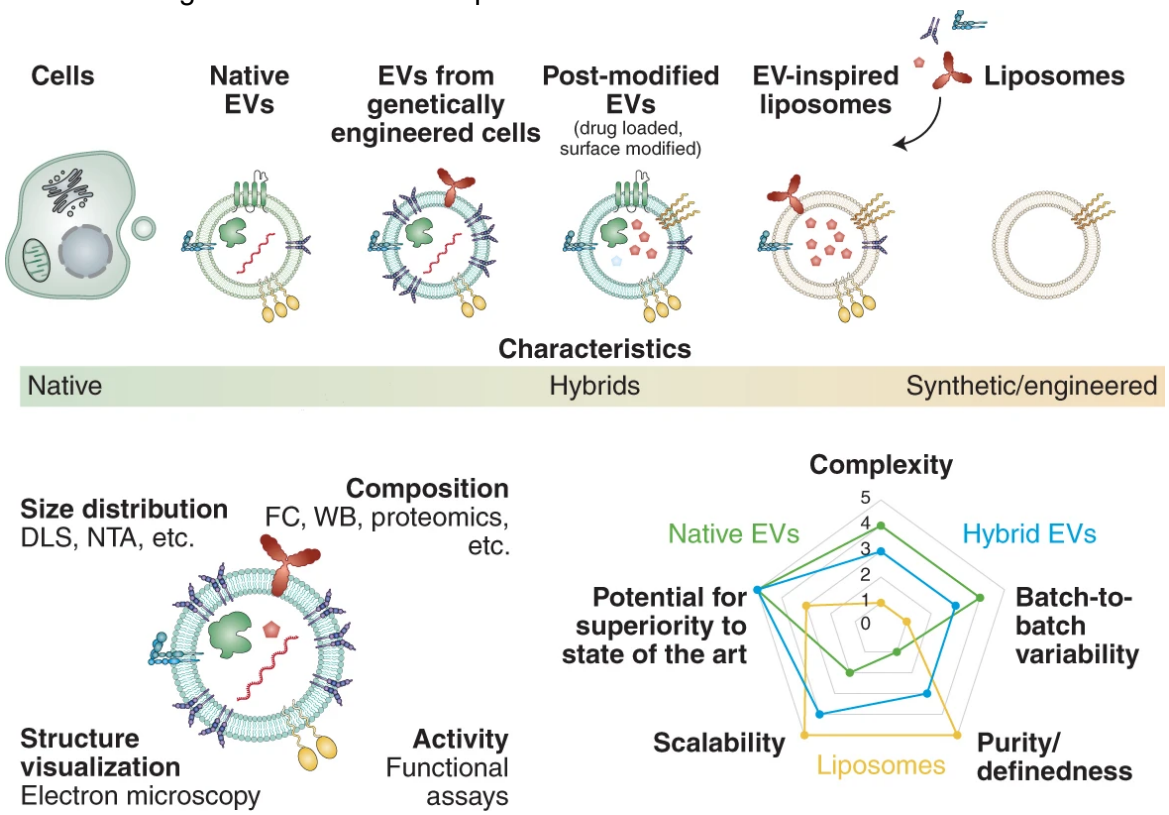


Figure 7. Classification of EVs and EVs-derived structures as drug delivery systems. EVs-derived nanosystems include EVs originated from genetically engineered cells, modified EVs actively loaded with external cargos or EVs functionalized with specific surface antigens. Moreover, EVs-derived nanosystems also include EVs-derived hybrid LNPs, containing fragments of both EVs and LNPs. Native and synthetic structures present several differences in terms of physicochemical properties, composition and activity. Native and EVs-derived systems are characterized by superior structural and compositional complexity and higher batch-to-batch variability, as well as reduced scalability, meanwhile synthetic systems own higher reproducibility, scalability and purity. Image reprinted with permission from ref. [268]; Copyright © (2021) Springer Group.

A summary of the main methodologies, advantages, limitations and examples is presented in **Table 3**. Further details about the exact composition, physicochemical properties and biological effects are reviewed in detail elsewhere.

Table 3. Summary of EVs-derived hybrid NPs production strategies: advantages, limitations and examples.

Physical induction strategies				
Approach	**Advantages**		**Limitations**	
Coincubation	▪ Simplicity ▪ Electrostatic or hydrophobic interactions ▪ No membrane damage		▪ Limited to NPs with specific surface charge or composition ▪ Uncontrollable size ▪ Aggregation ▪ Unwanted products ▪ Low EE	
	Nanoparticle	**Cargo**	**Benefits**	**Ref.**
	▪ Liposomes	▪ pDNA and CRISPR/Cas9	▪ Functional delivery of plasmids into MSCs	302
	▪ Polyethyleneimine / Folic acid-coated EV	▪ siRNA and pDNA	▪ Enhance cellular uptake ▪ pDNA delivery ▪ Gene silencing	303
Sonication	▪ High fusion efficiency ▪ Simplicity		▪ Low EE ▪ Strict control of power and temperature to avoid major structural damages ▪ Uncontrollable size	
	Nanoparticle	**Cargo**	**Benefits**	**Ref.**
	▪ Polyethyleneimine	▪ siRNA and anti-miRNA	▪ Increased gene delivery efficacy ▪ Improved storage stability	304
Extrusion	▪ High fusion efficiency ▪ No aggregation and suitable size		▪ Limited EE ▪ Limited yield ▪ Structural damage ▪ Rearrangement of membrane surface	
	Nanoparticle	**Cargo**	**Benefits**	**Ref.**
	▪ Liposomes	▪ siRNA	▪ Reduced toxicity ▪ Intrinsic regenerative properties	305
	▪ Gold NPs	▪ No cargo	▪ Reduced macrophage uptake	306
	▪ Liposomes	▪ antagomiR	▪ Increased miRNA silencing	307
	▪ Liposomes	▪ Doxorubicin	▪ Differential cellular uptake and enhanced toxicity in cancerous cells ▪ pH-sensitive release	308

Sonication + Extrusion	**Nanoparticle**	**Cargo**	**Benefits**	**Ref.**
	▪ Liposomes	▪ Gemcitabine	▪ Specific targeting to pancreatic cancer cells ▪ Increased apoptotic therapeutic effect	309
	▪ Liposomes	▪ Nintedanib	▪ Enhanced cellular uptake ▪ Enhanced penetration in tissue	310
Freeze-thaw	▪ Simplicity ▪ No need of complex instrumentation		▪ Aggregation ▪ Content leakage ▪ Complex purification ▪ High risk of structural damage	
	Nanoparticle	**Cargo**	**Benefits**	**Ref.**
	▪ Zinc oxide nanocrystals	▪ No cargo	▪ Targeting specificity against Daudi cancer cells ▪ Ultrasound-responsive effect	311
	▪ Thermosensitive liposomes	▪ Granulocyte-macrophage colony-stimulating factor + docetaxel	▪ Preferential accumulation in tumour ▪ Inhibition tumour progression ▪ Increased cellular uptake	312
	▪ Thermosensitive liposomes	▪ Imiquimod + indocyanine green	▪ Enhanced cellular uptake ▪ Prolonged circulation time ▪ Photothermal-responsive release	313
Microfluidics + sonication	▪ High fusion efficiency ▪ Improved reproducibility ▪ Enhanced EE		▪ Strict control of power and temperature to avoid structural damage	
	Nanoparticle	**Cargo**	**Benefits**	**Ref.**
	▪ Polymeric NPs	▪ No cargo	▪ Reduced uptake by macrophages ▪ Enhanced homotypic targeting	314
	▪ Polymeric NPs + Cholesterol-AS1411 aptamer	▪ No cargo	▪ Reduced uptake by macrophages ▪ Increased accumulation in tumour	315
Chemical induction strategies				
PEG induction	▪ High fusion efficiency ▪ Simplicity		▪ Aggregation ▪ Uncontrollable size ▪ Potential contamination or chemical damage	
	▪ Liposomes	▪ siRNA	▪ Improved siRNA delivery	316

Abbreviations: CRISPR: clustered regularly interspaced short palindromic repeats; **EE:** entrapment efficiency; **EV:** extracellular vesicle; **miRNA:** microRNA; **MSC:** mesenchymal stem cells; **NPs:** Nanoparticles; **pDNA:** plasmid DNA; **PEG:** poly(ethylene glycol); **siRNA:** small interfering RNA.

2.3 Local administration route for drug delivery

The previously described therapeutic agents can be delivered following a wide variety of administration routes, following systemic or local administration approaches. Systemic administration requires delivering the administered therapeutic into the bloodstream, spreading across the entire circulatory system with the aim to reach the target organs and tissues[317]. This approach is commonly correlated with widely-spread distribution through the organism, convenient accessibility and quick onset of action in multiple organs and tissues that may be affected by systemic conditions[318]. Systemic administration of hydrogels and NPs include oral, transdermal and intramuscular routes, among others.

Oral administration has traditionally remained a highly popular delivery method considering its various benefits, including ease administration and high patient compliance and controlled and sustained drug release from gastric-resistant enteric formulations[319,320]. Administration of therapeutics *via* the gastrointestinal tract requires to assess the large variety of factors that can impact the dissolution, release and absorption of the dosage forms, including physiological factors such as the acidic environment, high enzyme concentration, presence of bile salts and the distribution of the mucosal absorptive surface within the gastrointestinal tract[321,322]. Appropriate absorption through the gastrointestinal mucosa is followed by systemic distribution of the administered drug. The development of novel drug delivery methods currently aims to overcome several highly limiting factors correlated with the oral administration route, including the variability of the absorption rates depending on the nature of the system, the acidic and enzymatic degradation and the first-pass metabolism activity caused by the liver[323–325].

Transdermal administration remains another highly explored route especially by the development of hydrogel formulations. Delivery of therapeutical agents following the transdermal route presents several advantages, including considerable patience acceptance and reduced invasiveness controlled release of the administered cargo due to the development of depot systems, reduction of the potential toxicity associated with the administered drugs, decrease of the enzyme-dependent drug degradation risk, as well as evasion of first-pass metabolism[326–329]. Nonetheless, the delivery of molecules across the different physiological barriers that conform the stratum corneum remains challenging and commonly depends on the development of polymeric systems such as hydrogels, among others[330].

Intramuscular administration is an alternative administration routes that is based on the delivery of therapeutics into muscle tissue and subsequent expansion through systemic circulation[331]. Similarly to the transdermal route, the main advantages of the intramuscular route include sustained release of cargos from depot systems, decreased drug degradation risk and evasion of first-pass metabolism[332]. However, administration of therapeutics through intramuscular injection requires special attention, since it is correlated with patient discomfort and can even cause pain and tissue damage at the injection site[333].

Other administration routes focus on the local administration of therapeutic agents, which are administered directly into the desired tissue or site of action avoiding the systemic circulation of therapeutics. This approach targets specific organs or tissues and is especially suitable for the treatment of local pathologies, since it allows for rapid absorbance on the site of action and reduces the systemic exposure of the administered therapeutic and minimizes general side effects and first-pass metabolism[334]. By administering the cargo directly into the target it is possible to reduce the dose required to achieve the optimal therapeutic efficacy[335]. Moreover, the development of depot systems allows to achieve a prolonged release of the desired therapeutics precisely at the desired site of action[336]. Despite its numerous advantages, the

local administration of therapeutics requires the intervention of highly qualified professionals, since it involves the injection of therapeutics or implants in specific tissues[334].
Intra-articular administration allows to locally inject therapeutics to the joint space, making it a highly suitable administration route for the delivery of drugs to the synovial fluid and the treatment of inflammatory and degenerative musculoskeletal conditions such as osteoarthritis, rheumatoid arthritis and tendinopathies[337,338]. Several studies have highlighted the positive effects of encapsulating small molecules, biological therapeutics, different types NPs or even living cells into injectable hydrogels or hydrogel MPs[339,340].
Zeng *et al.*[341] developed an injectable gallic acid-grafted gelatine hydrogel suitable for intra-articular administration without affecting the motion of the affected knee. The hydrogel, which was formed following transglutaminase-mediated enzymatic crosslinking, was loaded with liposomes containing teriparatide, an active recombinant human peptide catalogued as a parathyroid hormone analogue that has been approved by the Food and Drug Administration (FDA) for the treatment of osteoporosis[342]. The hydrogel also showcased anti-inflammatory and reactive oxygen species (ROS)-scavenging properties due to the presence of phenolic hydroxyl groups from gallic acid[341]. The *in vivo* studies conducted in mice confirmed the sustained release of teriparatide for over 20 days and showed an increase in chondrocytes proliferation, as well as an increase in the expression of anabolic proteins and a down-regulation of catabolic and inflammatory proteins[341]. The formulation protected the cartilage layer from degradation, promoted the synthesis of glycosaminoglycans and reduced the degeneration progression[341].
In another study, Chun *et al.*[343] designed an injectable methoxy polyethylene glycol-*b*-polycaprolactone (MPEG-CL) hydrogel, which owns thermogelling properties due to the similarities between its phase transition and the body temperature. The hydrogel matrix was suitable for the encapsulation of rat bone marrow MSCs due to the functionalization with the collagen mimetic peptide GFOGER, which possesses chondrogenic and osteogenic potential and has been used as cellular adhesion peptide[343]. *In vitro* studies indicated that the encapsulated cells increased the expression of chondrogenic markers such as β1, α2 and α11 integrins, indicating the chondrogenic differentiation potential of the formulation. Further *in vivo* studies developed in a rat osteochondral defect model showcased that after 4 weeks the encapsulated cells survived at the induced defect and predominantly expressed chondrogenic markers. Histological findings after 8 weeks showed that the MSCs-loaded system produced significant osteochondral regeneration in comparison with the direct administration of MSCs[343].
Song *et al.*[344] described an alternative poly(organophosphazene) (PPZ) NP-based hydrogel system for the sustained release of celecoxib, an anti-inflammatory drug, for the treatment of Achilles tendonitis. Following the amphiphilic structure and thermoresponsive mechanical properties of PPZ, celecoxib was encapsulated within its hydrophobic core at low temperatures and, subsequently, the formulation was injected and the hydrogel was formed under body temperature conditions[344]. *In vitro* release studies indicated a celecoxib sustained release over 28 days and *in vivo* gradual hydrogel degradation for more than 28 days. Moreover, a single injection of the celecoxib-loaded hydrogel was correlated with higher expression of anti-inflammatory cytokines (IL-4 and IL-10) and aligned collagen fibres, improved mechanical properties and reduced expression of pro-inflammatory markers (COX-2, TNF-α, IL-6)[344].
Huang *et al.*[345] proposed a novel approach for the treatment of osteoarthritis and the reduction of joint friction based on the administration of HA-based hydrogel MPs incorporating rapamycin-loaded soy phosphatidylcholine liposomes. Methacrylated-HA hydrogel MPs were formed by single-emulsion microfluidics and jellified *via* photopolymerization. Rapamycin-loaded liposomes were integrated within the polymer matrix based on non-covalent

interactions[345]. The formed MPs were capable of improving joint lubrication by exposing the encapsulated liposomes to their surface, creating self-renewable hydration layers, reducing the induced friction and smoothing the rolling mechanism. Moreover, the sustained release of rapamycin contributed to the maintenance of cellular homeostasis by regulating autophagy, an intracellular degradation system that is significantly reduced during osteoarthritis[345].
The previously described studies remain examples of the numerous advantages achieved by the local administration of drug delivery systems such as hydrogels and NPs for the treatment of inflammatory and degenerative musculoskeletal conditions. The design of suitable biomaterials and sustained release formulations can be optimized to improve the efficacy of the encapsulated cargos, reduce the administration frequency and achieve more significant therapeutical outcomes.

2.4 Tendon-related disorders

Musculoskeletal diseases include more than 150 pathologies and have been reported to affect 1.71 billion people worldwide[346]. Among the different musculoskeletal conditions, tendinopathies comprise a broad and multi-faceted range of disorders that prevent the ability of tendon to heal due to chronic deregulation of the tissue homeostasis[347]. Tendon physiology is characterized by the presence of highly packed and organized collagen fibres as predominant ECM structure[348,349] in combination with a complex range of cells, with a 95% of the total cell population corresponding to tenocytes and tenoblasts, followed by chondrocytes, vascular cells and synovial cells from the tendon sheaths[350]. Pathological tendons suffer major homeostasis alterations that affect the cellularity and composition of the ECM, modifying the microstructure of the tissue, altering the architecture of collagen bundles, enhancing the production of glycosaminoglycans and increasing microvasculature due to neoinnervation[8]. Tendon is responsible for the storage and transmission of substantial mechanical forces due to their physiological function[351]. Highly repetitive use and frequent exposure to demanding mechanical loading activities can lead to mechanical stress and potential injuries, which can result in various overlying pathological processes[352].
Tendinopathic disorders predominantly affect two anatomical areas: the upper and lower limbs. In the upper limb, the most commonly affected tendons are the rotator cuff and the common flexors and extensors located within the shoulder and elbow, respectively[353]. In the lower limbs, however, the Achilles tendon and *plantar fascia* from the heel, the patellar tendon from the knee and the *tibialis posterior* tendon from the ankle are the mostly affected areas[354]. It has been frequently described that tendinopathic disorders commonly affect workers with physically demanding professions and athletes due to heavy and repetitive loading of specific tendons required for mechanical activities[355]. However, recent studies have also focused on the high prevalence among patients with genetic predisposition, concomitant pathologies, such as metabolic and rheumatic disorders, as well with the excessive use of drugs like fluoroquinolone antibiotics or corticosteroids[356].
Tendon-related disorders commonly own higher prevalence ratios between athletes and workers in comparison with general population[357–359]. However, the incidence of tendinopathic disorders like lower limb tendinopathies among the general population correspond to 10.52 per 1,000 person and year, surpassing other musculoskeletal diseases, such as osteoarthritis[360,361]. As most musculoskeletal diseases, tendinopathies cause a considerably negative impact in the quality of life, including mental health, sport participation, social interactivity and work productivity[355]. Despite the recent surgical and therapeutical advances, the healing process of tendinopathic disorders requires prolonged recovery periods in order to

partially restore the initial mechanical properties of the tissue[362]. Therefore, tendon-related disorders have a significant impact on numerous healthcare systems due to the combination of high prevalence levels among the population and high costs associated with specific diagnosis, potential surgery procedures and planification of recovery training sessions[363].

2.4.1 Tendon structure and physiology

Tendon structure is based on a multi-unit hierarchical matrix predominantly formed by collagen, which is organized as fibrils and fascicles parallelly assembled following the tissue axis and immersed in a highly complex matrix[364] (**Figure 8**). Collagen hierarchical alignment along the tendon longitudinal axis is based on a series of repeated small units surrounded by a less fibrous matrix known as ground substance[365]. Collagen molecules are longitudinally organized and separated from each other by 40 nm following a quarter stagger conformation[366]. The structure is organized in clusters of five molecules attached to each other by intermolecular bonds forming pentafibrils, which are arranged as bound fibrils with diameter values that differ from 10 to 500 nm[364]. The hierarchical structure is followed by the association of fibrils in fibres and fascicles, which remain the largest subunit of the tissue, which can be covered by an additional section of connective tissue known as the interfascicular matrix that holds different fascicles together[367]. As a result of this highly anisotropic structure and the ability of fibres to stretch by extension and interfibrillar shearing, tendons are capable of withstanding the necessary uniaxial tensile strain forces[368].

Among the different types of collagen molecules, collagen type I is a fibrillar molecule that conforms most of the hierarchical tendon structure, since the 90% of the total collagen content corresponds to type I[369,370]. The tissue structure is also comprised of other fibrillar collagen types such as types III, V and XI. Collagen type III constitutes the second most predominant type, since it represents the 10% of the total collagen content. Type III is mostly localized at the interfascicular matrix and, despite its role is not still fully understood, it has been described to be responsible for the regulation of type I fibrils size[371,372]. Another significant fibrillar collagen type is type V, which is considered to be involved in the process of fibrillogenesis and is located at the centre of collagen I fibrils[373]. Other non-fibrillar collagen types are types VI, located at the pericellular matrix, and types XII and XIV, which are responsible for the molecular connections between type I and other biomolecules[374].

The described hierarchical structure is immersed in a highly complex ECM highly rich in water, specifically around 55-70% of the tendon wet weight[364]. The tendon ECM contains a considerable variety of proteoglycans, such as decorin, with highly important structural properties for the tissue due to their role promoting the sliding movement between collagen fibrils or the lubrication of the tissue[375]. Overall, the ECM is responsible for the maintenance of the tendon morphology and serves as the suitable substrate for cell adhesion, growth and differentiation.

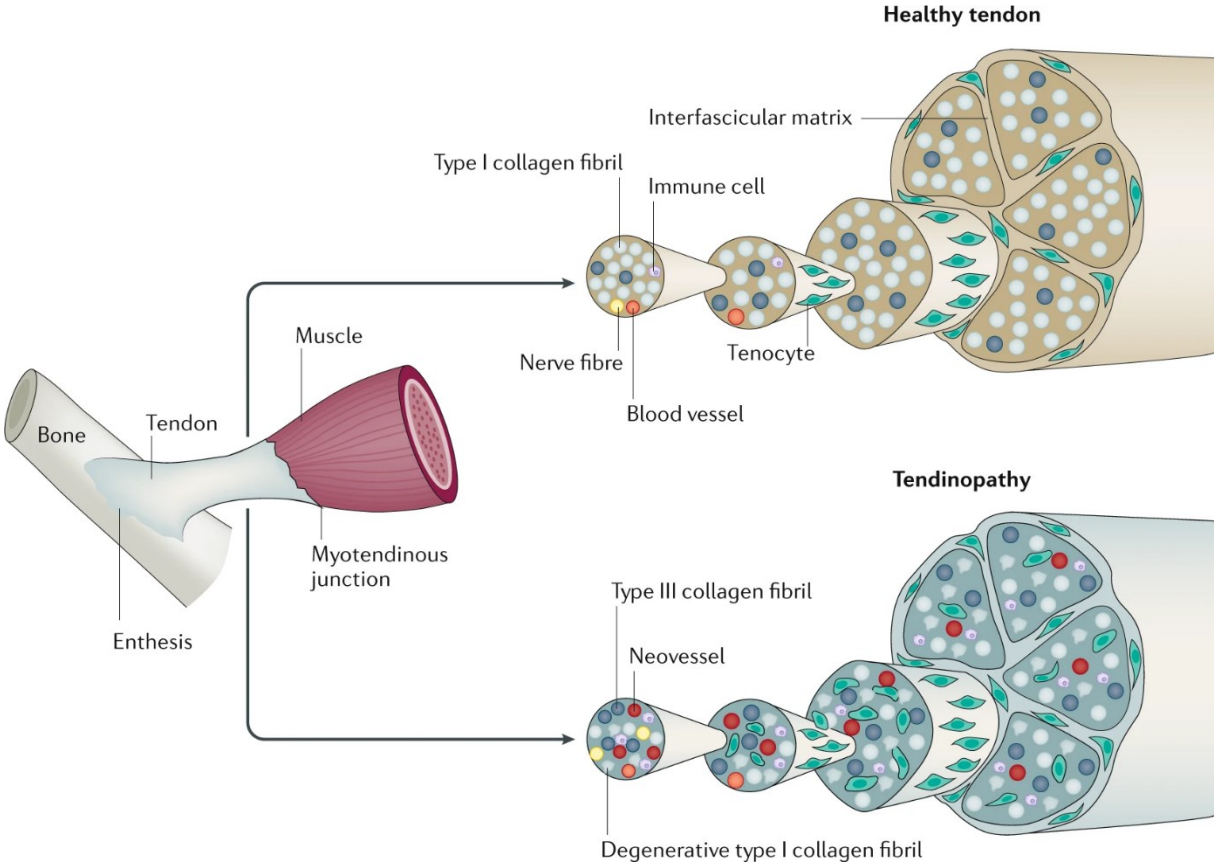


Figure 8. Tendon structural changes in tendinopathy. Non-affected tendon tissue is characterized by an organized ECM structure formed by parallelly oriented collagen fibrils, mainly formed by collagen type I, as well as proteoglycans and glycosaminoglycans. Tendinopathic tissue experiences a drastic change in the ECM structure with an increase in the number of collagen type III fibrils, disorganized collagen type I fibrils degeneration, neovascularization, neoinnervation, infiltration of inflammatory cells and glycosaminoglycans accumulation. Image reprinted with permission from ref[354]; Copyright © (2021) Springer Group.

2.4.2 Tenocytes and tendon progenitor stem cells

The highly complex ECM from tendon tissue is synthesized by the different types of cellular lineages that form tendons. From the total cell populations, the majority of cells constitute tenocytes and tenoblasts[376]. Tenocytes remain mature tendon cells that are anchored to the middle section of the primary fibre bundles along the tendon structure[377]. Their main properties include spindle shape with elongated nuclei, considerable number of free ribosomes, low concentration of pinocytotic vesicles and reduced amount of mitochondria[378]. On the contrary, tenoblasts are immature spindle-shaped cells located in the periphery of the primary fibre bundles[379]. Tenoblasts are characterized by their round shape with ovoid nuclei, low number mitochondria and a high concentration of pinocytotic vesicles[378]. Both types of cells are known to express specific tendon differentiation markers, including collagen type I, scleraxis, thrombospondin-4, tenomodulin and tenascin-C, among others[380]. These two predominant types of cells coexist with a minority of different cell types, which include immune cells, nerve cells and chondrocytes, predominantly located at the interfascicular matrix and the intersection with other tissues such as bone[8]. Moreover, tendon tissue has been characterized to also host a highly distinct type of stem cells known as tendon stem-progenitor cells (TSPCs).

TSPCs have been identified as distinctive cell populations with self-renewing and clonal properties, as well as the potential to differentiate into multiple types of cells[381]. TSPCs have been described to reside in particular tendon locations particularly enriched with two predominant proteoglycans, biglycan (Bgn) and fibromodulin (Fmod)[380]. TSPCs were initially identified by Bi *et al.* in murine patellar tendon samples, but several studies have been able to isolate different populations from tendon samples of other species and other anatomical sites, including *supraspinatus* and Achilles tendon[382]. Their proliferation rate is significantly faster in comparison with tenocytes and their morphology has been described to differ between spindle-type, convex-type and even rounded, depending on the source site and specie[376]. In comparison with tenocytes, TSPCs own slightly smaller cell sizes but considerably bigger nucleus. It has been described that human TSPCs express common markers in comparison with bone marrow-derived mesenchymal stem cells (BMSCs), including CD90, CD44, CD146 and Stro-I[383]. Despite initial studies indicated that TSPCs may predominantly reside within the tendon fascicles, it has also been illustrated that other subpopulations of stem cells reside within the peritendon area, with lower expression levels of certain stem cell markers, such as Sca-1 and lower tenogenic markers expression, including tenomodulin and scleraxis.[384] The peritendon-isolated stem cells showcased higher expression levels of vascular and pericyte makers, including endomyosin and CD133, as well as higher potential to differentiate into myofibroblasts[382].

Several studies have described the role that TSPCs and their interaction with ECM play in tendon homeostasis and regeneration. It has been suggested that TSPCs are partially responsible for different homeostatic tendon renewal mechanisms, since TSPCs have been described to regulate tenogenic gene expression and ECM composition based on the mechanical stimulus applied to the tissue[385–387]. TSPCs have also been identified as key mediators in tendon healing processes following their activation by the pro-inflammatory mediators[388]. In fact, TSPCs can regulate the inflammatory response by activation of the JNK and STAT3 pathways and upregulation of interleukin 10 (IL-10), an anti-inflammatory cytokine, as well as regulating the balance between metalloproteinase 3 (MMP3) and tissue inhibitor of metalloproteinase 3 (TIMP3), decreasing scar formation and fibrosis[388,389]. Other studies have described the anti-inflammatory paracrine effects exerted by TSPCS-derived exosomes, which additionally were responsible for modifying the immune inflammatory response by repolarizing the infiltrated macrophages. Specifically, studies indicate that TPSCs-derived exosomes can significantly decrease the presence of CCR7-expressing M1 phenotype macrophages and increase the CD163-expressing M2 phenotype macrophages[390].

TSPCs have also been identified as crucial agents based on their tendon lineage differentiation and their role on the production of crucial ECM components, since their differentiation potential can be activated by several growth factors and mechanical stimuli. Platelet-derived growth factor (PDGFBB), basic fibroblast growth factor (bFGF) and insulin-like growth factor-1 (IGF1) have been described to significantly increase cell proliferation, as well as collagen synthesis and ECM development[391,392]. Their effects have widely been described to remain mostly synergistic, since combination of different growth factors has shown to increase cell proliferation following a dose-dependent trend, as well as tenocyte chemotaxis, reduction of stemness markers in TSPCs and enhancement of tenogenic genes expression[391]. *In vitro* and *in vivo* studies with connective tissue growth factor (CTGF) described an increase in the recruitment of perivascular-derived TSPCs and tenogenic differentiation, since the increase in tendon expression markers and downregulation of other chondrogenic or osteogenic expression markers occurred simultaneously[393,394].

TSPCs are also responsible for the regulation of collagen type I production, fibre arrangement and reorganization of the ECM during the tissue remodelling phase[395]. This dynamic process mainly depends on the regulation of tenomodulin, a critical transcription factor. Regulation of collagen type I production and ECM regeneration is controlled by the expression of tenomodulin, as well as the expression of different metalloproteinases and their respective inhibitors[396].

2.4.3 Spectrum of tendon pathologies

Despite numerous theories, the term “tendinopathy” remains a generic term used to describe different types of clinical conditions that affect tendon tissue, either in a microscopic or macroscopic scale, and limit its functionality[397–399]. Even though that tendon-related disorders can be classified in different types of pathologies, tendinopathy remains a widely common concept.

Among the different conditions, tendinitis refers to the inflammation of tendon tissue and the subsequent activation of the innate immune system and multiple healing mechanisms[400] (**Figure 9**). Tendinitis may be originated by a wide range of factors, including repetitive and excessive mechanical loading of the tissue, causing microfractures within the tendon and triggering a series of proinflammatory phenomena[401]. However, some other factors such as genetic factors, nutrition or metabolic diseases are also correlated with changes within the ECM composition and the cell metabolism, which may trigger abnormal proinflammatory responses within the tissue[402]. Since the most common symptoms include swelling, pain and rigidity, the treatment generally aims to decrease inflammation and pain with the administration of non-steroidal anti-inflammatory drugs (NSAIDs) and minimize the tissue activity during the inflammatory stage.

On the contrary, tendinosis refers to the degeneration of the tendon tissue without the presence of a proinflammatory environment[397]. The affected tissue is characterized by an altered matrix architecture formed by a different ratio between collagen type I and type III, as well as other components (**Figure 9**). Tendinosis can be caused by multiple factors, including repetitive formation of microfractures by excessive use of the tissue, as well as incomplete tissue healing after previous injuries[403]. Macroscopically, the common white appearance of the tissue transforms into an amorphous greyish-brown structure with signs of mucoid degeneration, separation and loss of collagen fibres, neovascularization and fibrosis[403]. The pathology is histologically characterized by alteration in the composition of collagen, with an increased amount of collagen type III and a reduced presence of collagen type I, and degeneration of collagen fibres, which showcase altered orientation, loss of the transverse bands and modified length and diameter[404]. Affected tendon tissue suffers changes in the cell density, with some areas characterized by an increase in round-shaped tenocytes with high metabolic activity and some other areas with reduced number of tenocytes with pyknotic nuclei[401]. Moreover, the affected tendons show neovascularization, fibrosis, and even calcification, as well as increased production of glycosaminoglycans[403]. This combination of pathological processes is correlated with an even higher risk of injury, since the tissue degeneration can eventually lead to loss of the tissue integrity, tissue degeneration and, in many cases, partial or complete rupture of the affected tendon.

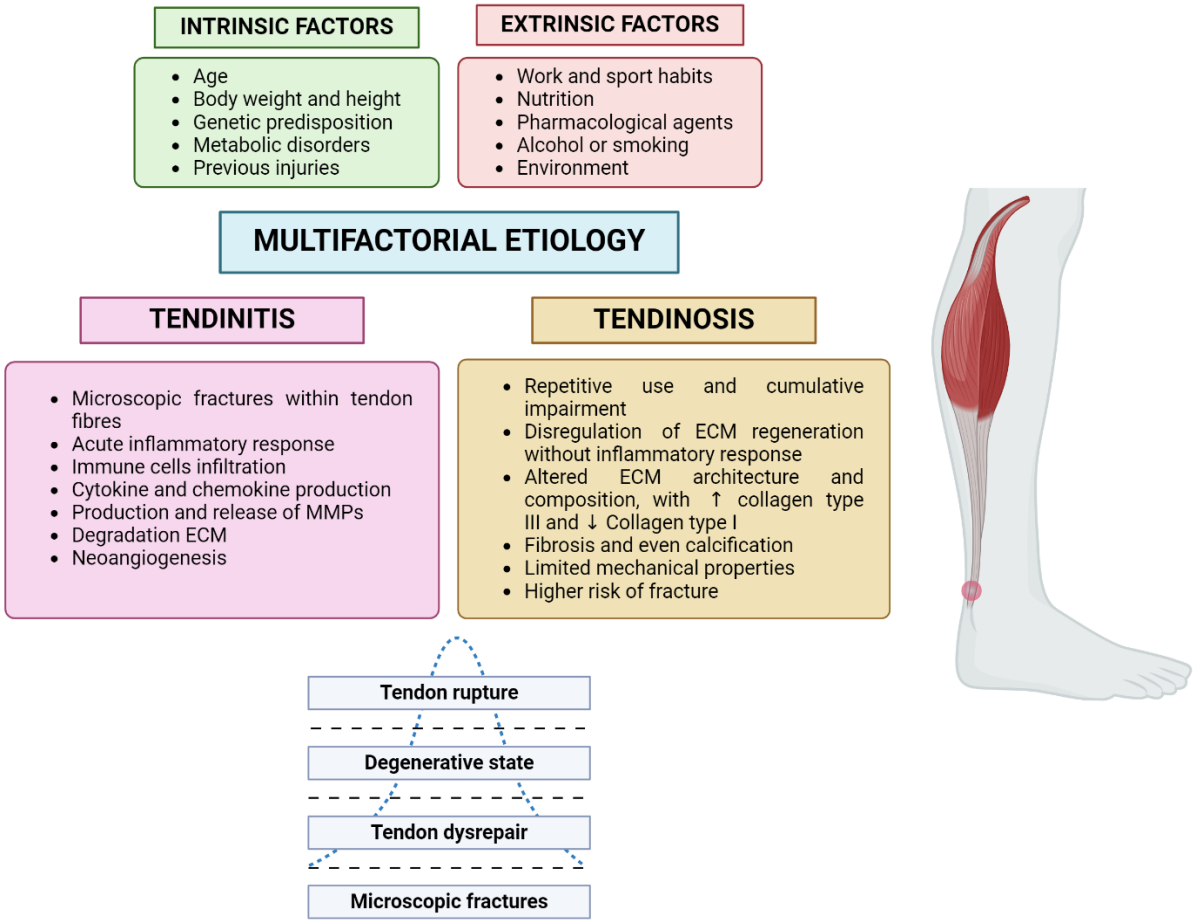


Figure 9. Classification of tendinopathic conditions. Tendinitis is characterized by the formation of microscopic fractures within tendon fibres, inducing an inflammatory response following the infiltration of immune cells, the release of proinflammatory cytokines and MMPs, further degradation of the ECM matrix and activation of fibroblasts and tenocytes, which induce angiogenesis and tissue regeneration. On the contrary, tendinosis is a non-inflammatory condition caused by a low reparation capacity of the tissue, altering the structure of the ECM matrix, increasing the ratio of collagen type III in comparison with collagen type I, inducing calcification and fibrosis of the tissue and limiting the mechanical properties of the tendon. Image created with Biorender.com.

Tendon rupture is characterized by the partial or complete ripping of tendon fibres in a localized tissue section. The condition can occur due to the application of a sudden extreme-load or mechanical force, or after the chronic weakening of the tissue due to excessive use, limiting the mechanical properties of the tissue and increasing the risk of rupture, even with application of low loads[405]. Since tendon rupture commonly induces fibrosis and the formation of scar tissue as a predominant healing mechanism, the regenerated tissue does not possess the same ECM morphology or composition. In fact, fibrotic tendons are incapable of fully withstand the same mechanical forces, which leads to a higher risk of suffering additional ruptures[406].

2.4.4 Tendon healing and remodelling

Tendon healing is described as a highly intricate process that includes three different sequential phases, including an initial inflammatory phase, followed by a proliferative stage

and a remodelling step[407]. Each phase involves a different combination of mediator cells and molecular signalling pathways (**Figure 10**).

The initial inflammatory phase is characterized by an initial responsible to the tissue injury *via* infiltration of inflammatory cells following an increase in the vascular permeability[397]. The phase initiates immediately after the injury and remains active for hours and even days, depending on the magnitude of the injury. The injured tissue initiates the inflammatory response by the expression of proinflammatory mediators such as tumour necrosis factor-alpha (TNF-α) and different types of interleukins, including IL1β and IL6, as well as oxidative stress-related agents[408]. Additionally, other neovascularization mediators like vascular endothelial growth factor (VEGF) are simultaneously released to increase the vascular permeability, allowing to increase the entry of immune cells to the affected tissue[409]. The recruited/infiltrated immune cells initially include neutrophils, followed by activation of pro-inflammatory phenotype macrophages (M1), which are responsible for the phagocytosis of cell debris and necrotic material[410]. Immune cells are responsible for the production of chemotactic and angiogenic cytokines and growth factors to not only increase the vascularization of the affected tissue, but also induce the proliferation of tenocytes and fibroblasts, which initiate the synthesis of ECM components, predominantly collagen type III[411]. In fact, fibroblasts are described to migrate from the epitenon to the injured site, whereas tenocytes from the surrounding areas detect the predominant presence of proinflammatory mediators and activate different tenogenic intracellular pathways[407].

Subsequently, the proliferation phase initiates days after the injury and occurs during weeks and even 1 or 2 months[401]. Previously recruited fibroblasts and resident tenocytes increase the synthesis of collagen, predominantly collagen type III, followed by the synthesis of other components, including proteoglycans[407]. The produced material constitutes a primitive ECM matrix substrate, since the organization and deposition of the produced material does not follow the original architecture of tendon tissue. The injured tissue remains highly vascularized and immune cells, such as macrophages, experience a phenotype switch to a pro-regenerative phenotype (M2) and the production of anti-inflammatory mediators such as transforming growth factor β1 (TGF-β1)[410]. The crossroad between degenerative and reparative inflammatory healing remains highly critical and tendon homeostasis strictly depends on the delicate balance between both types of processes.

Finally, the remodelling phase is characterized by the reorganization and remodulation of the newly formed precursor ECM matrix, replacing collagen type III fibres with collagen type I and reducing the production of ECM components and infiltrated cells[407]. Collagen fibres are reorganized and aligned following the direction of the tendon longitudinal axis and the mechanical properties of the tissue are progressively restored[405]. Previously infiltrated cells, mainly fibroblasts and macrophages, are responsible for the secretion of MMPs and the degradation of scar tissue formed by excessively produced ECM components[397]. Tenocytes are described to continue producing ECM components and supporting the reorganization of collagen type I fibres, since the remodelling stage requires a precise control of the ECM synthesis and degradation equilibrium. Tendon maturation is slowly achieved by increasing interfibrillar crosslinking among the tissue, improving its tensile strength, elasticity and mechanical resistance. Despite the intricate remodelling process, it has been described that the regenerated tendons significantly differ from the original ECM structure, organization and composition. In fact, healed tendons cannot recover the original mechanical properties of the tissue and show higher risk of suffering new injuries and even rupturing[406].

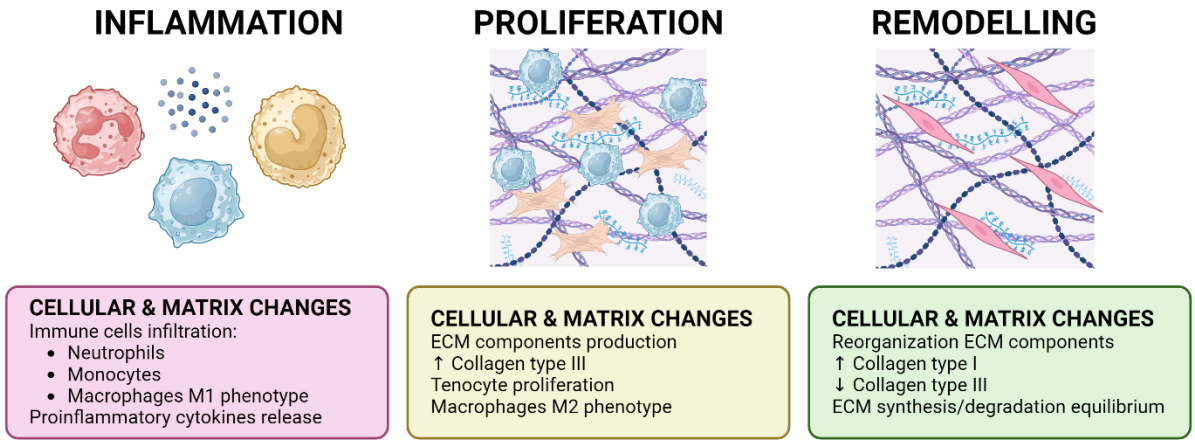


Figure 10. Tendon healing and remodelling. The process is divided into three different stages, with an initial inflammatory stage characterized by an increase in tendon vascularization, infiltration of immune cells and secretion of cytokines. During the following phase, a proliferative stage, fibroblasts migrate into the tissue and join tenocytes in the production of ECM components, forming a primitive ECM matrix. Finally, during the remodelling stage, tenocytes coordinate the reorganization of ECM and collagen fibres, as well as optimizing the balance between ECM synthesis and degradation with the assistance of both fibroblasts and macrophages. Adapted with Biorender.com with permission from ref. [412]; Copyright © (2018) Springer Group.

2.4.5 Traditional therapeutical tools and current hydrogel and nanotechnology-based approaches for local tendon delivery

Tendinopathy has traditionally been treated following different types of strategies with the aim to reduce the symptomatology. enhance tendon regeneration and improve the mechanical properties of the tissue. Possible treatment strategies include conventional therapies, which include passive administration of therapeutics or physiotherapy-based activities, as well as surgical interventions[11].

Conventional therapies generally include the combination of different types of approaches. Physiotherapy and exercise-based activities are some of the most common methods, since they can be easily individualized depending on the specific characteristics of the affected individual and the specific type of tendon injury and location[413–415]. Studies suggest that tendon loading isometric exercises can provide an acute analgesic effect and partially reinforce the tissue mechanical response[416]. However, the treatment of tendon-related disorders frequently requires the combinatory use of different approaches, including different types of therapeutics. Oral administration of non-steroidal anti-inflammatory drugs (NSAIDs) is considered a common initial option for the treatment of pain and inflammatory symptomatology, but its limited tissue-specific delivery and frequent adverse effects after its long-term use remain major disadvantages[417]. Local administration of corticosteroids remains another traditional approach for the treatment of pain and inflammation, even though research has highlighted that repeated administration of corticosteroids can affect the tendon regenerative process and increase the risk of new injuries and even ruptures[418,419]. Other non-invasive therapeutic options include therapeutic ultrasonography, low-level laser therapy and extracorporeal shockwave therapy[8].

Cellular-based therapies have recently been discussed as a potential alternative following the administration of progenitor/stem cells or autologous tenocytes. The performed pilot studies

via the administration of BMSCs or adipose-derived mesenchymal stem cells (ADSCs) were correlated with improvements in the mechanical properties of the affected tissue, as well as the administration of autologous tenocytes[420,421]. However, cell-based therapies require more extensive studies to assess their efficacy and safety, since the direct use of stem cells as therapeutical agents is correlated with significant risks. Local injection of platelet-rich plasma (PRP) has also been studied as a cell-derived therapeutical tool. Its preparation derives from the degranulation of autologous blood concentrate, allowing to achieve an autologous cocktail with different types of growth factors[422]. Despite being widely studied for the treatment of different types of tendinopathies, the efficacy of PRP injection has not been clearly demonstrated[423–425].

Surgical intervention of ruptured tendon is another common approach, usually in combination with other therapies. Surgical procedures are performed following the removal of the damaged tendon and adhesions surrounding the tissue, the decompression of the affected tissue or the grafting of the affected tendon with either autograft or allograft samples[417]. Surgical interventions have been optimized to be as minimally invasive as possible following the application of image techniques and arthroscopy-based procedures[426].

During the past decade, numerous studies have showcased the numerous benefits correlated, not only with the use of stem cells-based therapies, but following the study of stem cells-derived secreted biomolecules, including EVs or their conditioned medium, highly rich in growth factors, cytokines and nucleic acids[427,428]. Specifically, hMSCs have been extensively used for the isolation of their secretome and EVs. The hMSCs do not generally raise specific ethical concerns usually associated with other types of stem cells because they can be obtained from different source tissues, including bone marrow or adipose tissue[429–431]. Moreover, hMSC-derived biomolecules possess immunomodulatory and pro-regenerative properties, as it has been described in numerous studies[432,433]. Lui *et al.* studied the applicability of ADSCs-derived EVs in tendinopathy, proving that the obtained EVs were responsible for increasing both proliferation and migration of TSPCs, as well as increasing the protein expression of tenogenic markers such as tenomodulin, collagen type I and scleraxis[434]. Moreover, ADSCs-EVs exerted immunomodulatory properties, increasing the presence of M2 phenotype macrophages, and improved the collagen fibre structure of the regenerating tissue[434]. Chen *et al.* reported that BSMCs-derived EVs owned a remarkable immunomodulatory potential, increasing the percentage of M2 phenotype macrophages and the expression of M2 markers[435]. Moreover, the administration of EVs improved the mechanical properties of ACL tendon healing, increasing the stiffness of the tissue and improving the interface between tendon and bone[435]. hMSCs-derived EVs have also been studied in combination with different types of biomaterials, including fibrillar scaffolds and hydrogels. Ao *et al.* developed a fibrin hydrogel formulation for the encapsulation and controlled release of BSMCs-EVs[436]. The formulation, which was studied in an *in vivo* rat patellar tendon injury model, was responsible for increasing the production of collagen type I and its deposition within the ECM matrix, enhancing the expression of tendon-related markers and improving mechanical properties such as the modulus and stress at failure[436]. Additionally, the administration of the developed system was correlated with an increase in the proliferation of TSPCs during the early phase of the healing process[436]. Yin *et al.* similarly encapsulated ADSC-EVs in a collagen-based hydrogel and studied its effect in an *in vivo* rat rotator cuff tendon injury model[437]. The developed system was correlated with higher ECM collagen fibres alignment, upregulation of tendon-associated markers such as tenascin-C and tenomodulin and improved maximum tensile forces after the injury[437].

Several studies have also focused on the use of other types of stem cells, including amniotic epithelial stem cells (AECs). AECs are perinatal stem cells isolated from the innermost section of the placenta and have gained special attention due to their similar characteristics in comparison with hMSCs and their multilineage differentiation abilities[438]. Moreover, they are extensively available, have reduced ethical issues in comparison with the majority of stem cells and, importantly, have no risk of tumorigenicity, which remains a major concern with many other types of cells[439]. AECs have been described to possess significant immunomodulatory and anti-inflammatory properties, making them ideal candidates for the isolation of potentially therapeutic biomolecules with pro-tenogenic differentiation properties[440]. Barboni *et al.* developed a tendon biomimetic 3D *in vitro* system based on a polymeric scaffold structure engineered with ovine AECs and characterized their produced conditioned media[441]. The isolated conditioned medium produced by engineered AECs exerted a significant immunosuppressive effect in *in vitro* studies, inhibiting the proliferation of peripheral blood mononuclear cells (PBMCs) and exerting a pro-tenogenic paracrine effect to non-engineered AECs cultures[441]. Exposition to the conditioned medium was responsible for inducing a tendon-like elongated morphology, increasing the expression of tendon related genes and enhancing the production of tendon markers, such as tenomodulin[441]. Lim *et al.* studied the properties of human AECs-EVs as immunomodulatory and antifibrotic therapeutic tools[442]. Specifically, AECs-EVs increased the percentage of M2 phenotype macrophages, reduced the M1 phenotype and suppressed the proliferation of T cells[442].

Other novel therapeutic strategies for the treatment of tendinopathies have been proposed following the development of novel drug delivery technology. The design of new NPs and hydrogel-based tools allows to encapsulate different types of cargos, including small molecules, biological drugs and even living cells, in a stable and protective system. Therefore, local controlled delivery of specific therapeutics aims to reduce the initial inflammatory stage of the pathology and enhance tendon regeneration improving the mechanical properties of the healed tissue. Different approaches have focused on the use of NPs-based formulations produced with different materials, including lipid-based NPs and synthetic polymeric NPs, encapsulated within polymeric hydrogels, hydrogel microspheres and scaffolds.

Different studies have focused on the use of LNPs for the delivery of nucleic acids as a potential therapeutical approach for the treatment of tendinopathies. **Table 4** summarizes different novel approaches based on the application of different NPs-based and hydrogels-based systems for the treatment of tendinopathic disorders.

Table 4. Summary of relevant delivery systems developed for the treatment of tendinopathic disorder, including their loaded cargo, production method and effect.

Type of system	Cargo	Technique	Therapeutic effect	Ref.
LNPs	▪ SMAD3 siRNA and collagen type I mRNA	▪ Microfluidics	*In vitro* studies: ▪ Significant silencing SMAD3 and TGFβ1 ▪ Increase BMP2 expression and collagen type I production ▪ Dual antifibrotic and pro-regenerative effect	443
LNPs encapsulated in nanofibres	▪ miR29a	▪ Microfluidics production of LNPs and electrospinning fabrication of nanofibres	*In vitro* studies: ▪ Decrease of collagen type III production and nuclear translocation of NF-κB ▪ Immunomodulatory effect: increase in M2 phenotype macrophages. *In vivo* studies: ▪ Accelerated recovery of Achilles tendon rupture. ▪ Improved mechanical properties. Reduction of inflammatory cells infiltration.	444
Lactoferrin-immobilized and heparin-anchored PLGA NPs	▪ No inner cargo	▪ Single emulsion solvent evaporation	*In vitro* studies: ▪ Lactoferrin sustained release over 28 days ▪ Anti-inflammatory effects in cultured tenocytes *In vivo* studies: ▪ Reduced gene expression of COX-2, IL-1β, IL-6, TNF-α. Increased gene expression of IL-4 and IL-10 ▪ Improved collagen matrix organization ▪ Superior tissue stiffness and tensile strength	445
PLGA NPs coated in polydopamine-functionalized sutures	▪ VEGF and bFGF	▪ Double emulsion solvent evaporation	*In vitro* studies: ▪ Controlled release of both cargos for more than 30 days *In vivo* studies: ▪ Improved tendon gliding excursion and higher strength ▪ Reduced adhesion formation	446
PLGA NPs in HA/DBCO-PEG-DBCO hydrogels	▪ Metformin	▪ Double emulsion solvent evaporation	*In vitro* studies: ▪ Metformin prolonged release over 21 days ▪ Suppression of TGF-β1-induced cell proliferation *In vivo* studies: ▪ Reduction of tissue adhesion ▪ Improved tendon gliding ▪ Decrease of fibrotic markers	447

Polydopamine-functionalized gelatin MPs	▪ Human exfoliated deciduous teeth stem cells (HEDSCs)	▪ Single emulsion solvent evaporation	*In vitro* studies: ▪ Increase in the gene expression of pluripotency markers *Sox2* and *Oct4* ▪ Reduction DNA damage responses and ROS accumulation ▪ Upregulation tenogenic markers *In vivo* studies: ▪ Enhanced regeneration ECM matrix with an increase of aligned collagen type I fibres. ▪ Reduced infiltration inflammatory cells ▪ Decreased expression of chondrogenic markers	448
Dopamine-functionalized methacrylate gelatin MPs	▪ Hepatocyte growth factor (HGF)	▪ Microfluidics	*In vitro* studies: ▪ HGF sustained release over 28 days ▪ Anti-inflammatory and antioxidant effect in H_2O_2-induced tenocytes with a significant decrease of intracellular ROS *In vivo* studies: ▪ Reduction of inflammatory cells infiltration and pro-inflammatory cytokines	449
PAMAM dendrimers encapsulated in gelatin-methacryloyl MPs immersed in an HA hydrogel and PCL nanofibres	▪ SMAD3 siRNA	▪ Microfluidics for the preparation of LNPs and MPs, electrospinning for the fabrication of nanofibres	*In vitro* studies: ▪ SMAD3 knockout efficiency of 75% ▪ NPs responsive release after MMP-2-mediated degradation of MPs ▪ siRNA prolonged release *In vivo* studies: ▪ Reduction of peritendinous adhesion tissue formation ▪ Unidirectional release of siRNA NPs toward peritendinous tissue for selective transfection of fibroblasts	450

Abbreviations: bFGF: basic fibroblast growth factor; **BMP2:** bone morphogenic protein 2; **COX-2:** cyclooxygenase 2; **DBCO:** dibenzocyclooctyne; **ECM:** extracellular matrix; **HA:** hyaluronic acid; **HEDSCs**: human exfoliated deciduous teeth stem cells; **HGF:** hepatocyte growth; **IL:** interleukin; **LNPs:** lipid nanoparticles; **MMP-2:** matrix metallopeptidase 2; **mRNA:** messenger RNA; **miR29a:** microRNA 29a; **MPs:** microspheres; **NF-Kb:** nuclear factor kappa B subunit; **NPs:** Nanoparticles; **PEG:** poly(ethylene glycol); **PLGA:** poly(lactic-co-glycolic acid); **ROS:** reactive oxygen species; **siRNA:** small interfering RNA; **SMAD3:** Mothers against decapentaplegic homolog 3; **TGFβ1:** transforming growth factor beta; **TNF-α:** tumour necrosis factor alpha; **VEGF:** vascular endothelial growth factor.

3 Aims of the study

The pharmacological treatment of tendon-related disorders mainly focuses on the symptomatic relief of pain and inflammatory symptomatology, since no therapeutical tools capable of switching the inflammatory state and supporting the regeneration and restitution of the original ECM are used. Novel drug delivery-based technologies remain a promising alternative for the development of novel drug formulations designed to support tendon regeneration by the delivery of multiple biologically complex cargos, such as nucleic acids or stem cells-derived conditioned media. Hence, the main aim of this dissertation was to develop diverse hydrogel formulations and nanosystems as potential therapeutical tools for tissue engineering and the treatment of different tendinopathy-related conditions. First, a polymeric hydrogel MPs-based system was developed as a potential drug vehicle and cell encapsulation system. Subsequently, the system was optimized with different precursor polymers for the encapsulation and controlled release of a complex biological conditioned medium, followed by the study of its immunomodulatory potential. Finally, extracellular vesicles were engineered in combination with LNPs to develop a hybrid nanosystem for the delivery of collagen type I mRNA in pathological TSPCs as a potential pro-regenerative approach.

More specifically, the objectives of the present study were:

1. To produce and optimize an *in situ* gellable iEDDA-crosslinked PEG hydrogel MPs-based system *via* microfluidics, to characterize its physicochemical properties and study its potential use for the encapsulation of complex biological cargos, such as proteins and living cells, as a promising therapeutical tool (**I**).

2. To develop an adapted *in situ* gellable iEDDA-crosslinked HA and PEG hydrogel system functionalized with heparin for the encapsulation and sustained release of AECs-derived conditioned medium and to evaluate the immunomodulatory potential of the system (**II**).

3. To produce hMSC-EVs derived hybrid lipid NPs (MSC-Hyb) using a microfluidic-sonication technique, to characterize the hybrid nature of the system and to assess its potential as a mRNA delivery nanosystem for the delivery of collagen type I mRNA in pathological human TSPCs (**III**).

4 Experimental

This section summarizes the experimental methods used for the studies described in the thesis. The detailed description of the material and methods can be found in the original publications (**I–III**).

4.1 Hydrogels and nanoparticles production

4.1.1 Polymers functionalization and hydrogel formation (I-II)

The 4-arm PEG-tetrazine (PEG-Tz) was obtained following the 4-arm 20 kDa PEG-amine functionalization with Tz-COOH previously described by Anseth. *et al.* [451,452] with some modifications. Briefly, 100 mg of 4-arm 20 kDa PEG-amine (0.005 mmol which correspond to 0.02 mmol-NH_2) were dissolved in 5 mL of N-methyl-2-pyrrolidinone (NMP) and mixed with triethylamine (2× to -NH_2, 0.04 mmol) in a dry and argon-purged round-bottom flask under argon atmosphere during 15 min. Separately, Tz-COOH (2.5× to -NH_2, 0.05 mmol) were dissolved in NMP and reacted with O-(Benzotriazol-1-yl)-N,N,N',N'-tetramethyluronium hexafluorophosphate (HBTU, 2.5× to -NH_2, 0.05 mmol) under argon atmosphere during 5 min. Subsequently, the activated Tz-COOH was added to the initial PEG-amine mixture and the functionalization was conducted during 15 h at room temperature under argon atmosphere. The obtained product was precipitated in 10-fold volume excess of cold diethyl ether (-20 ºC), centrifuged, dried overnight under vacuum, dialyzed against ultrapure water for 48 h and lyophilized. PEG-TZ was additionally functionalized with heparin (PEG-TZ-HEP), following the previously described protocol[453]. Briefly, heparin was mixed with N-hydroxysuccinimide (NHS) and N-(3-Dimethylaminopropyl)-N-ethylcarbodiimide (EDC) in MilliQ-water following a 2:1 molar ratio between EDC and NHS and a 5:1 molar excess of EDC in comparison to the amount of heparin carboxylic groups. The mixture was kept on ice (4 °C) during 15 min to activate the heparin carboxylic groups. Subsequently, PEG-TZ was dissolved in MilliQ-water at 4 °C and added to the previously activated heparin solution following a molar ratio of 0.25:1 heparin to PEG-TZ. The functionalization was conducted overnight at 4 °C and the obtained product was dialyzed against ultrapure water for 48 h and lyophilized.

PEG-norbornene (PEG-Nb) was obtained following the 6 kDa PEG functionalization with 5-norbornene-2-carboxylic acid previously described by Alge *et al*[452] with some modifications. Firstly, 5 g 6 kDa PEG (0.83 mmol, 0.83 mmol -OH) dissolved in 15 mL anhydrous dichloromethane and added in a dry and argon purged round-bottom flask with 4-(dimethylamino) pyridine (0.5x to -OH, 0.4167 mmol) and pyridine (5x to -OH, 4.17 mmol). Separately, 5-norbornene-2-carboxylic acid (10 COOH :1 -OH, 8.33 mmol) was dissolved in 10 mL anhydrous dichloromethane in another dry and argon purged vessel and mixed with diisopropylcarbodiimide (0.5x to Nb, 4.17 mmol) during 45 min at room temperature under argon atmosphere to obtain dinorbornene anhydride. The obtained product was filtered to remove the resultant urea salts and, subsequently, added to the original mixture containing PEG. The functionalization was conducted overnight at room temperature and under argon atmosphere. The obtained product was precipitated in 10-fold volume excess of cold diethyl ether (-20 ºC), centrifuged, dried overnight under vacuum, dialyzed against ultrapure water for 48 h and lyophilized. HA was similarly functionalized with 5-norbornene-2-carboxylic acid to obtain HA-norbornene (HA-NB), following the protocol described by Feng *et al.*[454] with some modifications. Firstly, 1 g HA (0.05 mmol which correspond to 0.2 mmol -OH) was dissolved in 10 mL deionized water at room temperature under constant stirring. After its complete

dissolution, 5 mL dimethylformamide (DMF) were slowly added, and the pH of the solution was adjusted to 10 by 5 M sodium hydroxide (NaOH) solution. In another dry and argon purged vessel, 5-Norbornene-2-carboxylic acid (1:1 to -OH) was dissolved in 5 mL DMF and mixed with diisopropylcarbodiimide (0.5:1 M to 5-Norbornene-2-carboxylic acid) during 1 h at room temperature under argon atmosphere to obtain dinorbornene anhydride. The obtained product was filtered to remove the resultant urea salts. Subsequently, dinorbornene anhydride was added dropwise to the HA solution maintaining the pH of the solution at 10. The functionalization was conducted overnight at 4ºC. The obtained product was three time precipitated in 10-fold volume excess of cold ethanol-DMF (1:1 v/v) and centrifuged. Afterwards, the product was dialyzed against ultrapure water for 48 h and lyophilized. All the obtained polymers were dissolved in deuterated dimethyl sulfoxide-d_6 (DMSO) and characterized by proton nuclear magnetic resonance (^{1}H-NMR) to study the performed functionalization with an Ascend 400 MHz NMR spectrometer (Bruker, Switzerland). The functionalization degree of the polymers was calculated based on the area associated with specific protons of the added moieties. Bulk hydrogels were prepared at different concentrations of different polymers maintaining a 1:1 ratio between the two reactive groups following the previously estimated modification degrees. Each polymer was dissolved in Milli-Q water and, subsequently, both precursor polymers were briefly mixed and left to crosslink during a few minutes.

4.1.2 Hydrogel microspheres production (I)

MPs were fabricated by single emulsion in a glass capillary microfluidics chip with co-flow geometry. The design of the microfluidic system consisted in two different glass capillaries aligned in a co-flow geometry. Firstly, the inner glass capillary (outer diameter 1.00 mm; 1B100-6, World Precision Instruments, USA) was shaped using a micropipette puller (P-97, Sutter Instrument, USA) and accurately sanded obtaining a final inner diameter of approximately 100 µm. The inner capillary was introduced into an outer glass capillary (with an inner diameter of 1.10 mm; T150-6, World Precision Instruments, USA) and coaxially aligned.

For the preparation of the microspheres, different polymer concentrations were studied without modifying the 1:1 ratio between the two reactive groups based on the obtained modification degrees. Firstly, different aqueous inner phases were prepared with each of the two precursor polymers. 10% (w/v) PEG-Tz in 1× phosphate buffer solution (PBS, pH 7.4) and 13.5% (w/v) PEG-NB in 1× PBS precursor solutions were connected to a T-junction capillary, which was connected to the inner capillary of the glass microfluidics chip. Meanwhile a paraffin oil 1% Span 80 solution was injected from the outer glass capillary, both precursor solutions were simultaneously mixed and injected through the inner glass capillary. A 3D coaxial flow was obtained thanks to the injection of both phases in the same direction. Flow rates for both inner phases were set at 200 µL/h, meanwhile the outer phase was injected at 20 mL/h. The spherically shaped droplets of polymer precursors immersed in an oil outer phase were recollected from the microfluidics platform into a recollection bath under 50 rpm shaking for their crosslinking. Subsequently, MPs were centrifuged at 95 g (Hettich EBA 21, Germany) for 5 min, the oil and surfactant traces were aspirated, and the remaining MPs were immersed in 1× PBS. This washing and centrifuging procedure was repeated thrice to ensure the complete removal of oil and surfactant traces. Finally, the obtained MPs were stored at 4 ºC until further use.

4.1.3 Hybrid nanoparticles production (III)

Empty and mRNA-loaded LNPs were prepared by NanoGenerator Flex (Precigenome LLC San Jose, CA, USA) using a staggered herringbone micromixer chip (Precigenome LLC San Jose, CA, USA). The organic phase consisted in lipid mixture formed by ALC-0315:DSPC:cholesterol:ALC-0159 dissolved in ethanol at a 0.5:0.1:0.385:0.015 molar ratio. mRNA loading was performed by preparing an aqueous phase with eGFP mRNA or COL 1A1 mRNA immersed in 0.1 M citrate buffer (pH 5), following a N:P ratio of 15:1. Empty and mRNA-loaded MSC-Hyb were prepared with a similar protocol with some additional steps. In this case, EVs from hMSC were resuspended and added to the aqueous phase following weight ratios between EVs and total lipid weight of 1:100, respectively.
For the preparation of both types of formulations, both precursor solutions were injected into the chip at a 4 mL/min total flow rate maintaining a 3:1 ratio between the aqueous and the organic phase. Meanwhile, the chip was immersed in a sonication bath under 30 Hz and 50 W at 4 ºC. The combination of sonication with microfluidics has been described as a suitable method to disrupt their lipidic structure and subsequently reassemble in the presence of additionally added synthetic lipids to form a hybrid structure combining materials from both origins. The obtained LNPs and MSC-Hyb were dialyzed overnight at 4 ºC using 10 kDa Slide-A-Lyzer dialysis cassettes immersed in PBS 1× to change the pH to 7.4 and separate the non-capsulated mRNA.

4.2 Physicochemical characterization

4.2.1 Morphological and physicochemical evaluation: Scanning electron microscopy (SEM) and Fourier-transform infrared spectroscopy (FTIR) (I-II)

Fourier transform infrared (ATR-FTIR) spectroscopy (Bruker Vertex 70, Bruker, USA) was used to study the hydrogels' structure. Dried hydrogels were studied in the range of 3500-500 cm^{-1} with a resolution of 2 cm^{-1} and FTIR spectra were recorded using OPUS 8.1 software.
Scanning electron microscopy (SEM Quanta FEG 250, FEI, USA) was used to study the inner structure of the hydrogel MPs at an accelerating voltage of 5.0 kV. Samples were previously immersed in cryostat embedding medium and frozen in liquid nitrogen. Samples were sectioned in 15 µm thin segments (Leica Cryostat CM1950, Leica Biosystems, Germany), which were placed over a silica substrate, dried overnight under vacuum at room temperature, and coated with a 10 nm platinum layer.

4.2.2 Rheological studies (I-II)

The hydrogel systems were characterized in terms of rheological properties using a TA Instruments DHR-2rheometer (TA Instruments, USA), with a 20 mm diameter stainless steel plate-and-plate geometry (parallel plate). Previously, gels were prepared and immersed in PBS at 37 ºC overnight before being loaded into the lower plate. Subsequently, strain sweep measurements were conducted with a gradual strain variation from 0.1% to 1000% and frequency values at 25 ºC and 1 Hz. Subsequently, frequency sweep measurements were performed modifying the applied oscillatory frequency from 20 to 0.1 rad/s meanwhile the strain was maintained at 1% following the linear viscoelastic range and the temperature was maintained at 25 ºC. Moreover, time sweep measurements were conducted with both precursor polymer solutions quickly mixed and injected above the lower plate, allowing the gel to cure. Therefore, the variation of G' and G'' was monitored under constant strain, angular frequency and temperature values of 1%, 1 Hz and 25 ºC, respectively.

4.2.3 Swelling studies (I-II)

The swelling index of the hydrogels was determined after immersing dried hydrogels in 1× PBS at 37 ºC. The swelling index was calculated at specific timepoints following two different methodologies, either by determining the diameter of disc-shaped hydrogels or hydrogel MPs using optical microscopy (Nikon SMZ645, Japan) and software analysis (ImageJ software) and subsequently calculation of the hydrogel volume, or by weighting hydrogels after carefully removing the excess of water on their surface. At each timepoint, the swelling index was calculated based on the volume following Equation (**1**):

$$\text{Swelling index (v/v)} = \frac{V - V_0}{V_0} \quad (\mathbf{1})$$

where, V corresponds to the volume of swollen hydrogels at a particular timepoint and V_0 corresponds to the volume of the dried hydrogels.

4.2.4 Dynamic light scattering (DLS), electrophoretic light scattering (ELS) and nanoparticle tracking analysis (NTA) (III)

Dynamic light scattering (DLS) was used to assess the average size (Z-average) and PDI of the developed NPs, whereas electrophoretic light scattering (ELS) was used to determine their ζ-potential using a Zetasizer Nano ZS instrument 1000HSa (Malvern Panalytical, Malvern, UK) equipped with a He-Ne laser of 633 nm and a detector angle of 173º. Samples were diluted 1:50 (v/v) with filtered (0.22 μm) Milli-Q water in disposable polystyrene cuvettes in triplicate to determine the size and PDI. Samples were equally diluted in disposable folded capillary cells (DTS1070, Malvern, UK) to determine the ζ-potential. Particle size and concentration of NPs were additionally measured using NP tracking analysis (NTA) on a NanoSight NS500 (Malvern Panalytical, Malvern, UK) with a sCMOS camera. Samples were diluted 1:1000 (v/v) with filtered (0.22 μm) Milli-Q water to obtain an ideal particle per frame value (20-200 particles/frame). The following settings were set according to the manufacturer: Camera level was increased until clearly visualize particles without exceeding 20% signal saturation, which corresponded to a camera level 12. Five measurements of 1 min were performed under a cell temperature of 25 ºC and pump rate of 30 μL/min. The detection threshold was set for a maximum of 10% non-distinct particles and blue cross count was limited to a maximum of 5 per frame. Moreover, autofocus was adjusted to avoid unclear particles. The recorded videos were analyzed using NanoSight Software NTA 3.1 Build 3.1.46 with a sensitivity level of 5.dl

4.2.5 Cryo-transmission electron microscopy (Cryo-TEM) (III)

Glow-discharged electron microscopy grids, Quantifoil holey carbon R 1.2/1.3 Cu 300 mesh, were used to vitrify NPs immersed in RNAse free water using a Leica EM GP plunger. Data collection of the Cryo-EM grid screening was performed using a ThermoFisher Scientific Talos Arctica operating at 200 kV.

4.2.6 Hybridization studies: Fluorescence resonance energy transfer (FRET) and surface markers analysis (III)

The fusion process between the precursor synthetic lipids and EVs was studied using a previously described FRET-based lipid mixing assay[455,456]. In brief, LNPs and MSC-Hyb were

prepared equally containing a 1.5 molar ratio of two types of lipids conjugated with both donor fluorescent molecules, 18:1 1,2-dioleoyl-sn-glycero-3-phosphoethanolamine-N-(lissamine rhodamine B sulfonyl) ammonium salt (Rhodamine-PE), and 18:1 1,2-dioleoyl-sn-glycero-3-phospho-L-serine-N-(7-nitro-2-1,3-benzoxadiazol-4-yl) ammonium salt (NBD-PS). Activation of NBD at its excitation wavelength is followed by the transferring of energy to Rhodamine in a FRET process that mainly depends on the distance between the two fluorophores. Lipid mixing was monitored following the NBD fluorescence intensity, with excitation at 460 nm and emission at 535 nm. The addition of external agents is correlated with the dilution of both fluorophores within the lipid membrane and an increase on the distance between them, causing an increase of NBD fluorescence. Maximum NBD fluorescence intensity was measured after dissolving the obtained LNPs and MSC-Hyb in Triton X-100 1% (w/v) during 10 min at 37 ºC.

A calibration curve between the percentage of maximal NBD fluorescence and the percentage of addition of external material into the lipid structure was prepared with a series of formulations with different amounts of both conjugated lipids, simulating the effect caused by an increase in the distance between both fluorochromes. The value of the non-dissolved standard formulation with 1.5 molar ratio of both conjugated lipids, considered as minimum fluorescence intensity (FI), was subtracted from all the other values, and the change of NBD fluorescence was calculated according to Equation (**2**):

$$NBD\ fluorescence\ increase\ (\%) = \frac{[NBD\ FI - Min\ (NBD\ FI)]}{[Max\ (NBD\ FI) - Min\ (NBD\ FI)]}\ x\ 100 \qquad (\mathbf{2})$$

where, NBD FI was the fluorescence measured from a sample, Max (NBD FI) was the maximum NBD fluorescence measured after dissolving the sample in Triton X-100 1% (w/v) during 10 min at 37 ºC, and Min (NBD FI) was the minimum fluorescence intensity from the standard LNPs formulation with lowest NBD signal.

Analysis of EVs surface markers was performed using the human MACSPlex Exosome kit (Miltenyi Biotec, Bergisch-Gladbach, Germany), following the standard short protocol for tubes provided by the manufacturer. Briefly, EVs and MSC-Hybrids (10 µg of protein quantified by MicroBCA), as well as LNPs or PBS as blank control, were diluted in 120 µL of MACSPlex buffer. Samples were incubated with 15 µL capture beads (including all the antibody-coated beads) and 15 µL of detection antibody cocktail (i5 µL of each antibody type including CD9, CD63 and CD81, all conjugated to APC). Samples were mixed and incubated protected from light under agitation for 1 h at room temperature. Subsequently, samples were washed twice for 15 min using 0.5 mL MACSPlex buffer and centrifuged at 3000 g for 5 min at room temperature. Finally, samples were measured by BD LSRFortessa™ Cells Analyzer (BD Bioscience, USA) flow cytometry. The results were analyzed with FlowJo™ software v.10 (Tree Star, Inc., USA). APC mean fluorescence intensity (MFI) background values corresponding to the PBS blank control were subtracted from each APC MFI value obtained from all the samples.

4.3 Drug loading and *in vitro* drug release studies

4.3.1 Drug loading degree in hydrogel systems (I-II)

The entrapment efficiency and loading degree of the developed hydrogel systems were determined by dissolving the loaded samples in a mildly acidic phosphate buffer. After the complete degradation of the samples, the amount of drug in the supernatant was determined. The total protein content was determined using micro-BCA protein assay (Thermo Fisher, USA)

(**I-II**) and vascular endothelial growth factor (VEGF) and amphiregulin (AREG) (**II**) were determined using specific ELISA assays (ThermoFisher, USA; MyBiosource, USA) respectively, following manufacturer's instructions.
The entrapment efficiency (EE) and loading degree (LD) values were calculated according to Equations (**3**) and (**4**):

$$EE\ (\%) = \frac{Cargo\ released\ from\ the\ loaded\ hydrogel\ (\mu g)}{Initial\ amount\ of\ cargo\ (\mu g)}\ x\ 100 \quad (\mathbf{3})$$

$$LD\ (\%) = \frac{Cargo\ released\ from\ the\ loaded\ hydrogel\ (\mu g)}{Total\ mass\ of\ hydrogel\ (\mu g)}\ x\ 100 \quad (\mathbf{4})$$

4.3.2 In vitro drug release (I-II)

In vitro release studies were performed in Hank's balanced salt solution-(N-[2-hydroxyethyl]piperazine-N'-[2-ethanesulfonic acid]) (HBSS-HEPES, pH 7.4) and 2-(N-morpholino) ethanesulfonic acid (HBSS-MES (pH 5.5) (**I**) and 1× PBS (**II**). The hydrogel systems were immersed in 5 mL of medium at 37 ºC. The complete release medium was removed at specific timepoints, from 5 min to 14 days. After the complete removal of release medium at each timepoint, equal volume of fresh buffer was immediately added. Subsequently, samples obtained at each timepoint were quantified using micro-BCA protein assay and specific ELISA assays. Afterwards, the obtained data was analysed following a series of different kinetic models such as zero-order, first-order, Higuchi and Korsmeyer-Peppas models as described in Equations (**5-9**):

$$\text{Zero} - \text{order model: } \frac{\mathrm{Mt}}{\mathrm{M}\infty} = \mathrm{kt} \quad (\mathbf{5})$$

$$\text{First} - \text{order model: } \ln\left(1 - \frac{\mathrm{Mt}}{\mathrm{M}\infty}\right) = \mathrm{n}\ln\mathrm{t} + \ln\mathrm{k} \quad (\mathbf{6})$$

$$\text{Higuchi model: } \frac{\mathrm{Mt}}{\mathrm{M}\infty} = \mathrm{kt}^{1/2} \quad (\mathbf{7})$$

$$\text{Korsmeyer} - \text{Peppas model: } \ln\frac{\mathrm{Mt}}{\mathrm{M}\infty} = \mathrm{n}\ln\mathrm{t} + \ln\mathrm{k} \quad (\mathbf{8})$$

$$\text{Weibur model: } \ln\left[-\ln\left(1 - \frac{\mathrm{Mt}}{\mathrm{M}\infty}\right)\right] = \beta\ln t_d + \beta\ln\mathrm{t} \quad (\mathbf{9})$$

where, M_t/M_∞ corresponds to the proportion of protein released at time *t*; *k* corresponds to the corresponding release constant according to each specific model; *n* corresponds to the release exponent; t_d corresponds to the lag time before the drug release; *β* corresponds to a constant describing the shape of the release curve.

4.3.3 mRNA loading and quantification assay in hybrid nanoparticles (III)

The EE of the loaded LNPs and MSC-Hyb was determined by quantifying the loaded mRNA using Quant-iT RiboGreen RNA Reagent. NPs were dissolved in Triton X-100 (2%, v/v) and incubated during 10 min at 37 ºC to quantify the complexed RNA. Samples were subsequently diluted in TE buffer (1×) to obtain a final Triton X-100 concentration of 0.5%, according to the maximum concentration recommended by the manufacturer. The NPs were simultaneously dissolved in TE buffer (1×) to quantify the non-complexed RNA. The calibration curves of mRNA were prepared in Triton X-100 (0.5%, v/v) and in TE buffer (1×) within a range from 5-1000 ng/mL. The RiboGreen assay was performed following the manufacturer's protocol. The standards corresponding to the calibration curve were resuspended and subsequently 20 µL of each standard were loaded into the wells of the provided 96-well plate. Then, 180 µL of either Triton X-100 (0.5% v/v in TE buffer 1×) or TE buffer (1×) were added. Moreover, volumes

of 200 µL from the diluted samples were loaded into the wells of the provided 96-well plate, where the RiboGreen reagent was resuspended by pipetting. The plate was incubated for 10 min in the dark and the concentration of RNA was determined in Nunclon Delta Surface black 96-well plates (ThermoFisher Scientific, Waltham, MA, USA) by fluorescence measurement using a Tecan Infinite® 200 Pro microplate reader (Tecan Trading AG, Switzerland), specifically, with an excitation wavelength of 458 nm and an emission wavelength of 520 nm. The EE was calculated according to Equation (**10**):

$$EE\ (\%) = \frac{Concentration\ of\ mRNA\ quantified\ (ng\ mL^{-1})\ x\ Volume\ of\ sample\ (mL)}{Initial\ amount\ of\ mRNA\ added\ (ng)}\ x\ 100 \qquad (10)$$

4.4 *In vitro* cell studies

For the *in vitro* cell studies, the following cell types were used: human primary tenocytes, isolated from the extensor indicis proprius of a 58-years-old patient, and RAW 264.7 (American Type Culture Collection, USA) (**I**). Perypheral Blood Monocytes Cells (PBMC) isolated from the blood of anonymous healthy donors, and ovine amniotic epithelial stem cells (AEC) isolated from the amniotic membrane (AM) of three pregnant Appenninica sheep during mid-gestation (**II**). Human primary tendon progenitor stem cells (TSPC) from pathological Achilles tendon from different 43 and 51-years-old patients during surgery for the reconstruction of injured Achilles tendon, and immortalized Chinese Hamster Ovary cells (CHO) (American Type Culture Collection, USA) (**III**). RAW 264.7, PBMCs and CHO were maintained in a BB16 gas incubator (Heraeus Instruments GmbH, Germany) at 37 ºC, 5% CO_2 and 95% relative humidity. Human primary tenocytes, AECs and TPSCs were grown and maintained in an ESCO CelCulture® CO_2 incubator (ESCO Scientific), at 37 °C, 5% of CO2 and 95% relative humidity. Human primary tenocytes and TSPCs used for the *in vitro* studies in publications **I** and **III** were maintained and used between passage 2 and 5. AECs used for the obtention of the AEC-CM were used at passage 0 in publication **II**.

4.4.1 Cell lines and culture conditions (I-III)

RAW 264.7 were cultured in DMEM supplemented with 10% (v/v) fetal bovine serum (FBS), 1% (v/v) MEM non-essential amino acids (NEAA), 1% (v/v) l-glutamine and 1% (v/v) penicillin and streptomycin (PEST). Human primary tenocytes were grown and maintained in DMEM-F12 medium supplemented with 10% (v/v) FBS, 1% (v/v) PEST and 200 µM of Ascorbic acid. PBMCs were cultured in RPMI 1640 medium with 10% FBS and 1% (v/v) PEST. AECs were cultured in α-MEM, supplemented with 10% inactivated FBS, 1% L-Glutamine, 1% amphotericin B, and 1% PEST, along with 25 µM Progesterone (P4). TSPCs were cultured in in α-MEM, supplemented with 10% inactivated FBS, 1% amphotericin B, and 1% PEST. CHO cells were cultured in HAM'S F-12 supplemented with 10% FBS and 1% PEST.

4.4.2 Cell-cytocompatibility studies (I-III)

CellTiter-Glo® luminescence assay was used to assess the cytocompatibility of the developed systems based on the quantification of adenosine triphosphate (ATP) produced by the tested cells after being treated with the different systems. RAW 264.7 and human primary tenocytes were seeded in a 96-well plate following a density of 1×10^4 cells/cm^2 and let to attach overnight. Human TSPCs and CHO were seeded in a 96-well plate (Corning, USA) following a density of 5×10^3 cells/cm^2 and 1×10^4 cells/cm^2, respectively, and also let to attach overnight. Then, cells were treated with different concentrations of the tested hydrogel or NPs system, whereas cells

with Triton X-100 were used as positive control and cells with only cell medium were used as a negative control. Cells were incubated at predetermined conditions, 37ºC, 5% CO_2 and 5% relative humidity, during different times of incubation. Subsequently, cells were washed twice with HBSS-HEPES (pH 7.4) and immersed in 100 µL CellTiter-Glo®/HBSS-HEPES (1:1). Luminescence was read with a Varioskan™ LUX multimode microplate reader.

4.4.3 PBMCs activation and macrophages polarization studies (II)

The immunomodulatory properties of the AEC-CM-loaded system were evaluated by analysing the proliferation of peripheral blood mononuclear cells (PBMC). PBMCs were activated with phytohemagglutinin (PHA) at a final concentration of 10 µg/mL. A total of 2×10^5 PHA-stimulated PBMC were then plated and cultured for 72 hours and 7 days with the AEC-CM derived from immune-activated AEC (stimulated with LPS) and encapsulated within the hydrogel system. PBMC activation was measured using the CellTiter96 Aqueous One Solution Cell Proliferation Assay according to the manufacturer's instructions.
The immunomodulatory properties of AEC were further evaluated by assessing the macrophage M1 polarization towards the M2. For monocyte isolation, PBMCs were plated in each Nuclon™ Delta surface treated 35 mm petri dishes at 3×10^6 to PBMCs/mL in 2 mL and allowed to adhere in a 5% CO_2 container at 37° for 2 h. Non-adherent cells were removed by thorough washing with RPMI 1640. Adherent cells were harvested after 15 min of incubation in Accutase. For macrophage differentiation, cells were then centrifuged at 350×*g* for 5 minutes and cultured in non-treated 12 well plates at a cell density of 3×10^5 cells/mL with Macrophage serum free medium (SFM) + 10% FBS + 1% PEST enriched with 100 ng/mL of granulocyte-macrophage colony stimulating factor (GM-CSF) for 5 days. Cells were then stimulated with either 100 ng/ml LPS and 20 ng/ml IFN-γ (M1 stimulation), 40 ng/ml IL-4 and 40 ng/ml IL-13 (M2 stimulation) or remained untreated for 48 h. Furthermore, without removing the stimulus, AEC-CM-loaded hydrogels were added to M1 macrophages with a transwell set up. After 48 h of treatment, the macrophages were harvested for flow cytometry analysis by incubating in Accutase for 15 min. Cells were transferred to a V bottom 96-well plated and centrifuged at 350×*g* for 5 min. The supernatant was discarded, and the macrophages were resuspended in FC block solution and incubated for 10 minutes at room temperature. Then, the cell pellets were immunostained with APC anti-CD86 and PE anti-CD206 antibodies at a concentration of 2 µg/mL in PBS at 4°C for 30 min in the dark. Subsequently, the cells were washed twice with PBS and analysed using flow cytometry. For each group, cells without antibody staining served as the negative control. The fold change of MFI in each sample was calculated by subtracting the MFI of the unstained samples and normalizing against the negative control. All flow cytometry data were analysed using FlowJo software.

4.4.4 Cellular uptake of rhodamine-labelled hybrid nanoparticles (III)

TSPCs and CHO cells were seeded in 24-well plates at a density of 5×10^3 cells/cm^2 and 1×10^4 cells/cm^2, respectively, and left to attach overnight. Subsequently, rhodamine-labelled NPs were suspended at the following concentrations: 100 and 200 µg/mL and added to the seeded cells for 24 and 48 h. Afterwards, cells were washed with PBS, detached with trypsin-EDTA, washed twice with PBS and resuspended in 300 µL of PBS. The uptake was analysed by FACS Verse Flow Cytometer (BD FACSVerse, BD Biosciences, IT).

4.4.5 Transfection efficiency with eGFP mRNA model-loaded hybrid nanoparticles(III)

TSPCs and CHO cells were seeded in 24-well plates at a density of 5×10^3 cells/cm^2 and 1×10^4 cells/cm^2, respectively, and left to attach overnight. eGFP mRNA-loaded NPs were suspended in cell media at the following concentrations: 100 and 200 µg/mL and added to the seeded cells. Cells with only medium were used as negative control and cells with Lipofectamine RNAiMAX at the concentration suggested by the provider were used as positive control. Cells were incubated for 48 h and, afterwards, washed with PBS, detached with trypsin-EDTA, washed twice with PBS and resuspended in 300 µL of PBS. The percentage of eGFP-positive cells was measured by FACS Verse Flow Cytometer (BD FACSVerse, BD Biosciences, IT).

4.4.6 Efficacy studies with collagen I mRNA-loaded hybrid nanoparticles (III)

TSPCs were seeded in 6-well plates at a density of 5×10^3 cells/cm^2 and left to attach overnight. COL1A1 mRNA-loaded NPs and empty NPs were added at a concentration of 200 µg/mL for 48 h. Non-treated TSPCs in cell media were used as a negative control. Subsequently, cells were washed with 1× PBS, detached with trypsin-EDTA and washed twice with 1× PBS. Subsequently, Western Blotting was conducted to quantify the production of collagen type I from each sample. Protein extraction from the obtained cell pellet was conducted with RIPA Lysis and Extraction buffer 1× in combination with 1× Protease and Peptidase Inhibitor cocktail. Afterwards, samples were incubated on ice for 45 min and centrifuged at 13000×*g* for 20 min at 4 ºC. Protein lysate supernatants were collected and quantified using micro-BCA assay. A standard curve with different concentrations of bovine serum albumin (BSA) within a range between 0-200 µg/mL was prepared. Finally, protein samples were prepared by mixing 25 µg of protein with 1× Laemmli buffer and 5% 2-mercaptoethanol to obtain a final volume of 25 µL. Samples were boiled at 95 ºC for 5 min. Gel electrophoresis with 8% nitrocellulose gels was performed by loading 25 µg of each sample and running the gel for 2 h at 80 V. Proteins were transferred to a nitrocellulose membrane using a Turbo Transfer system. Blocking was performed immersing the membrane in 10% non-fat dry milk for 1 h at room temperature. Subsequently, the membrane was incubated overnight at 4 ºC under mild shaking with rabbit anti-human type I collagen antibody (Abcam, ab264074, USA) at 1:1000 in 1× PBS 5% non-fat dry milk and 0.1% Tween-20. A mouse anti-human beta Tubulin (Santa Cruz, sc166729, USA) was used as a lading control at 1:1000. Subsequently, goat anti-rabbit IgG-HRP secondary antibody and goat anti-mouse IgG-HRP (Abcam, USA) were added as secondary antibodies and incubated for 1 h at room temperature under mild shaking. Enhanced chemiluminescence assay (ECL) was used to develop the membranes using a luminescent image analyser incorporated with a CCD camera. Quantification of the mean densitometry of the obtained protein bands was performed using ImageJ. Results were normalized to the loading control and expressed as fold change respectively to the untreated samples.
Qualitative determination of collagen type I was also conducted by immunostaining. TSPCs were seeded on 13 mm^2 coverslips at a 5×10^3 cells/cm^2 and the procedure was performed according to the previously described protocol. Afterwards, cells were washed with 1× PBS, fixed with 3.7% PFA for 30 min at room temperature, permeabilized with 0.1% Triton X-100 for 5 min and blocked with 1% BSA for 1 h. Incubation with mouse monoclonal anti COL1A1 primary antibody (1:100, Sigma-Aldrich, Milan, Italy) was performed overnight at 4 ºC. Afterwards, samples were incubated with DyLight 488 horse anti-mouse IgG (1:500, BioLegend, CA, USA) antibody for 1 h at room temperature. Cell nuclei were stained with DAPI (1:1000) for 5 min. Samples were visualized and image acquisition was performed with an

inverted Leica laser-scanning confocal microscope (TCS SP5; Leica Microsystems, Wetzlar, Germany) at 63× magnification and equipped with an Apo 63X/1.4 NA oil immersion objective.

4.5 Ethical permits (I-III)

Patients involved in the study agreed with their recruitment, participation, and sample collection by signature of a informed consent, approved by the Helsinki and Uusimaa Hospital District ethics committee (HUS/2785/2020) and by the institutional review board (HUS/234/2020) (**I**) as well as the Institutional Review Board of San Giovanni di Dio e Ruggi D'Aragona Hospital (Salerno, Italy) (Review Board prot./SCCE n. 151 achieved on 29 October 2020) (**III**). PBMC cells were isolated according to the internal blood sampling licenses of the Finnish Red Cross (**II**).

4.6 Statistical analysis

Statistical analysis was performed with GraphPad Prism 10 (GraphPad Software, Inc., La Jolla, CA, USA). The experiments conducted in the described studies were performed at least in triplicate and the results correspond to the mean ± standard deviation (S.D.). Each figure includes a complete description of the statistical method used for the analysis of the presented data.

5 Results and Discussion

Drug delivery systems like hydrogels and NPs have been described as promising approaches capable of overcoming the numerous limitations correlated with conventional treatment methods in multiple fields, including the treatment of tendon-related disorders. Here, different hydrogel and NPs-based systems were developed as potential therapeutic tools for the treatment of different tendinopathy-derived conditions. In publications **I** and **II**, an *in situ* gellable iEDDA-crosslinked hydrogel formulation was developed and used for the production of macroscale hydrogels and hydrogel MPs *via* microfluidics. Both systems were characterized in terms of physicochemical properties, morphological characteristics, swelling and rheological behaviour and drug loading and release of biologically complex cargos, including AEC-derived secretome. *In vitro* studies in PBMCs and macrophages were conducted to assess the immunomodulatory activity of the secretome-loaded system. In publication **III**, an hMSC-EVs-derived hybrid nanosystem was developed as a potential mRNA delivery system. The formulation was studied in terms of physicochemical and morphological properties, hybridization degree, mRNA loading and cytocompatibility. *In vitro* efficacy studies were performed in pathological TSPCs to assess the transfection efficacy as collagen type I mRNA delivery agents.

5.1 Physicochemical characterization of bulk hydrogels and hydrogel microspheres

5.1.1 Precursor polymers functionalization and hydrogels fabrication (I-II)

In publications **I** and **II**, different synthetic and natural polymers were functionalized with the aim of adding two specific chemical moieties, tetrazine and norbornene, to obtain the different precursor polymers capable of producing the developed hydrogel systems. In publication **I**, 4-arm 20 kDa PEG amine and 6 kDa PEG were functionalized following previously described protocols[451,457] to obtain 4-arm PEG-TZ and PEG-NB. ^{1}H-NMR was conducted to characterize the structure of both modified precursor polymers. In agreement with numerous literature reports, the obtained spectrum for 4-arm PEG-TZ showcased different peaks at δ 10.5 ppm, 8.4 ppm and 7.8 ppm, which corresponded to tetrazine group protons, whereas the spectrum of PEG-NB included two specific peaks at δ 6.1 ppm and 5.9 ppm, which correlated to different norbornene group protons. The estimated modification degree of 4-arm PEG-TZ and PEG-NB, approximately 85 and 75% respectively, remained in accordance with other previously reported studies [451,457]. The specific ^{1}H-NMR spectra are shown in the Supporting Information of the respective publication. In publication **II**, 4-arm PEG-TZ and HA-NB were used as precursor polymers. 4-arm PEG-TZ was functionalized following the same procedure performed in publication **I** and HA-NB was functionalized following a previously described protocol with some modifications [454]. Following functionalization, ^{1}H-NMR analysis of 4-arm PEG-TZ remained in correlation with the previous publication, as well as the previously estimated modification degree. The HA-NB spectra also showed the presence of specific peaks at δ 6 ppm and 6.5 ppm corresponding to norbornene protons, with a modification degree of approximately 30%. The specific ^{1}H-NMR spectra are also shown in the Supporting Information of the respective publication.

The preparation of hydrogel MPs and bulk hydrogels was conducted with different the concentration of both precursor polymers but maintaining a constant 1:1 ratio between tetrazine and norbornene groups based on the estimated modification degrees. In publication

I, optimization of hydrogel MPs production *via* microfluidics was conducted by studying the effect of modifying both inner and outer flow rates ratios in the microfluidics setup. Studies were conducted maintaining a constant outer phase flow rate while altering the inner phase flow rate from 50 to 500 µL/h. Specifically, different inner flow rates were studied under constant outer phase flow rates, including 10, 20, 50 and 75 mL/h (**Figure 11A**). The produced MPs were observed by the light EVOS microscope to measure the MPs diameter using ImageJ software and, subsequently, calculate the coefficient of variation.

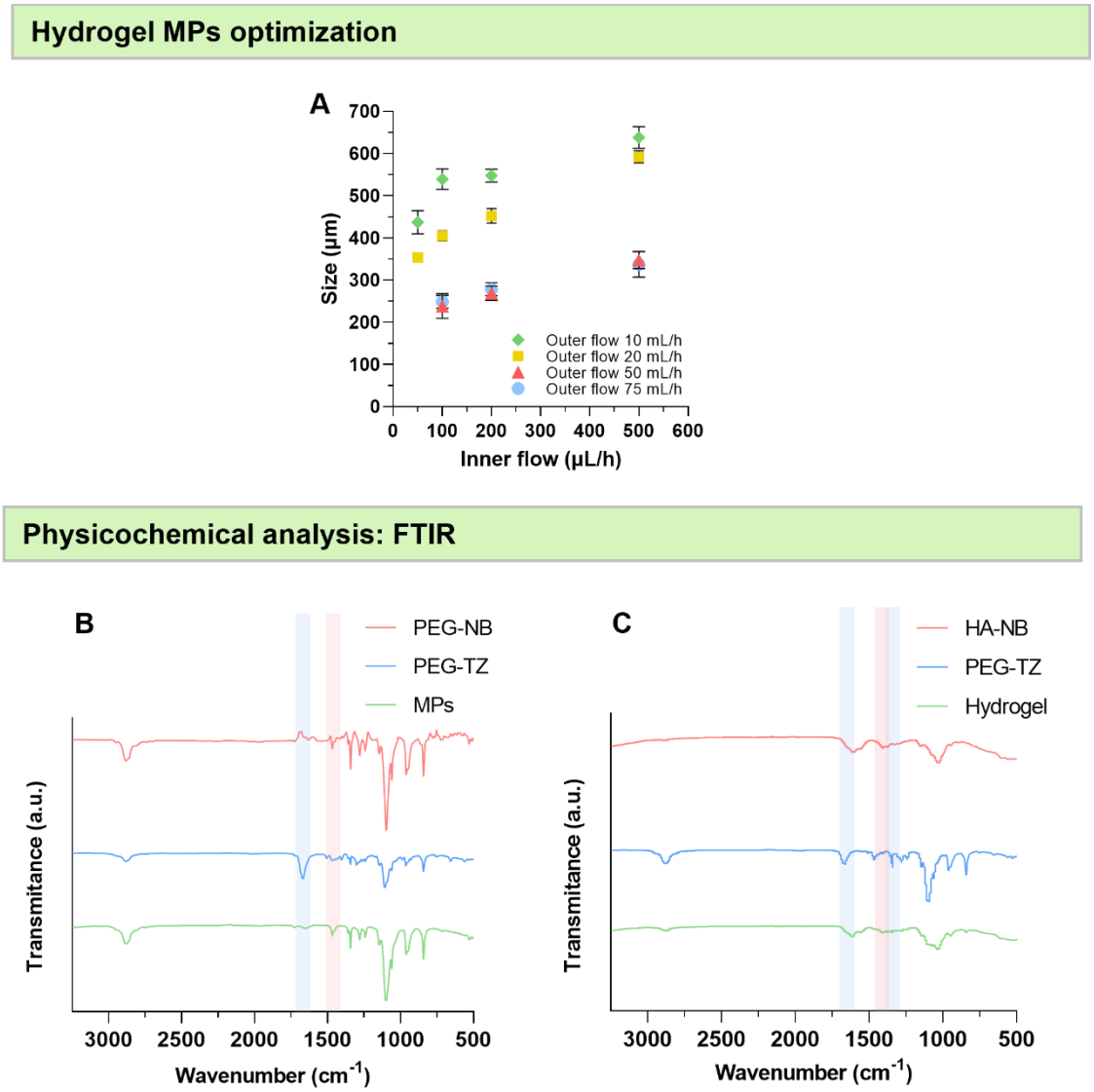


Figure 11. Hydrogel MPs optimization and physicochemical analysis. (A) Optimization graph considering the size of the produced MPs, inner flow rates and the outer flow rates. **(B)** ATR-FTIR spectra of 4-arm PEG-TZ, PEG-NB and hydrogel MPs. FTIR spectra were recorded in the range of 3500-500 cm^{-1} with a resolution of 2 cm^{-1}. (C) ATR-FTIR spectra of HA-NB, 4-arm PEG-TZ and HA-PEG hydrogel. FTIR spectra were recorded within the 3500-500 cm^{-1} range with a resolution of 2 cm^{-1}.

The optimization studies confirmed that MPs with sizes varying from 225 µm to 625 µm could be produced by a single microfluidics platform. As expected, MPs showed higher average sizes after increasing the inner flow rates while maintaining constant outer flow rates, whereas MPs owned lower average sizes after increasing the outer flow rates while maintaining

constant inner flow rates. Moreover, no significant changes were observed in terms of polydispersity index. For instance, after maintaining the inner phase flow rate of 100 µL/h, increasing the outer phase flow rate from 10 mL/h to 50 mL/h reduced the MPs average size to the half, with a final size of 225 µm. In stark contrast, after keeping the outer phase flow rate at 20 mL/h, increasing the inner phase flow rate from 50 µL/h to 500 µL/h increased the MPs average size from 330 µm to 580.

5.1.2 Morphological and physiochemical evaluation: SEM and FTIR analyses (I-II)

The physicochemical properties of the developed hydrogel MPs and bulk hydrogels were studied by FTIR. In publication **I**, the analysis of 4-arm PEG-TZ confirmed the presence of the tetrazine group double bound between C=N[458], shown by the band at 1670 cm^{-1} (**Figure 11B**). Other characteristic bands correlated with the structure of the polymer can also be observed, including a specific band around 1080 cm^{-1} corresponding to the C-O stretching and a band around 2850 cm^{-1} corresponding to the C-H stretching [459]. PEG-NB analysis also confirmed the presence of the C=C bond from norbornene[460] due to the presence of a band at 1480 cm^{-1}. The analysis of the crosslinked hydrogel MPs showed a clear decrease of the band at 1670 cm^{-1} due to the abolition of C=N bonds caused by the coupling of both groups and the release of gaseous nitrogen.

Morphological analysis: SEM

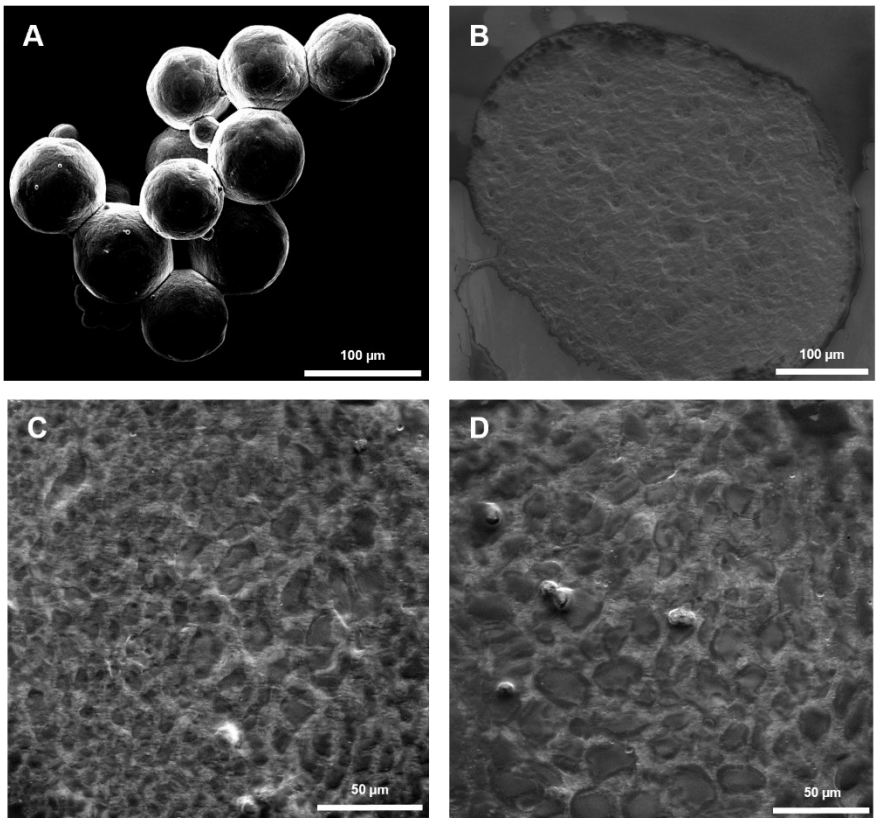


Figure 12. Morphological analysis of MPs and bulk hydrogels. (A) MPs external morphology by SEM. Scale bar 100 µm. **(B)** Inner matrix of MPs by SEM. Scale bar 100 µm. **(C)** Inner matrix of HA-PEG hydrogels by SEM. Scale bar 50 µm. **(D)** Inner matrix of HA-PEG-HEP hydrogels by SEM. Scale bar 50 µm.

Therefore, the obtained results suggested the successful crosslinking between both precursor polymers. In publication **II**, 4-arm PEG-TZ showed the same previously described spectrum, whereas HA-NB showcased a characteristic band at 1450 cm^{-1} corresponding to the C=C bond from norbornene. Moreover, the formed bulk hydrogel system similarly showcased the absence C=N and N=N bonds and confirmed the crosslinking of the structure (**Figure 11C**).
The morphological characterization studies were conducted using SEM. In publication **I**, the developed hydrogel MPs (**Figure 12A-B**) showcased an external regular surface with no visible pores. SEM images from the sectioned MPs indicated a highly porous inner structure with pore sizes reaching from 10 µm to 20 µm, similarly to the inner structure of other iEDDA-crosslinked systems[461]. A highly similar inner structure was also observed in the bulk hydrogel system developed in publication **II** (**Figure 12C-D**). As it has been previously described, the observed highly porous hydrogel matrix can be correlated with the release of 1 equivalent of nitrogen per reaction, as an inert byproduct of the iEDDA reaction between TZ and NB[462,463].

5.1.3 Rheological characterization (I-II)

The study of the rheological properties of both disc-like bulk PEG hydrogels and hydrogel MPs was conducted with a rotational rheometer in publication **I**. All the samples were prepared, allowed to swell during 24 h in 1× PBS (pH of 7.4) and characterized by strain sweep measurements and frequency strain measurements. Moreover, time sweep measurements were performed immediately after mixing both precursor polymer solutions and applying the precursor polymers mix above the lower plate to study the gelation kinetics of the system. Strain sweep measurements of bulk PEG hydrogels (**Figure 13A**) indicated that the system owns a stable behaviour until strain values of 10%. As expected, the storage modulus G' values of formulations with different precursor polymers concentrations were reported to increase after increasing the precursor polymers concentration. Successively, frequency sweep measurements (**Figure 13B**) were performed within the linear viscoelastic range. The detected G' values remained stable during the different measurements, following the rheological studies performed with numerous covalently crosslinked hydrogel networks[464,465]. Furthermore, the obtained G' values, detected as 1349 Pa for 10% PEG-TZ and 2978 Pa for 20% PEG-TZ, remained similar to other PEG-derived hydrogel systems crosslinked with the same type of approach[466,467].
The rheological properties of the hydrogel MPs were also assessed and measurements were conducted maintaining all the parameters previously used for the characterization of bulk PEG hydrogels. Strain sweep measurements showed considerably lower G' values, detected around 950 Pa, in comparison to same precursor polymers-formed bulk hydrogels (**Figure 13C**). This can be correlated to the macroscopic differences between of both samples, since bulk hydrogels constitute a single crosslinked polymer structure, whereas MPs remain a succession of separately formed micro-sized spheres. However, no statistically significant differences were observed between both MPs formulations with different precursor polymers concentrations, mainly due to the resemblance between the detected G' values. Similarly, frequency sweeps (**Figure 13D**) exhibited constant G' values and confirmed the storage modulus differences previously observed between bulk PEG hydrogels and MPs, despite showcasing a highly similar rheological behaviour.
Time sweep studies of both precursor polymer solutions showed that the storage modulus started to increase approximately 120 s after mixing both precursor polymers (**Figure 13E**). The G' values continued to increase for more than 600 s, time when the gelation of the system was completed. In this particular case, the observed gelation kinetics were highly favourable

since, prior to their crosslinking, both precursor polymers could quickly combine in the microfluidic platform and produce the MPs before the hydrogel matrix crosslinks.

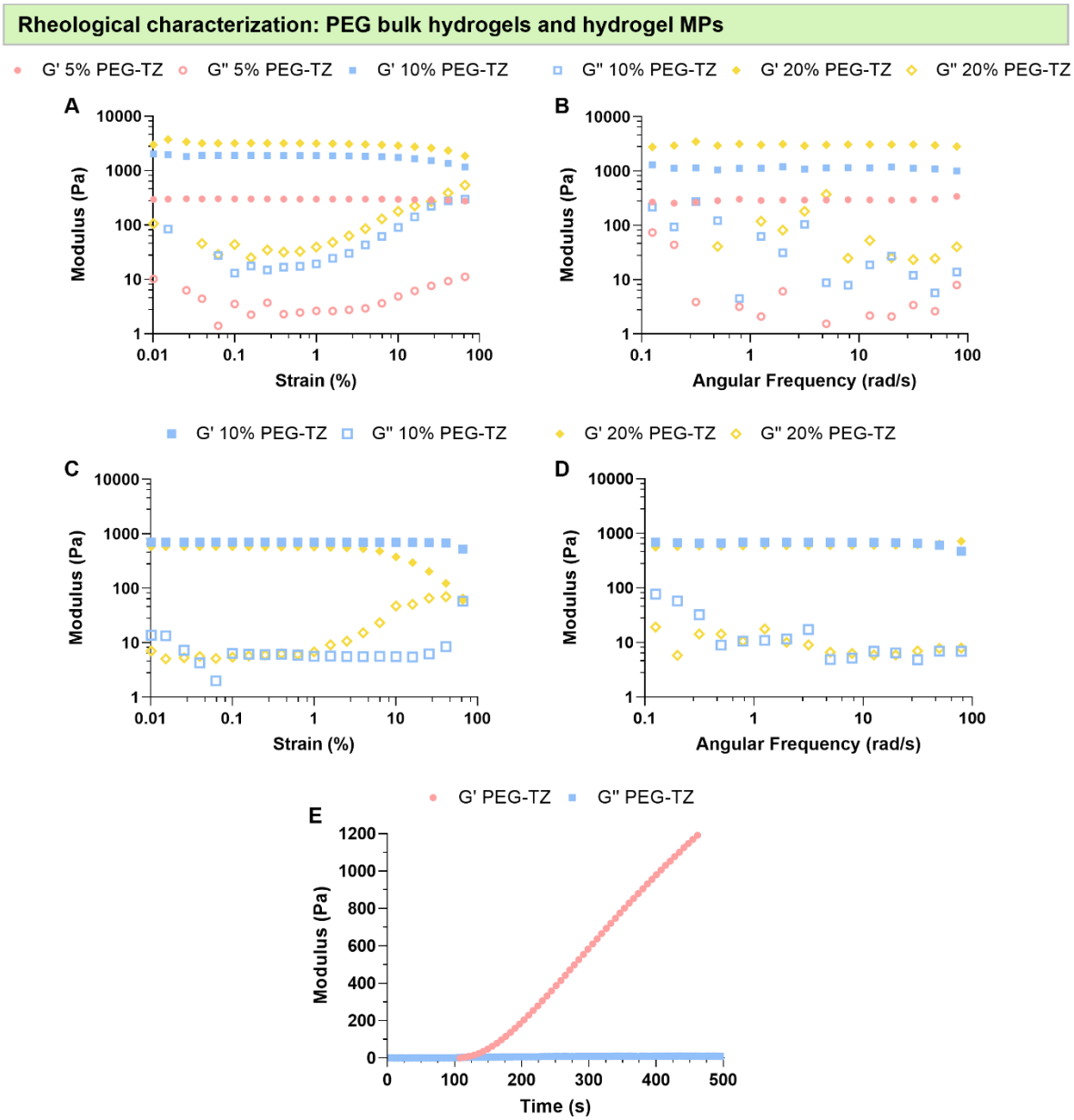


Figure 13. Rheological characterization of PEG bulk hydrogels and hydrogel MPs. (A) Strain sweep of bulk hydrogel with 5% PEG-TZ, 10% PEG-TZ and 20% PEG-TZ. **(B)** Frequency sweep of bulk hydrogel with 5% PEG-TZ, 10% PEG-TZ and 20% PEG-TZ. **(C)** Strain sweep of MPs with 10% PEG-TZ and 20% PEG-TZ. **(D)** Frequency sweep of MPs with 10% PEG-TZ and 20% PEG-TZ. **(E)** Time sweep of bulk hydrogel 10% PEG-TZ.

In publication **II**, HA-PEG and HA-PEG-HEP bulk hydrogels with disc-like morphology were similarly characterized. Strain sweep measurements of both types of hydrogels confirmed that both systems owned almost identical G' and G'' profiles, which showed a highly stable trend until 10% strain (**Figure 14A**). Subsequently, frequency sweep measurements were conducted within the previously described linear viscoelastic range. HA-PEG and HA-PEG-HEP showed again identical behaviour, with constant G' values up to 930 and 1110 Pa, respectively (**Figure 14B**). Several studies have described that the combination of HA with other synthetic polymers is usually conducted with the aim to improve the rheological properties of standard HA-based

hydrogels. The obtained results indicated that both hydrogel formulations showed similar G' and G'' values in comparison with other HA-PEG hydrogel formulations with a similar initial polymer concentration[468–470]. Moreover, time sweep measurements showed that the developed HA-PEG system experienced a G' crossover with G'' after approximately 200 ± 84 s following the mixing of both polymers (**Figure 14C**). Subsequently, G' values continued increasing up until the complete gelation shortly after 500 s. The observed behaviour remained similar to other hydrogel systems with the same crosslinking principle and comparable concentration of precursor polymers[172,175,471].

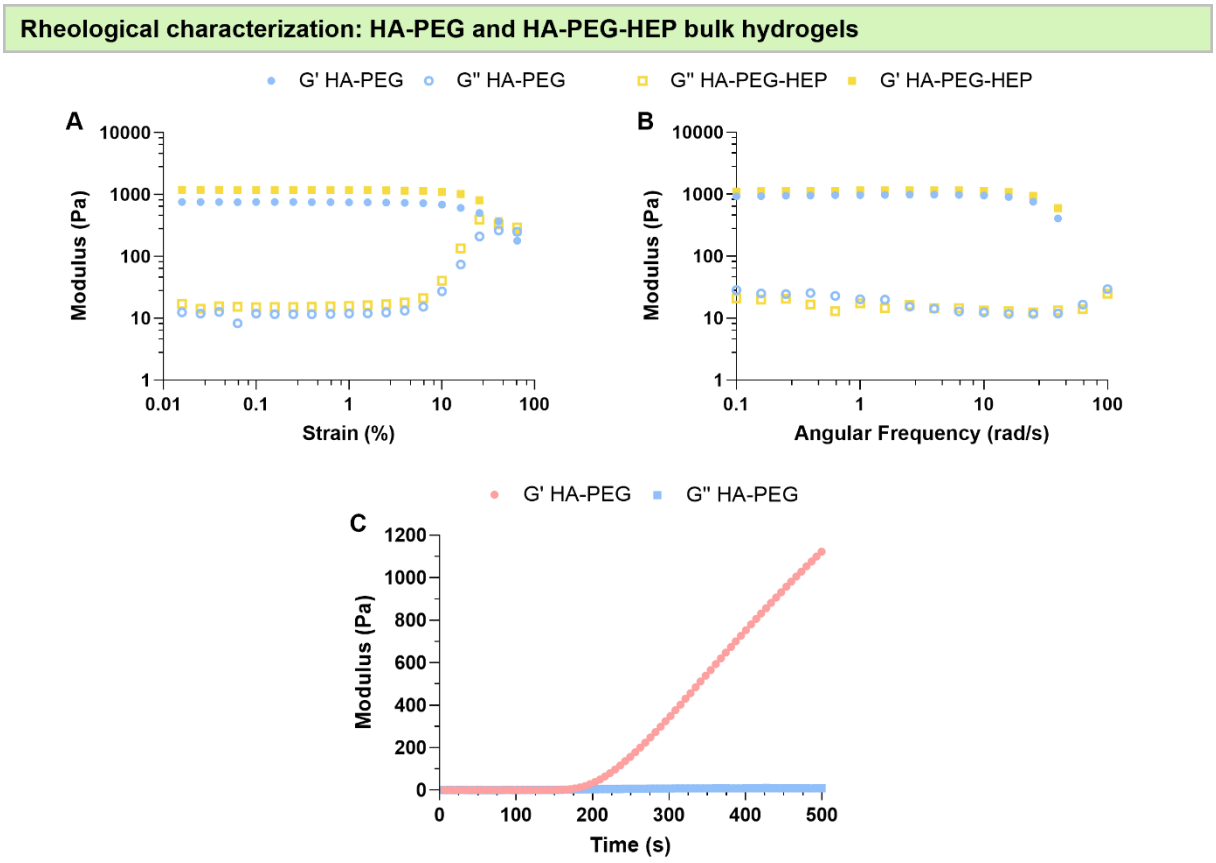


Figure 14. Rheological characterization of HA-PEG and HA-PEG-HEP bulk hydrogels. (A) Strain sweep measurements of HA-PEG and HA-PEG-HEP. **(B)** Frequency sweep measurements of HA-PEG and HA-PEG-HEP. **(C)** Time sweep measurements of HA-PEG and HA-PEG-HEP.

5.1.4 Swelling studies (I-II)

After studying the morphological and physicochemical properties of the developed systems, the swelling properties of the different types of hydrogels were investigated. In publication **I**, the hydrogel MPs with different concentrations of precursor polymers were immersed in a synovial fluid mimicking buffer with a high polyelectrolyte and protein content, and two different pH conditions. The selected pH conditions were pH 5.5, as a slightly acidic buffer mimicking the inflammatory environment, and pH 7.4. The swelling index was calculated based on the relationship between the MPs diameter at specific timepoints and the initial diameter before immersion.

The developed hydrogel MPs showcased a limited swelling index increase during the initial 5 min at both pH conditions (**Figure 15A-B**). The initial trend was followed by a plateau tendency

at pH 7.4 regardless of the precursor polymers concentration, since formulations with different amounts of 4-arm PEG-TZ maintained stable swelling index values around 1 and 1.4 during the complete development of the study. No major signs of volume differences or degradation were observed during the performed studies, which correlated with similar iEDDA-crosslinked PEG-based systems with persistent hydrolytic stability[172,472]. Contrary to the previously described trend, hydrogel MPs showcased a gradual increase in their swelling index at pH 5.5. The increase in the swelling index was observed until the complete degradation of MPs, approximately 8 days after the beginning of the study. Both formulations of 10% and 20% of 4-arm PEG-TZ showed major differences, with higher swelling index values correlated with reduced precursor polymers composition. Differences in the degradation of both systems may be explained by the PEG-NB esters bonds hydrolysis, which has been reported to be accelerated in acidic pH conditions by protonation of the ester bond at the carbonyl oxygen[473].

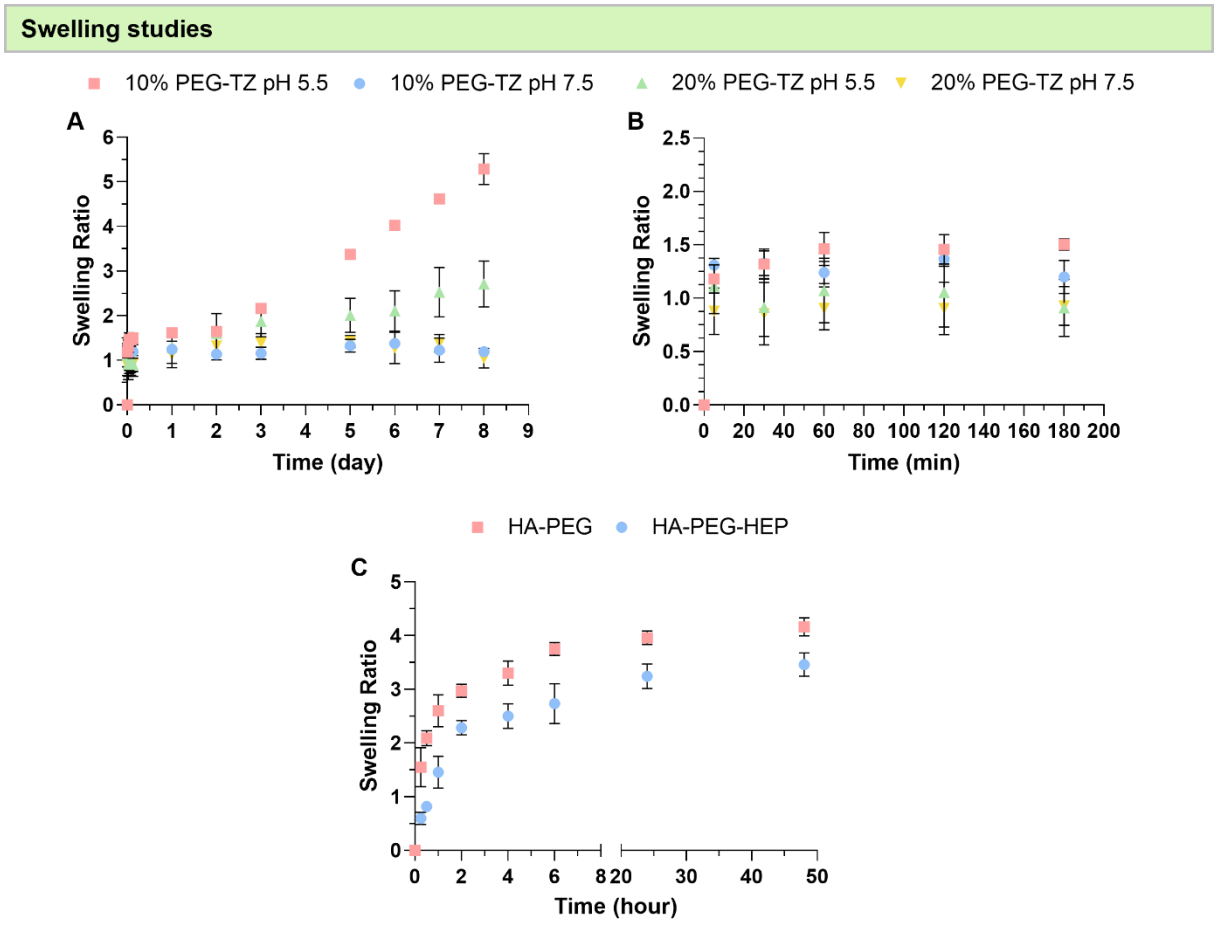


Figure 15. Swelling studies. (A) Swelling ratio of hydrogel MPs in synovial mimicking buffer at pH 5.5 and 7.4 and 37 ºC for 8 days. **(B)** Swelling ratio of hydrogel MPs in synovial mimicking buffer at pH 5.5 and 7.4 and 37 ºC during the initial 200 min. **(C)** Swelling ratio of HA-PEG and HA-PEG-HEP hydrogels incubated in 1× PBS at pH 7.4 and 37 ºC. Results are presented as mean ± SD (n≥3).

In comparison with bulk hydrogel systems, MPs might be more susceptible to this phenomenon due to spherical morphology of the MPs, since the surface area of the structure is increased in comparison with the comparable bulk hydrogel. Overall, hydrogel MPs showcased reduced swelling profiles and no degradation signs under the tested physiological conditions, as well as increased swelling indexes followed by gradual degradation under mildly acidic conditions.

In publication **II**, both PEG-HA and HA-PEG-HEP formulations were similarly studied in terms of swelling behaviour following volume changes after immersing dry hydrogels in 1× PBS at 37 ºC. The diameter of disc-shaped hydrogels was measured at specific timepoints to calculate the volume of each sample and compared to their respective initial dry values. The obtained results indicated that following their immersion, both types of hydrogels showed a quick initial swelling ratio increase during the first 2 h, reaching swelling indexes of approximately 2.9 and 2.4 for PEG-HA and PEG-HA-HEP hydrogels, respectively (**Figure 15C**). Subsequently, the swelling ratio of both formulations showed a limited and constant increase after 24 h, following a stable evolution after 48 and 72 h, with PEG-HA and HA-PEG-HEP swelling ratios of 4 and 3.5, respectively. Previous studies have extensively reported that HA and PEG-based hydrogels own high swelling ratio values due to the hydrophilic properties of both polymers[470,474]. A wide variety of factors, including the degree of crosslinking, the presence of additional moieties in the polymer network or the loading of cargos, can condition the swelling properties. Here, the developed PEG-HA and PEG-HA-HEP hydrogels showed similar swelling properties in comparison with other iEDDA-crosslinked hydrogels and reduced swelling degree values in comparison with other HA-based hydrogel formulations with different crosslinking methods[475,476]. Since it has been correlated that higher crosslinking degree or polymer modification degree can reduce the swelling index of the system[477], the observed reduction in the swelling degree can be explained by the crosslinking density achieved by the specific iEDDA crosslinking method of the developed system. Moreover, the developed HA-PEG and HA-PEG-HEP formulations owned comparable swelling properties. In fact, volume-based measurements did not show significant differences between the swelling behaviour of both types of formulations. Nevertheless, the macroporous structure of the developed hydrogels still showed a substantial swelling degree, suggesting that additional strategies should be implemented to minimize the swelling behaviour of HA-based systems, such as its functionalization with additional moieties[478], with the aim to improve the maintenance of the matrix structural integrity and improve the control of the encapsulated agents release[479].

5.2 Physicochemical characterization of hybrid nanoparticles (III)

5.2.1 Dynamic light scattering (size, PDI and ζ-potential) and nanoparticle tracking analysis (III)

In publication **III**, the physicochemical properties of the developed MSC-Hyb NPs and control LNPs were characterized by DLS, ELS and NTA. DLS analysis indicated that LNPs and MSC-Hyb owned average sizes of 168.7 nm and 178.6 nm, respectively (**Figure 16A**). Moreover, LNPs and MSC-Hyb measurements indicated PDI values of 0.135 and 0.245, respectively, indicating that MSC-Hyb owned higher average size and PDI values (**Figure 16B**). ELS analysis additionally revealed that the ζ-potential (**Figure 16C**) of LNPs and MSC-Hyb was -2.15 and -19.5 mV, respectively, revealing a considerable decrease of surface charge between both types of samples. The decrease of ζ-potential might be attributed to the addition of EV membrane into MSC-Hyb, considering EVs prevalently own a negative surface charge. NTA analysis of both types of systems indicated that LNPs and MSC-Hyb owned average sizes of 106 nm and 126.6 nm, respectively (**Figure 16D-E**). These values remain slightly lower values in comparison with those obtained by DLS, a phenomenon that may be explained by the differences between both techniques. Furthermore, considering that both samples were equally diluted 1:1000, the measured sample concentrations were respectively 6.80×10^{11} particles/mL for LNPs and 3.70×10^{11} particles/mL for MSC-Hyb. The obtained data confirms that the used microfluidic-sonication technique allows to obtain a significant particle

concentration despite the limited initial total lipid and EVs concentration. Interestingly, LNPs were correlated with a higher particle concentration, whereas MSC-Hyb showed a lower particle concentration similar to the initial particle concentration of EVs. Specifically, MSC-Hyb were prepared by adding MSC-EVs to the precursor aqueous phase following a protein to lipid ratio of 1:100 (w/w), which corresponded to an average particle concentration of 2.00×10^{10} particles/mL following NTA analysis.

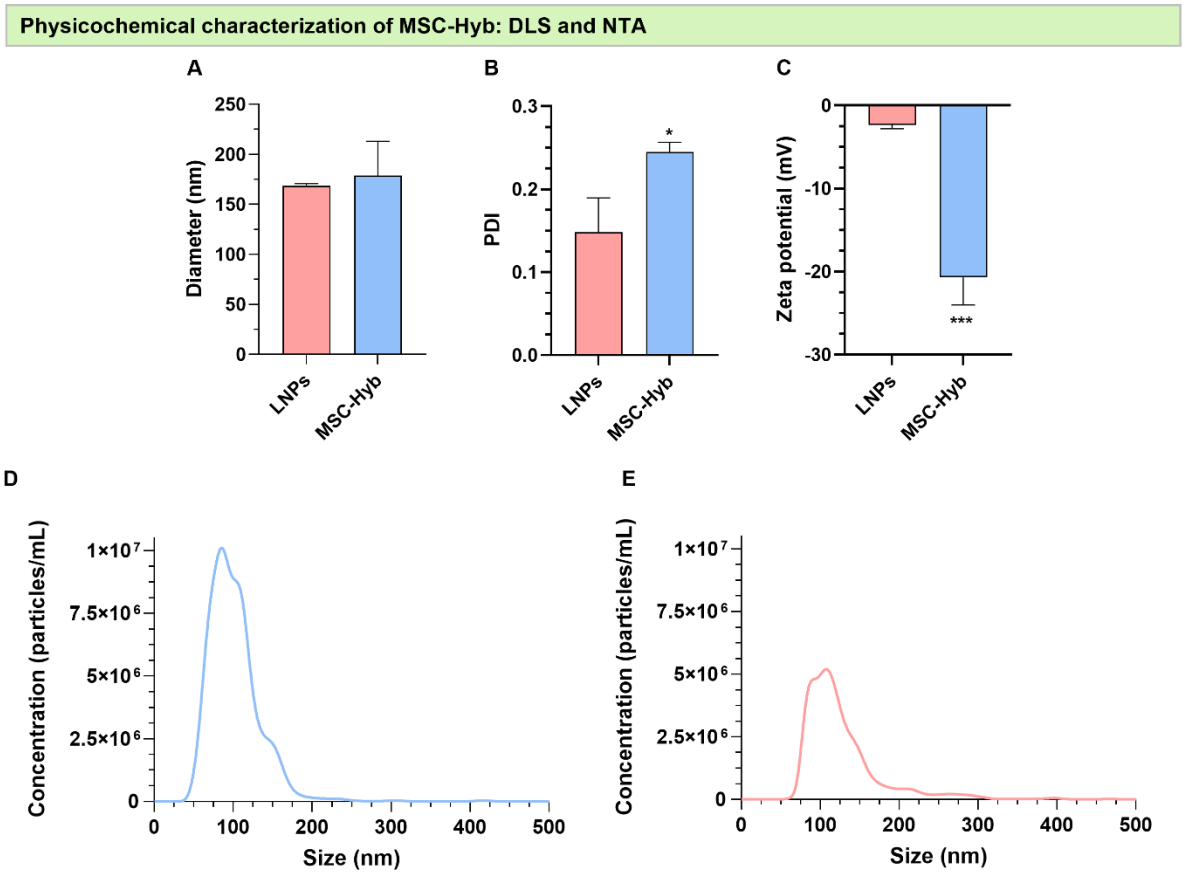


Figure 16. Physicochemical characterization of MSC-Hyb. (A) Average diameter of MSC-Hyb and LNPs as measured by DLS. **(B)** PDI of MSC-Hyb and LNPs as measured by DLS. **(C)** Surface charge (ζ-potential) of MSC-Hyb and LNPs as measured by ELS. (**D)** Size and particle concentration of LNPs determined by NTA. **(E)** Size and particle concentration of MSC-Hyb determined by NTA. Results are presented as mean ± SD (n≥3), and the samples were analysed with a paired Student's t-test, setting the probabilities *p< 0.05, **p< 0.01, *** p < 0.001.

5.2.2 Morphological evaluation (Cryo-TEM) and hybridization studies: FRET and surface markers analysis (III)

In publication **III**, the morphological evaluation of MSC-Hyb and control LNPs was performed *via* Cryo-TEM to confirm the size and size polydispersity data previously obtained by DLS and NTA. Cryo-TEM images revealed that MSC-Hyb and LNPs owned spherical shape and unilamellar structure, as reported for LNPs and EVs elsewhere[480,481]. Furthermore, the size and PDI data previously obtained by DLS was confirmed, since the observed LNPs were slightly smaller and more homogenous in comparison with MSC-Hyb (**Figure 17A**). Observation of MSC-Hyb confirmed the presence of slightly higher and more polydisperse NPs

(**Figure 17B**), probably due to the non-regular incorporation of membrane segments derived from EVs. Additionally, the obtained images did not show any aggregation signs, confirming the appropriateness of the used method for the development of NPs.
Hybridization studies were conducted to study the hybrid nature of the produced MSC-Hyb NPs. Firstly, FRET-based lipid mixing studies were conducted as previously reported[482,483] using fluorescent label-conjugated lipids, NBD-PS and Rhodamine-PE.

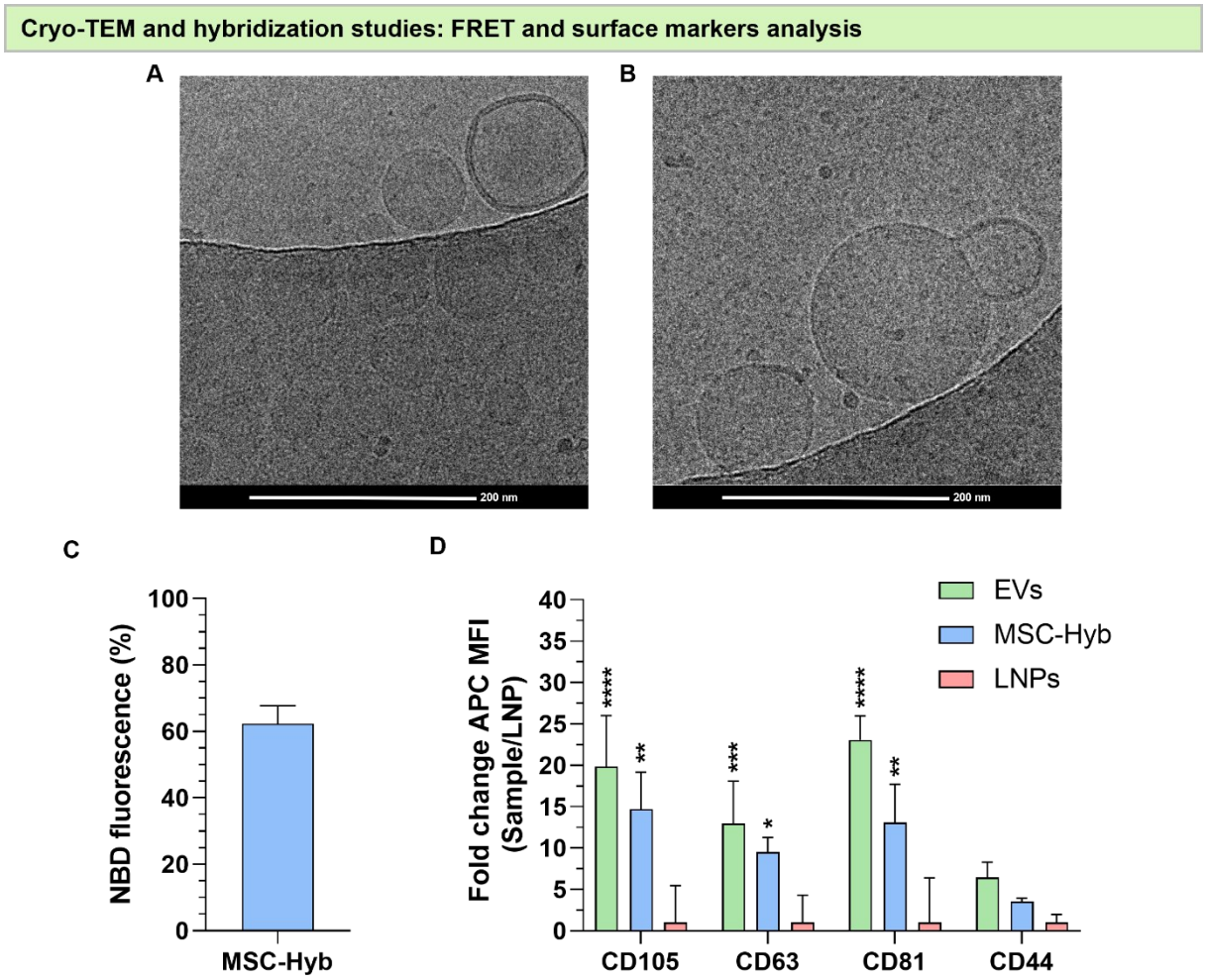


Figure 17. Morphological and hybridization studies of MSC-Hyb. (A-B) Cryo-TEM images revealing the morphological appearance of **(A)** LNPs and **(B)** MSC-Hyb. The highlighted scale bar in both images corresponds to 200 nm. **(C)** FRET assay in MSC-Hyb. **(D)** Analysis of CD105, CD63, CD81 and CD44 surface markers *via* MACSPlex Exosome kit in EVs, MSC-Hyb and LNPs targeting. APC MFI background values from PBS blank control were subtracted from each APC MFI value obtained from all the samples and results were represented as fold change relative to LNPs. Results are presented as mean ± SD (n≥3), and the samples were analysed with ordinary one-way ANOVA, followed by Turkey post-hoc test, setting the probabilities *p< 0.05, **p< 0.01, *** p < 0.001, **** p < 0.0001, comparing each EVs and MSC-Hyb sample with the corresponding LNPs sample.

The assay was used to detect the inclusion of external material into the lipid membrane thanks to the interaction between NBD, with an excitation wavelength of 460 nm, and Rhodamine, which receives fluorescence resonance energy from NBD depending on the distance between both fluorochromes. Therefore, it is possible to detect changes in the distance between both lipids within the lipid membrane following the incorporation of external components, since the

distance between both fluorophores increases and the emission of NBD at 535 nm increases due to the lack of interaction with nearby Rhodamine molecules. As it is shown in **Figure 17C**, the detected NBD fluorescence from MSC-Hyb NPs, which were prepared with a 1.5 molar ratio of each type of labelled lipid, increased up to a 62.34%. Based on the stablished calibration curve between the increase of NBD fluorescence and the hypothetical round of fusion, which can be observed in the Supporting Information of publication **III**, the produced MSC-Hyb NPs were estimated to own 28.99% of external material within the lipid membrane.
Secondly, the presence of EVs' surface markers on the surface of MSC-Hyb NPs was studied using a bead-based flow cytometry analysis tool, MACSPlex Exosome kit, capable of detecting several antigens. MSC-derived EVs have been described to own multiple specific antigen proteins such as CD81, CD69, which are highly common protein markers detected in EVs[484,485], and CD105 and CD44, highly expressed by MSC[486,487]. Bead-based analysis revealed that MSC-Hyb showed significant levels of these four proteins in comparison with LNPs (**Figure 17D**), confirming the presence of EVs-derived membrane fragments in the structure of MSC-Hyb NPs. Moreover, as expected, MSC-Hyb NPs showed a limited presence of EVs-derived material, since significantly lower levels of these four antigens were detected in comparison with the original EVs. Overall, the obtained results prove that the obtained MSC-Hyb NPs were detected by antibody-coated beads against specific EV antigens, confirming that MSC-Hyb NPs contain EVs-derived fragments.

5.3 Drug loading and *in vitro* drug release studies (I-III)

The EE and LD of the different cargos encapsulated within the different developed formulations were assessed to evaluate the loading of either proteins or nucleic acids within the proposed hydrogel MPs and NPs systems. In publication **I**, the developed hydrogel MPs were loaded with a model protein, BSA, to evaluate the potential use of the developed system as a protein delivery carrier. BSA-loaded MPs were prepared by adding and mixing BSA with both precursor polymer solutions, which were used for the production of MPs following the formerly reported procedure. Afterwards, both EE and LD were evaluated *via* the direct method, as previously described, obtaining estimated EE and LD values of 87.17 ± 2.41% and 4.36 ± 0.25%, respectively. The obtained values were correlated with the high hydrophilic nature of the loaded cargo and the fast crosslinking of the MPs system shorty after their formation *via* single emulsion. Furthermore, the mRNA EE of MSC-Hyb and standard LNPs was studied in publication **III** following direct Ribogreen assay-mediated quantification, as previously described. Direct determination of mRNA encapsulation revealed EE values of 51.45 ± 5.70% and 71.46 ± 4.13% for MSC-Hyb and LNPs, respectively. The decrease in the amount of encapsulated mRNA in MSC-Hyb may be correlated with the presence of several negatively charged components during the NPs formation procedure, including RNA, proteins or lipids derived from EVs, which may compete with the added mRNA and interact with the used ionizable lipid in the formulation[305]. Nonetheless, the obtained EE indicated the ability of the used method to encapsulate mRNA within MSC-Hyb NPs.
The *in vitro* release of protein cargos encapsulated in hydrogel MPs and bulk hydrogels was investigated to assess the drug release profile both types of systems. In publication **I**, the BSA release profile of hydrogel MPs with different concentrations of precursor polymers was studied at pH 5.5 with a mildly acidic buffer mimicking the inflammatory environment, and pH 7.4 mimicking physiological conditions. In both conditions, hydrogel MPs with different polymer content equally showcased a predominant burst release profile during the first 6 h (**Figure 18A**). After 1 day under pH 7.4 conditions, the hydrogel MPs released among the 80 and 90%

of the encapsulated BSA, depending on the concentration of precursor polymers, while the remaining percentage of encapsulated BSA was gradually released during the following days. Similarly, at pH 5.5, the hydrogel MPs did not show significant differences in comparison with the previously tested conditions, since approximately among the 87 and 95% of loaded BSA was released after 1 day. After analysing the initial 6 hours data based on different kinetic models, Korsmeyer-Peppas remained the most fitting model with the highest linearity (R^2) for both conditions and types of formulations, as it can be observed in the Supporting Information section of the respective publication. In all the cases, the release exponent (*n*) values remained lower or equal to 0.45, suggesting a Fickian diffusion-mediated release mechanism. The diffusion-governed release profile can be explained by the highly hydrophilic nature of the cargo and the MPs system, as well as the highly porous inner structure, which is conditioned by the polymer molecular weight and crosslinking density, as it has been previously reported in other comparable systems[488–490]

In publication **II**, the kinetics of AEC-CM loaded HA-PEG and HA-PEG-HEP hydrogels were evaluated. Both types of formulations were prepared and loaded with lyophilized AEC-CM immersed in both precursor polymers and hydrogels were formed with a disc-like morphology. The release kinetics of the loaded AEC-CM were evaluated by determination of the total protein concentration and the concentration of two specific proteins previously reported as predominant components of AEC-CM, VEGF and AREG[491,492]. As expected, both total protein content and the two specific growth factors showed an initial burst release during the earliest hours of the study, as it has been previously correlated with highly hydrophilic cargos[493–495]. However, the obtained results indicated significant differences depending on the type of formulation and the studied cargo. Total protein studies showed that HA-PEG-HEP and HA-PEG formulations experienced a substantial burst release of 50 and 60% of the total protein content, respectively (**Figure 18B**). After 24 h, around the 60 and 80% of the total protein content had been released from HA-PEG-HEP and HA-PEG hydrogels, respectively, followed by a sustained release of the remaining content up to 7 days in HA-PEG and 14 days in HA-PEG-HEP. Interestingly, the VEGF release profile showed an initial burst release of approximately 30 and 60% in HA-PEG-HEP and HA-PEG hydrogels, respectively (**Figure 18C**). After 24 h, the differences between both systems were maintained, with HA-PEG-HEP and HA-PEG releasing 40 and 70% respectively. The remaining VEGF was subsequently released in a sustained rate with highly significant differences. Specifically, HA-PEG-HEP gels showed a slow release, with only 60% of VEGF content released after 14 days, whereas HA-PEG gels released the complete amount of VEGF after 3 days. Similarly, AREG release studies also showed an initial burst release of 40 and 50% in HA-PEG-HEP and HA-PEG gels, respectively (**Figure 18D**). Afterwards, both systems showcased a sustained release, with HA-PEG gels releasing the total AREG content after 7 days and HA-PEG-HEP gels releasing up to the 65% after 7 days, followed by a slow-release trend for more than 21 days.

Heparin was used as functionalization moiety of the polymer matrix due to its physicochemical properties, since its structure with numerous sulphate groups and predominant negative charge allows to stablish electrostatic interactions with positively charged cargos like growth factors[496]. The release studies showcased that functionalization with heparin was correlated with reduction of the burst release degree of the monitored growth factor cargos, as well as more prolonged release of the remaining cargo. The reduction in the initial percentage of released cargo was considerably limited for the total protein content, but statistically significant for both VEGF and AREG, mainly due to the presence of electrostatic interactions between heparin and both studied components from AEC-CM. Data analysis of release kinetics also indicated that the highest correlation was obtained with Korsmeyer-Peppas, with reduced

exponent values below 0.43, suggesting that the release of AEC-CM was mediated by a Fickian diffusion mechanism.

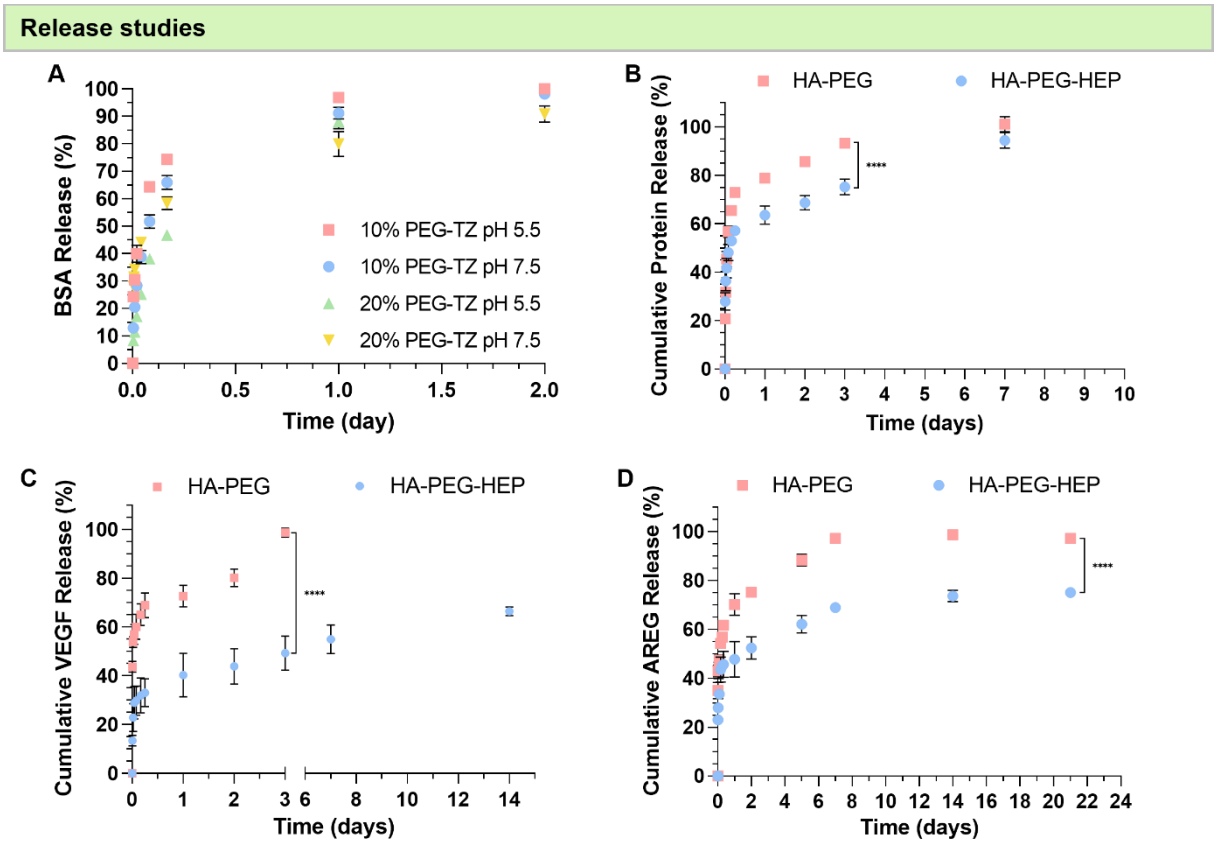


Figure 18. Release studies. (A) Cumulative BSA release from MPs at 37ºC under pH 5.5 and 7.4. **(B)** Cumulative total protein release profile from HA-PEG and HA-PEG-HEP hydrogels in 1× PBS at 37 ºC for 7 days. **(C)** Cumulative VEGF release profile from HA-PEG and HA-PEG-HEP hydrogels in 1× PBS at 37 ºC for 14 days. **(D)** Cumulative AREG release profile from HA-PEG and HA-PEG-HEP hydrogels in 1× PBS at 37 ºC for 21 days. Results are presented as mean ± SD (n≥3), and the samples were analysed with ordinary one-way ANOVA, followed by Turkey post-hoc test, setting at the probabilities *p< 0.05, **p< 0.01, *** p < 0.001, **** p < 0.0001 comparing each HA-PEG and HA-PEG-HEP sample within the same time point.

Altogether, the investigated systems showcased an initial diffusion-mediated burst release due to the high diffusion coefficient of the loaded cargo and the porous nature of the system. However, functionalization with heparin as additional moiety in the hydrogel structure proved to decrease the degree of burst released cargo and prolong the sustained release of the monitored cargos.

5.4 Cytocompatibility studies (I-III)

Following the development, optimization and characterization of the different hydrogel and NPs-based systems, the safety of the produced formulations was studied in different *in vitro* cellular models with the objective to determine the viability of using both types of systems for the delivery of therapeutics without inducing cellular toxicity due to their composition. The cytotoxicity of the developed hydrogel MPs and bulk hydrogels was evaluated in primary human tenocytes (**I-II**), whereas the cytotoxicity of MSC-Hyb NPs was studied in primary human TSPCs (**III**). Cytotoxicity was studied using an ATP-based luminescence assay after

exposing cells to different concentrations of hydrogel MPs and NPs during different periods of time ranging from 24-72 h. Therefore, dose-dependent cytotoxicity was evaluated to determine the highest safe concentration to use during the subsequent *in vitro* cellular studies.
In publication **I**, the cytocompatibility of the developed hydrogel MPs was assessed in primary human tenocytes as cellular model. Studies were conducted following the exposure of different concentrations of MPs, ranging from 5 µg/mL to 1000 µg/mL, during exposure times of 24 h and 72 h. The obtained data indicated that no statistically significant cell viability differences were observed for any of the tested concentrations of MPs following exposure times of 24 and 72 h (**Figure 19A-B**). These results were in agreement with other PEG-based systems, which have been described as highly biocompatible, and with previously reported iEDDA-crosslinked hydrogels, considering the bioorthogonal nature of both moieties[466,497].

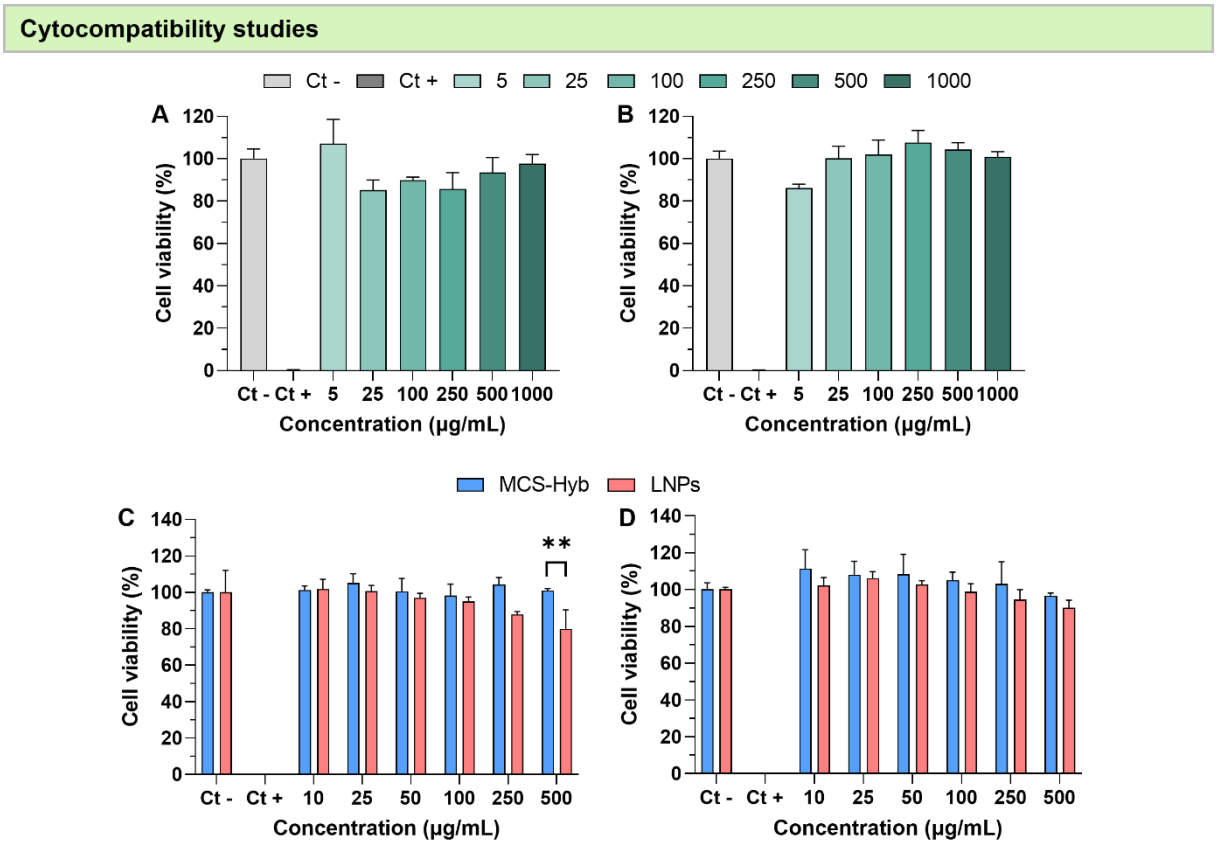


Figure 19. Cytocompatibility studies. (A-B) Cell viability of human primary tenocytes determined by CellTiter assay. Cells were incubated with MPs at different concentrations from 5 to 1000 µg/mL and cell viability was studied after 24 **(A)** and 48 h **(B). (C-D)** Cell viability of TSPCs incubated with MSC-Hyb and LNPs determined by CellTiter assay. Cells were incubated with MSC-Hyb and LNPs at different concentrations from 10 to 500 µg/mL and cell viability was studied after 24 **(C)** and 48 h **(D)**. Results are presented as mean ± SD (n≥3), and the samples were analysed with ordinary two-way ANOVA, followed by Turkey post-hoc test, setting the probabilities *p< 0.05, **p< 0.01, comparing each MSC-Hyb and LNPs sample with the untreated cells as well as each MSC-Hyb sample with the equivalent concentration LNPs sample.

In publication **III**, the cytocompatibility of MSC-Hyb and standard LNPs was evaluated in primary human TSPCs. Similarly, studies were conducted by exposing cells to different concentrations of both types of formulations, including 10, 25, 50, 100, 250 and 500 µg/mL, during incubation times of 24 and 48 h. The obtained results suggested that both formulations

owned high biocompatibility with TSPCs, since no statistically significant differences were observed after exposition for 24 and 48 h, including the highest concentration at 500 µg/mL (**Figure 19C-D**). Furthermore, no major statistically significant differences between LNPs and MSC-Hyb were observed at each specific concentration. Non-significant differences at high concentrations of 250 and 500 µg/mL for 24 h were observed, with MSC-Hyb NPs showing slightly higher cell viability values in comparison to LNPs, which may be attributed to the variability of the assay. Therefore, based on the obtained cell viability studies results, the following *in vitro* cellular studies were conducted with NPs concentrations of 100 and 200 µg/mL.

5.5 PBMCs activation and macrophages polarization studies (II)

The immunomodulatory potential of the AEC-CM-encapsulated hydrogel system developed in publication **II** was assessed to determine the biological activity of the AEC secretome after its encapsulation within the hydrogel formulation. PBMC activation was studied *via* CellTiter96 Aqueous One Solution Cell Proliferation Assay at different exposition times, including 3 and 7 days, in PHA-activated PBMCs after treatment with non-encapsulated AEC-CM, empty hydrogels and CM-loaded hydrogels with different concentrations of CM. **Figure 20A-B** shows that the encapsulation of AEC-CM in the hydrogel system significantly enhanced the immunomodulatory properties of the CM. After 3 days of exposure, the activation degree of PBMCs treated with AEC-CM decreased following a concentration-dependent trend, with non-diluted AEC-CM showing the most significant suppression, approximately a 60% ($p<0.001$ *vs.* PHA, **Figure 20A**). It is worth to mention that the observed effect in human immune cells caused by the use of ovine-conditioned media emphasizes the importance of xeno-cross talk between ovine-CM and human immune cells and provides insights into the wider applicability of the findings across species, as it has been previously reported[498]. Regarding the developed system, the empty hydrogel formulation (H) induced a minor immunosuppressive effect ($p<0.01$ *vs.* PHA, **Figure 20A**), whereas the hydrogel-encapsulated CM suppressed PBMC activation more effectively than the non-encapsulated equivalents at each concentration [$p<0.01$, H+AEC-CM (0.5:1) *vs.* AEC-CM (0.5:1); $p<0.001$, H+AEC-CM (1:1) *vs.* AEC-CM (1:1); $p<0.0001$, H+AEC-CM (2:1) *vs.* AEC-CM (2:1), **Figure 20A**]. The same tendency was observed after 7 days of exposition, since the hydrogel-encapsulated CM continued to exhibit a higher degree of PBMC inhibition in comparison to the non-encapsulated CM at each concentration. Moreover, in comparison with the data obtained after 3 days of treatment, a more pronounced suppression of PBMC activation was detected at each specific condition. The obtained data emphasizes the enhanced immunosuppressive potential of the encapsulated AEC-CM and suggests a synergistic effect between the hydrogel and the AEC-CM[499,500].

Following the obtained results regarding the PBMC activation assay, the study of human macrophage polarization was conducted to further analyse the immunomodulatory properties of the hydrogel-encapsulated AEC-CM. Following the previous studies, human PBMCs were isolated and treated to obtain M_0 macrophages, which were exposed to encapsulated and non-encapsulated ovine-CM during 48 h. The selected exposure time of 48 h was chosen following the early macrophage polarization dynamics, since the study aimed to detect changes occurred during the initial phenotype shifts[501]. The obtained results (**Figure 20 C-D**) revealed that all the tested conditions, including non-encapsulated AEC-CM, empty hydrogels and AEC-CM-loaded hydrogels, induced a change in macrophage polarization from the pro-inflammatory M1 phenotype towards the anti-inflammatory M2 phenotype. The described shift

was evidenced by a decrease in M1 marker CD86 MFI (**Figure 20C**) and an increase in the M2 marker CD206 MFI (**Figure 20D**). Specifically, the M1 marker CD86 experienced the most significant MFI reduction and M1 phenotype suppression after the treatment with the hydrogel-encapsulated AEC-CM. Treatment with the non-encapsulated AEC-CM and the empty hydrogel also decreased CD86 MFI, but in a lower degree in comparison with the encapsulated CM ($p<0.05$ vs. H +AEC-CM, **Figure 20C**). Similarly, M2 marker CD206 showcased similar results, with the non-encapsulated AEC-CM and the empty hydrogel increasing CD206 MFI, whereas the hydrogel-encapsulated AEC-CM substantially increased CD206 MFI to a higher extent ($p<0.05$ vs. H +AEC-CM, **Figure 20D**).

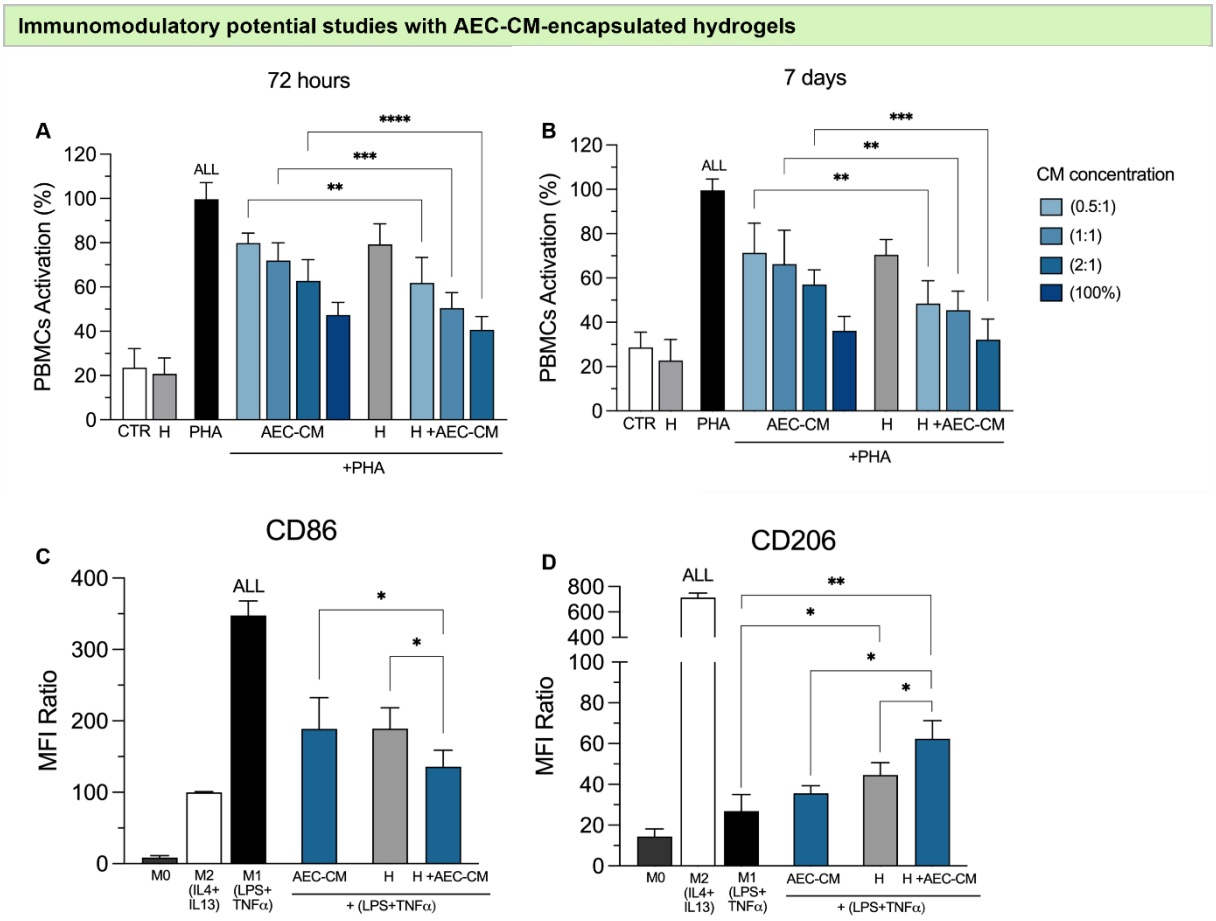


Figure 20. Immunomodulatory potential studies of hydrogel-encapsulated AEC-CM. (A-B) PBMCs activation after **(A)** 72 h and **(B)** 7 days of culture with PHA and treated with different concentrations non-encapsulated AEC-CM and hydrogel-encapsulated AEC-CM (H+AEC-CM). **(C)** CD86 expression of human macrophages treated with non-encapsulated AEC-CM, empty HA-PEG-HEP hydrogel (H) or hydrogel-encapsulated AEC-CM (H+AEC-CM) for 48 h. **(D)** CD206 expression of human macrophages treated with non-encapsulated AEC-CM, empty HA-PEG-HEP hydrogel (H) or hydrogel-encapsulated AEC-CM (H+AEC-CM) for 48 h. Results are presented as mean ± SD (n≥3) and represent independent sets of experiments (n=3 biological replicates in each group per set; each biological replicate assayed in at least 3 technical replicates). Data was analysed with ordinary one-way ANOVA, followed by Turkey post-hoc test, setting the probabilities *p< 0.05, **p< 0.01, ***p<0.001, and ****p<0.0001, respectively.

The obtained findings suggest that the hydrogel formulation may be responsible for the enhancement of the innate immunomodulatory activity of AEC-CM. This phenomenon may be

attributed to the nature of the hydrogel system, specifically due to its predominant HA composition. HA has been commonly reported as an immunosuppressive agent capable of inducing M2 phenotype changes in macrophages[502–504]. Therefore, the hydrogels not only reduced the initial burst release and facilitated the sustained release of different AEC-CM components, but also cause an intrinsic biological effect. The positive effect synergizes with the innate effect of the AEC-CM and enhances the therapeutic potential of the combined treatment[505], since the hydrogel is no longer considered as a simple passive carrier. Therefore, the combined approach using the hydrogel-encapsulated AEC-CM showed a clear advantage in promoting anti-inflammatory macrophage polarization, further underscoring its potential in therapeutic applications.

5.6 Cell–nanoparticles interactions: Quantitative cell uptake studies (III)

In publication **III**, the interaction between both types of NPs and primary human TSPCs was assessed by quantitatively studying the cellular internalization efficiency of both formulations, considering cell internalization remains a critical step for the cytoplasmatic delivery of mRNA. Both types of NPs, LNPs and MSC-Hyb, were prepared using Rhodamine-PE, a fluorescent-labelled phospholipid with an excitation wavelength of 546 nm and an emission wavelength of 567 nm. Following the cell-cytocompatibility studies, we chose NPs concentrations of 100 and 200 µg/mL due to their high cytocompatibility profiles. LNPs and MSC-Hyb were incubated with both types of cells for 48 h and, therefore, samples were analyzed by flow cytometry. **Figure 21A** shows that cell uptake of MSC-Hyb NPs was significantly decreased in comparison with LNPs after 48 h of incubation. Both MSC-Hyb NPs and LNPs showed a dose-dependent uptake behaviour in TSPCs, which showed a significant internalization degree, 31.61 and 53.96 MFI fold change, after incubation with 100 µg/mL of either MSC-Hyb NPs or LNPs, respectively. The increase of dose to 200 µg/mL of both types of NPs showed a slightly increased internalization degree, with 60.53 and 89.12 MFI fold change values corresponding to MSC-Hyb NPs and LNPs, respectively.

It has been widely described that NPs cellular internalization can occur *via* different endocytosis processes, which can be clearly influenced by the physicochemical properties of each NP formulation, including size and ζ-potential. Moreover, cellular uptake can also be influenced by the presence of specific biological moieties on the surface of NPs systems. The lower internalization rates of MSC-Hyb NPs in comparison with LNPs may be explained by the different physicochemical properties between both types of NPs, especially regarding their surface charge, since MSC-Hyb NPs own a more negative surface charge. Moreover, it has also been previously described that non-modified EVs can show different uptake ratios in comparison with other lipid-based systems. In this case, despite the presence of specific antigens on the surface, the predominant negative charge of MSC-Hyb NPs reduced to a certain extent the number of electrostatic interactions with the negatively charged membrane of both types of cells. Nonetheless, MSC-Hyb NPs still showed high cell uptake rates and proved to be promising NPs-based systems for intracellular delivery.

5.7 Quantification of the transfection efficiency of the hybrid nanoparticles (III)

Consequently, the use of MSC-Hyb NPs and LNPs as functional mRNA delivery agents was assessed following the previously described cell uptake studies conducted in publication **III**. We studied the efficiency of both MSC-Hyb and LNPs in terms of cytoplasmatic delivery of mRNA, which previously requires endosomal escape of the mRNA cargo after NPs uptake. eGFP mRNA was used as a model mRNA cargo for studying the transfection efficiency of both

MSC-Hyb NPs and LNPs in TSPCs. **Figure 21B** showcases the percentage of eGFP positive cells detected by flow cytometry after incubating TSPCs with 100 and 200 µg/mL of both types of NPs for 48 h. TSPCs incubation with 100 and 200 µg/mL of eGFP mRNA-loaded MSC-Hyb NPs induced an increase in the percentage of eGFP positive cells of approximately 17.72% and 21.49%. Both values remained significantly lower in comparison with the percentage of eGFP positive cells detected after incubation with 100 and 200 µg/mL of LNPs, which were confirmed to be 85.49% and 78.47%, respectively.
The decrease in the percentage of eGFP positive cells can either be explained by the lower uptake degree of MSC-Hyb in comparison to LNPs, as well as the significantly lower mRNA encapsulation efficiency in MSC-Hyb. Therefore, the obtained results indicated that MSC-Hyb NPs are suitable for the delivery of functional mRNA in TSPCs primary cells with decreased transfection efficiency in comparison with synthetic LNPs. Considering the previously showed data, including cell viability, quantitative cell uptake and transfection efficiency studies, a concentration of 200 µg/mL for both MSC-Hyb NPs and LNPs was chosen as the appropriate concentration for the following in vitro efficacy studies based on the observed safety profile and its transfection efficiency.

Quantitative cell-uptake and quantitative transfection efficiency of MSC-Hyb NPs

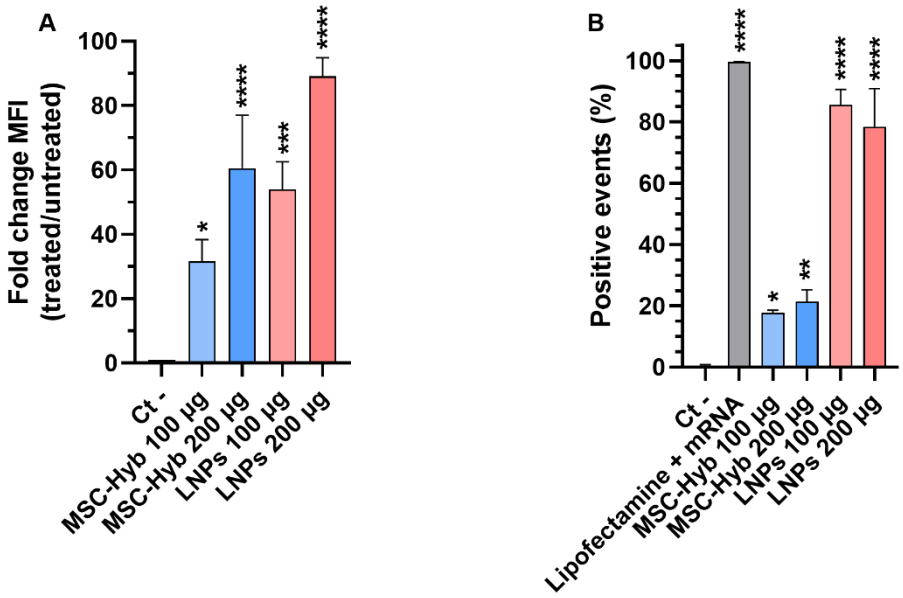


Figure 21. Quantitative cell-uptake and quantitative transfection efficiency studies of MSC-Hyb NPs. (A) Quantitative cell uptake studies in TSPCs using flow cytometry. TSPCs were incubated for 48 h at 37ºC with 100 and 200 µg/mL of Rhodamine-PE labelled MSC-Hyb NPs and LNPs. Results were expressed as fold change of PE MFI relative to the negative control. **(B)** Transfection efficiency of eGFP mRNA-loaded MSC-Hyb and LNPs in TSPCs cells after 48 h. TSPCs cells were incubated for 48 h at 37ºC with 100 and 200 µg/mL of MSC-Hyb and LNPs and, subsequently, transfection efficiency was assessed by flow cytometry analysis. Results were expressed as percentage of eGFP positive TSPCs. Results are represented as mean ± SD (n≥3), and represent independent sets of experiments, including biological and technical replicates. Data was analysed with ordinary one-way ANOVA, followed by a Turkey post-hoc test, setting the probability at * $p < 0.05$, ** $p < 0.01$, *** $p < 0.001$, **** $p < 0.0001$, comparing each condition with the negative control.

5.8 *In vitro* efficacy studies with COL1A1 mRNA-loaded hybrid nanoparticles(III)

Tendinopathic TSPCs have been described to increase the production of collagen type III, which deposits in a disorganized manner during the initial stages of tendon healing. Simultaneously, the ratio between collagen type I and collagen type III is altered, since the production of collagen type I remains low in comparison with non-pathological tendons[380,506]. The synthesis of collagen type I is considered a critical process since the deposition of organized collagen I fibres within tendon bundles allows to improve the tissue mechanical properties and reduce tissue adhesion[354]. In fact, enhancement of collagen I production remains a partial solution, since it needs to be combined with other factors, such as the application of appropriate mechanical stimuli, among others[507,508]. Until now, several studies have been focused on the beneficial effects regarding collagen I production caused by the administration of growth factors and stem cells-derived culture media[436,509], as well as the simulation of mechanical stress conditions in combination with bioengineered materials and different *in vitro* culture models[510]. However, alternative approaches based on the administration of COL1A1 mRNA to the affected TSPCs with the aim to enhance collagen I production have also been considered[511,512]. Hence, after studying the capability of MSC-Hyb to deliver functional mRNA, we assessed the *in vitro* potential of MSC-Hyb as COL1A1 mRNA delivery agents for pathological TSPCs. TSPCs were treated with 200 µg/mL of COL 1A1 mRNA-loaded MSC-Hyb NPs and LNPs, as well as with empty MSC-Hyb NPs and LNPs, during 48 h of exposition. Moreover, non-treated TSPCs immersed in cell culture medium were used as negative control. Afterwards, collagen I production was evaluated by quantitative western blot analysis, as well as qualitative immunofluorescence studies. **Figure 22A-C** showcased Western Blot analysis of alpha-1 collagen I protein expression from TSPCs from three different donors after incubation with the different treatment groups. Two predominant and distinctive bands were observed around 180 kDa and 35 kDa, respectively, corresponding to the procollagen alpha-1 chain and procollagen type I carboxy-terminal peptide (PICP)[513]. Analysis of the procollagen alpha-1 chain band did not reveal significant differences between the different groups treated with either mRNA-loaded or empty MSC-Hyb and LNPs, possibly due to the already noticeable basal expression of procollagen alpha-1 chain in non-treated TSPCs. Nevertheless, analysis of the PICP band revealed a statistically significant increase in TSPCs treated with mRNA-loaded LNPs and MSC-Hyb NPs, with 1.96 and 1.92 relative fold change values, respectively.

Collagen type I holds a triple-helical structure with terminal globular propeptide domains, including both amino and carboxy-ended domains. Specifically, procollagen type I has a heterodimeric structure that consists in two α1 chains and one α2 chain assembled as a trimeric structure shortly after their secretion[514]. Assembly of this trimeric structure requires endopeptidase-mediated cleavage of each chain at specific amino and carboxy terminal sites. Thus, this process is responsible for the segmentation of the structure in three different fragments: collagen type I, which forms collagen fibrils that form the ECM, and two released procollagen type I terminal peptides, one with an amino terminal (PINP) and one with a carboxy terminal (PICP)[515]. Previous studies have reported that detection of PICP constitutes a suitable marker to study the production of collagen type I in different tissues, including bone and skin[516,517]. For example, detection of PICP in fibroblasts, either in cell extracts or culture supernatants, has traditionally been considered an efficient method to study the production of collagen type I[518,519]. Hence, the obtained data seems to indicate that MSC-Hyb NPs are equally capable of delivering functional mRNA as LNPs due to the significant increase in the production of PICP in TSPCs treated with mRNA-loaded MSC-Hyb and LNPs. Interestingly,

exposition to empty LNPs was responsible for a decrease in the levels of PICP, in contrast to empty MSC-Hyb NPs, which slightly increased PCIP production. Despite the increase observed after the treatment with empty MSC-Hyb was found to be non-significant, this may be explained due to the partial EV content of MSC-Hyb NPs, since studies performed with MSC-EVs in tenocytes show a significant increase in collagen type I production[520,521]. Collagen I immunostaining and confocal microscopy imaging were also performed to qualitatively determine the production of collagen type I in TSPCs. As it can be observed in **Figure 22D**, the obtained images suggest that TSPCs treated with 200 µg/mL of MSC-Hyb and LNPs for 48 h experienced a certain increase in collagen type I in comparison with non-treated TSPCs. Overall, the obtained data regarding protein production suggested that mRNA-loaded MSC-Hyb can equally increase the production of collagen type I in comparison with LNPs, confirming the *in vitro* potential of MSC-Hyb NPs as COL1A1 mRNA delivery agents for pathological TSPCs.

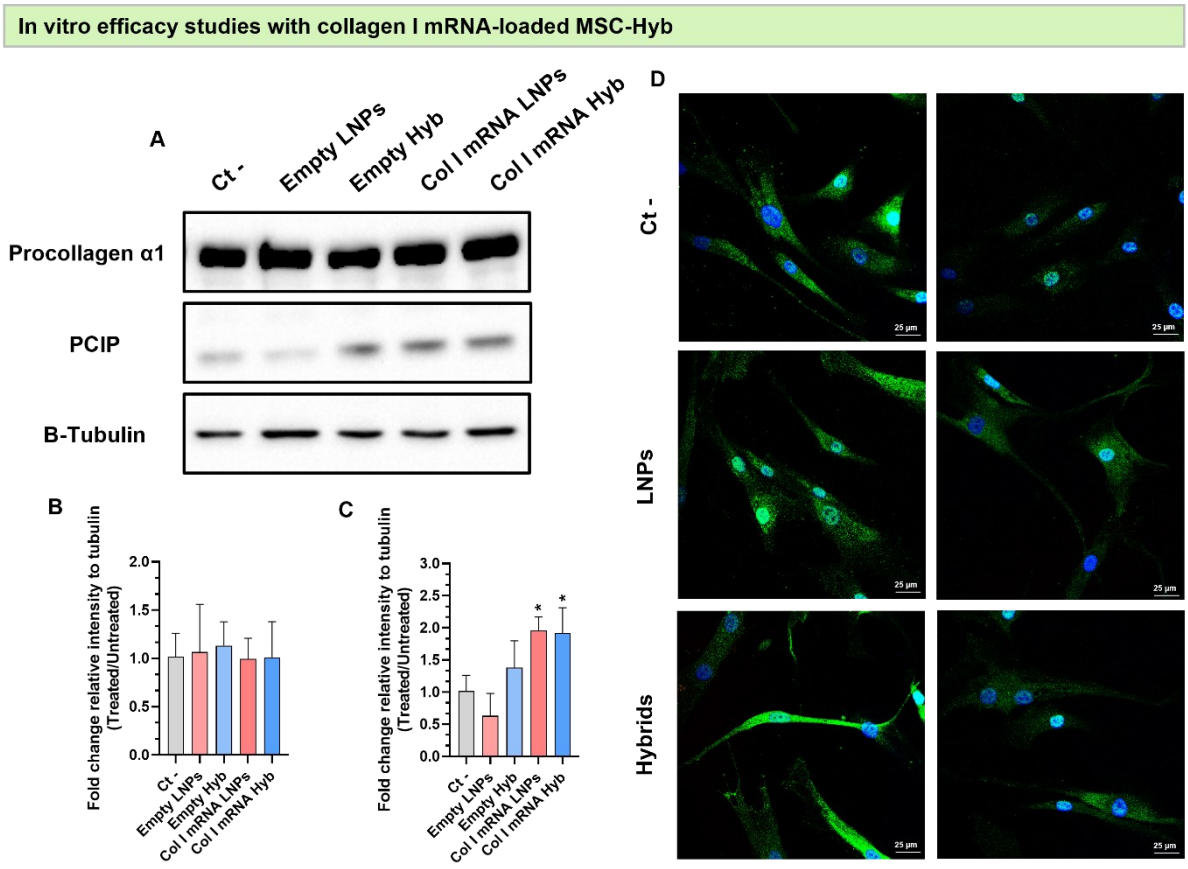


Figure 22. *In vitro* efficacy studies with collagen I mRNA-loaded MSC-Hyb. (A) Protein expression analysis by Western Blot of collagen type I in TSPCs. Cells were incubated during 48 h with empty LNPs, empty MSC-Hyb, Col 1A1 mRNA-loaded LNPs and Col I mRNA-loaded MSC-Hyb before proceeding with cell lysis and protein extraction. Western Blot bands are shown, including procollagen α1 and PCIP, as well as β-Tubulin, used as housekeeping protein. **(B-C)** Densitometric analysis of procollagen α1 expression **(B)** and PCIP expression **(C)** normalized to β-Tubulin and represented as fold change values relative to the negative control. Results are represented as mean ± SD (n≥3), including biological replicates, and the data was analyzed with ordinary one-way ANOVA, followed by a Turkey post-hoc test, setting the probability at *p < 0.05, comparing each condition with the negative control. **(D)** Immunofluorescence staining confocal fluorescence microscope images of collagen type I in 2D cultured TSPCs. TSPCs were treated with 200 µg/mL of COL1A1 mRNA-loaded LNPs and

MSC-Hyb for 48 h. Collagen type I was stained using an anti-collagen type I antibody and an Alexa 488-conjugated secondary antibody (green). DAPI was used to stain the nuclei (blue).

6 Conclusions

Drug delivery continues revolutionizing the biomedical field by combining novel technologies in drug formulation and recently acquired knowledge in terms of molecular biology and pathogenesis. Innovative hydrogels and NPs formulations can be designed to efficiently encapsulate biological cargos without altering their structure or modifying their activity, improving their stability in biological conditions, and controlling their release kinetics or even deliver specific cargos intracellularly. Therefore, the development of drug delivery systems remains a highly promising alternative for the treatment of numerous pathologies in comparison with conventional therapeutics.

In this thesis, different hydrogel and NPs-based systems were produced and loaded with biologically complex cargos to tackle different conditions commonly derived from tendinopathies.

Firstly, in **publication I**, monodisperse *in-situ* gellable iEDDA-crosslinked PEG hydrogel MPs were developed *via* W/O emulsification using a glass microfluidics platform. The functionalized precursor polymers, 4-arm PEG-TZ and PEG-NB, owned fast reaction kinetics and were used to produce highly uniform MPs with a size range between 200 µm and 600 µm with a single microfluidic device by just altering the flow parameters. The morphological characterization studies showcased that the produced hydrogel MPs owned considerably porous inner structure and uniform surface area. Moreover, the rheological properties of the produced MPs were in agreement with the behaviour of other analogous covalently crosslinked hydrogel systems, with storage modulus G' values of up to 3000 Pa. The swelling properties of the MPs were characterized by a reduced swelling degree and slow degradation behaviour under physiological conditions, in contrast to a high swelling degree and fast degradation behaviour under mildly acidic conditions. The potential of the developed hydrogel MPs to encapsulate protein-based cargos was studied, confirming that the MPs own a high protein loading capacity, with an EE of 87%, and a predominant burst release behaviour, with almost 90% release during 24 h. Furthermore, *in vitro* studies confirmed that the produced MPs did not induce cytotoxicity in primary human tenocytes, proving that iEDDA-crosslinked MPs remain a potential protein encapsulation carrier system for biomedical applications.

Subsequently, in **publication II**, a modified *in-situ* gellable iEDDA-crosslinked hydrogel formulation was developed following functionalization of HA and PEG. Both successfully functionalized precursor polymers, HA-NB and 4-arm PEG-TZ, as well as heparin-modified 4-arm PEG-TZ, were employed to develop a hydrogel system with fast-crosslinking kinetics and a gelation time of 500 s after mixing both precursor solutions. Physicochemical and morphological characterization studies verified the covalent crosslinking of the formulation and its highly porous inner matrix. Heparin-modified hydrogels showed a reduced initial burst release of the protein fraction and different predominant growth factors from AEC-CM, specifically 30 and 40% of both VEGF and AREG. The reduced initial release was followed by a prolonged sustained release over time, with only a 60% of both growth factors released after 14 days. The therapeutic efficacy of the encapsulated AEC-CM efficacy was evident in the significant suppression of PBMC activation, since the combination of the hydrogel with AEC-CM enhanced the immunosuppressive effects observed with non-encapsulated AEC-CM. Moreover, the system induced a pronounced shift in macrophage phenotype towards the M2 phenotype, with the encapsulated AEC-CM inducing a stronger effect compared to the non-encapsulated. Therefore, the developed hydrogel formulation not only gradually released AEC-CM, but also amplified its biological effects, providing a synergistic therapeutic approach for immunomodulation and tissue regeneration. Further studies should be performed to gain a

better understanding of the immunomodulatory potential of the system in *in vivo* animal models. Efficacy studies could be performed in different tendon injury models, including studies in the same animal species or in other animal models to further study the xeno-compatibility off AEC-CM. Initially, safety and tissue penetration degree studies after local administration of the formulation should be performed to further investigate the tissue compatibility of the system. Subsequently, the modulatory potential of the locally administered system should be assessed following the analysis of the predominant phenotypic profile of macrophages isolated from the affected tissue. Moreover, histological analysis of the injured area should be performed to study the inflammatory state of the injured tissue after the local administration of the system, as well as studying the protein production and gene expression of specific pro-inflammatory mediators and pro-regenerative markers.

In **publication III**, MSC-EVs derived hybrid NPs were produced by microfluidic-sonication for mRNA encapsulation. The produced MSC-Hyb NPs owned moderately higher size and PDI values, 178.6 nm and 0.245 respectively, more negative ζ-potential, -19.5 mV, and reduced mRNA EE in comparison with standard LNPs. The performed physicochemical and EVs-derived surface antigens analysis confirmed the hybrid nature of the produced NPs, which showed the presence of EVs-derived surface proteins, including CD63, CD81 and CD105. Furthermore, MSC-Hyb NPs were found to be highly biocompatible and did not significantly reduce human TSPCs viability even after incubation with the highest concentration of 500 µg/mL. MSC-Hyb NPs proved to be feasible agents for the internalization and cytoplasmatic delivery of functional mRNA with reduced internalization rates and mRNA transfection efficacy in comparison with LNPs. Moreover, exposition to MSC-Hyb NPs loaded with COL1A1 mRNA caused a 2-fold increase in procollagen type I carboxy-terminal peptide production in TSPCs, similarly to LNPs. However, despite the efforts, the production of EVs-derived hybrid NPs remains a challenging task mainly due to the limited available knowledge regarding EVs composition and its impact on the development of hybrid NPs, as well as the limited tools available to fully characterize the conformation and structure of hybrid NPs. More in-depth studies may help to gain a better understanding of the observed limitations regarding the loading of mRNA-based cargos or reduced cell internalization, as well as to improve the drug delivery capabilities of the described nanosystems. Moreover, additional studies should be conducted to further support the functional delivery of COL1A1 mRNA, including ex vivo and in vivo studies in different models. Firstly, ex vivo studies should be performed to appropriately study the degree of tissue penetration achieved by MSC-Hyb NPs after their local administration in the tissue. Secondly, in vivo studies in animal models would be appropriate to assess the functional delivery of COL1A1 mRNA. Efficacy studies should include quantification of collagen type I production of the injured tissue after the administration of NPs and histological analysis of the injured tissue to study the ECM collagen structure. Quantification of pro-regenerative protein modulators should also be conducted to gain a better understanding of the pro-regenerative effect of the administered system. Moreover, after isolation of the specific tendons, mechanical studies of the injured tendons should be performed to study of the viscoelastic, dynamic and quasi-static mechanical properties of the tissue after the administration of the developed formulation.

In conclusion, the described work presents multiple alternatives for the development of hydrogel and NPs-based drug delivery systems for tendon therapy. The designed drug delivery systems showcased high potential as versatile platforms for the treatment of tendinopathy-derived conditions. With the aim to further study their promising applications, future perspectives may focus on the study of their efficacy in multiple *in vivo* models to further assess the efficacy of the produced systems. Additional studies must ensure that the developed

systems can successfully penetrate into the injured tissue after their local administration and remain safe, following the obtained results. Furthermore, the *in vivo* efficacy of the produced systems must be assessed, performing histological analysis of the treated tissues, studying their mechanical properties and assessing the degree of ECM regeneration.

References

1. Allen, T. M. & Cullis, P. R. Drug Delivery Systems: Entering the Mainstream. *Science (1979)* **303**, 1818–1822 (2004).
2. Li, C. *et al.* Recent progress in drug delivery. *Acta Pharm Sin B* **9**, 1145–1162 (2019).
3. Gao, J., Karp, J. M., Langer, R. & Joshi, N. The Future of Drug Delivery. *Chemistry of Materials* **35**, 359–363 (2023).
4. Bruno, B. J., Miller, G. D. & Lim, C. S. Basics and Recent Advances in Peptide and Protein Drug Delivery. *Ther Deliv* **4**, 1443–1467 (2013).
5. Zhong, R. *et al.* Hydrogels for RNA delivery. *Nature Materials 2023 22:7* **22**, 818–831 (2023).
6. Mitchell, M. J. *et al.* Engineering precision nanoparticles for drug delivery. *Nature Reviews Drug Discovery 2020 20:2* **20**, 101–124 (2020).
7. Cieza, A. *et al.* Global estimates of the need for rehabilitation based on the Global Burden of Disease study 2019: a systematic analysis for the Global Burden of Disease Study 2019. *The Lancet* **396**, 2006–2017 (2020).
8. Riley, G. Tendinopathy—from basic science to treatment. *Nature Clinical Practice Rheumatology 2008 4:2* **4**, 82–89 (2008).
9. Briggs-Price, S. *et al.* Incidence, demographics, characteristics and management of acute Achilles tendon rupture: An epidemiological study. *PLoS One* **19**, e0304197 (2024).
10. Čretnik, A. & Košir, R. Incidence of Achilles tendon rupture: 25-year regional analysis with a focus on bilateral ruptures. *Journal of International Medical Research* **51**, (2023).
11. Irby, A., Gutierrez, J., Chamberlin, C., Thomas, S. J. & Rosen, A. B. Clinical management of tendinopathy: A systematic review of systematic reviews evaluating the effectiveness of tendinopathy treatments. *Scand J Med Sci Sports* **30**, 1810–1826 (2020).
12. Maffulli, N., Longo, U. G., Loppini, M. & Denaro, V. Current treatment options for tendinopathy. *Expert Opin Pharmacother* **11**, 2177–2186 (2010).
13. Hoffman, A. S. The origins and evolution of “controlled” drug delivery systems. *Journal of Controlled Release* **132**, 153–163 (2008).
14. Park, H., Otte, A. & Park, K. Evolution of drug delivery systems: From 1950 to 2020 and beyond. *Journal of Controlled Release* **342**, 53–65 (2022).
15. Vargason, A. M., Anselmo, A. C. & Mitragotri, S. The evolution of commercial drug delivery technologies. *Nature Biomedical Engineering 2021 5:9* **5**, 951–967 (2021).
16. Hicks, H. R., Carreras, B. A., Holmes, J. A. & Langer, R. New Methods of Drug Delivery. *Science (1979)* **249**, 1527–1533 (1990).
17. Sultana, A., Zare, M., Thomas, V., Kumar, T. S. S. & Ramakrishna, S. Nano-based drug delivery systems: Conventional drug delivery routes, recent developments and future prospects. *Med Drug Discov* **15**, 100134 (2022).
18. Patra, J. K. *et al.* Nano based drug delivery systems: recent developments and future prospects. *Journal of Nanobiotechnology 2018 16:1* **16**, 1–33 (2018).
19. Ganta, S., Devalapally, H., Shahiwala, A. & Amiji, M. A review of stimuli-responsive nanocarriers for drug and gene delivery. *Journal of Controlled Release* **126**, 187–204 (2008).
20. Petros, R. A. & Desimone, J. M. Strategies in the design of nanoparticles for therapeutic applications. *Nature Reviews Drug Discovery 2010 9:8* **9**, 615–627 (2010).
21. Tibbitt, M. W., Dahlman, J. E. & Langer, R. Emerging Frontiers in Drug Delivery. *J Am Chem Soc* **138**, 704–717 (2016).
22. Leuner, C. & Dressman, J. Improving drug solubility for oral delivery using solid dispersions. *European Journal of Pharmaceutics and Biopharmaceutics* **50**, 47–60 (2000).
23. Uppal, S., Italiya, K. S., Chitkara, D. & Mittal, A. Nanoparticulate-based drug delivery systems for small molecule anti-diabetic drugs: An emerging paradigm for effective therapy. *Acta Biomater* **81**, 20–42 (2018).
24. Lee, K. Y. & Yuk, S. H. Polymeric protein delivery systems. *Prog Polym Sci* **32**, 669–697 (2007).
25. Paunovska, K., Loughrey, D. & Dahlman, J. E. Drug delivery systems for RNA therapeutics. *Nature Reviews Genetics 2022 23:5* **23**, 265–280 (2022).

26. Shin, H. *et al.* Recent Advances in RNA Therapeutics and RNA Delivery Systems Based on Nanoparticles. *Adv Ther (Weinh)* **1**, 1800065 (2018).
27. Poon, W., Kingston, B. R., Ouyang, B., Ngo, W. & Chan, W. C. W. A framework for designing delivery systems. *Nature Nanotechnology 2020 15:10* **15**, 819–829 (2020).
28. Blanco, E., Shen, H. & Ferrari, M. Principles of nanoparticle design for overcoming biological barriers to drug delivery. *Nature Biotechnology 2015 33:9* **33**, 941–951 (2015).
29. Thakur, S., Thakur, V. K. & Arotiba, O. A. History, Classification, Properties and Application of Hydrogels: An Overview. 29–50 (2018) doi:10.1007/978-981-10-6077-9_2.
30. Buwalda, S. J. *et al.* Hydrogels in a historical perspective: From simple networks to smart materials. *Journal of Controlled Release* **190**, 254–273 (2014).
31. Lee, S. C., Kwon, I. K. & Park, K. Hydrogels for delivery of bioactive agents: A historical perspective. *Adv Drug Deliv Rev* **65**, 17–20 (2013).
32. Cascone, S. & Lamberti, G. Hydrogel-based commercial products for biomedical applications: A review. *Int J Pharm* **573**, 118803 (2020).
33. Wheeler, J. C. *et al.* Evolution of hydrogel polymers as contact lenses, surface coatings, dressings, and drug delivery systems. *J Long Term Eff Med Implants* **6**, 207–217 (1996).
34. Liu, X., Liu, J., Lin, S. & Zhao, X. Hydrogel machines. *Materials Today* **36**, 102–124 (2020).
35. Lee, K. Y. & Mooney, D. J. Hydrogels for tissue engineering. *Chem Rev* **101**, 1869–1879 (2001).
36. Kopeček, J. Hydrogel biomaterials: A smart future? *Biomaterials* **28**, 5185–5192 (2007).
37. Holback, H., Yeo, Y. & Park, K. Hydrogel swelling behavior and its biomedical applications. *Biomedical Hydrogels* 3–24 (2011) doi:10.1533/9780857091383.1.3.
38. Kim, S. W., Bae, Y. H. & Okano, T. Hydrogels: Swelling, Drug Loading, and Release. *Pharmaceutical Research: An Official Journal of the American Association of Pharmaceutical Scientists* **9**, 283–290 (1992).
39. Dreiss, C. A. Hydrogel design strategies for drug delivery. *Curr Opin Colloid Interface Sci* **48**, 1–17 (2020).
40. Foudazi, R., Zowada, R., Manas-Zloczower, I. & Feke, D. L. Porous Hydrogels: Present Challenges and Future Opportunities. *Langmuir* **39**, 2092–2111 (2023).
41. Li, J., Illeperuma, W. R. K., Suo, Z. & Vlassak, J. J. Hybrid hydrogels with extremely high stiffness and toughness. *ACS Macro Lett* **3**, 520–523 (2014).
42. Arakaki, K. *et al.* Artificial cartilage made from a novel double-network hydrogel: In vivo effects on the normal cartilage and ex vivo evaluation of the friction property. *J Biomed Mater Res A* **93A**, 1160–1168 (2010).
43. Bodugoz-Senturk, H., Macias, C. E., Kung, J. H. & Muratoglu, O. K. Poly(vinyl alcohol)–acrylamide hydrogels as load-bearing cartilage substitute. *Biomaterials* **30**, 589–596 (2009).
44. Ahmed, E. M. Hydrogel: Preparation, characterization, and applications: A review. *J Adv Res* **6**, 105–121 (2015).
45. Tibbitt, M. W. & Anseth, K. S. Hydrogels as extracellular matrix mimics for 3D cell culture. *Biotechnol Bioeng* **103**, 655–663 (2009).
46. Geckil, H., Xu, F., Zhang, X., Moon, S. & Demirci, U. Engineering Hydrogels as Extracellular Matrix Mimics. *Nanomedicine* **5**, 469–484 (2010).
47. Rehmann, M. S. *et al.* Tuning and Predicting Mesh Size and Protein Release from Step Growth Hydrogels. *Biomacromolecules* **18**, 3131–3142 (2017).
48. Appel, E. A., Forster, R. A., Rowland, M. J. & Scherman, O. A. The control of cargo release from physically crosslinked hydrogels by crosslink dynamics. *Biomaterials* **35**, 9897–9903 (2014).
49. Hegab, R. A. *et al.* Effect of network mesh size and swelling to the drug delivery from pH responsive hydrogels. *J Appl Polym Sci* **137**, 48767 (2020).
50. Varaprasad, K., Raghavendra, G. M., Jayaramudu, T., Yallapu, M. M. & Sadiku, R. A mini review on hydrogels classification and recent developments in miscellaneous applications. *Materials Science and Engineering: C* **79**, 958–971 (2017).
51. Ullah, F., Othman, M. B. H., Javed, F., Ahmad, Z. & Akil, H. M. Classification, processing and application of hydrogels: A review. *Materials Science and Engineering: C* **57**, 414–433 (2015).
52. Willner, I. Stimuli-Controlled Hydrogels and Their Applications. *Acc Chem Res* **50**, 657–658 (2017).

53. Deng, Z., Yu, R. & Guo, B. Stimuli-responsive conductive hydrogels: design, properties, and applications. *Mater Chem Front* **5**, 2092–2123 (2021).
54. Li, J. & Mooney, D. J. Designing hydrogels for controlled drug delivery. *Nature Reviews Materials 2016 1:12* **1**, 1–17 (2016).
55. Worch, J. C. *et al.* Stereochemical enhancement of polymer properties. *Nature Reviews Chemistry 2019 3:9* **3**, 514–535 (2019).
56. Katyal, P., Mahmoudinobar, F. & Montclare, J. K. Recent trends in peptide and protein-based hydrogels. *Curr Opin Struct Biol* **63**, 97–105 (2020).
57. Shi, L. *et al.* Self-Healing Polymeric Hydrogel Formed by Metal–Ligand Coordination Assembly: Design, Fabrication, and Biomedical Applications. *Macromol Rapid Commun* **40**, 1800837 (2019).
58. Arkenberg, M. R., Nguyen, H. D. & Lin, C. C. Recent advances in bio-orthogonal and dynamic crosslinking of biomimetic hydrogels. *J Mater Chem B* **8**, 7835–7855 (2020).
59. Madl, C. M., Heilshorn, S. C., Madl, C. M. & Heilshorn, S. C. Bioorthogonal Strategies for Engineering Extracellular Matrices. *Adv Funct Mater* **28**, 1706046 (2018).
60. Ashley, G. W., Henise, J., Reid, R. & Santi, D. V. Hydrogel drug delivery system with predictable and tunable drug release and degradation rates. *Proc Natl Acad Sci U S A* **110**, 2318–2323 (2013).
61. Hosaka, S., Ozawa, H. & Tanzawa, H. Controlled release of drugs from hydrogel matrices. *J Appl Polym Sci* **23**, 2089–2098 (1979).
62. Brandl, F. *et al.* Hydrogel-based drug delivery systems: Comparison of drug diffusivity and release kinetics. *Journal of Controlled Release* **142**, 221–228 (2010).
63. Meenach, S. A., Anderson, K. W. & Hilt, J. Z. Hydrogel Nanocomposites: Biomedical Applications, Biocompatibility, and Toxicity Analysis. 131–157 (2009) doi:10.1007/978-0-387-78608-7_7.
64. Pei, X., Wang, J., Cong, Y. & Fu, J. Recent progress in polymer hydrogel bioadhesives. *Journal of Polymer Science* **59**, 1312–1337 (2021).
65. Clegg, J. R., Adebowale, K., Zhao, Z. & Mitragotri, S. Hydrogels in the clinic: An update. *Bioeng Transl Med* e10680 (2024) doi:10.1002/BTM2.10680.
66. Zöller, K., To, D. & Bernkop-Schnürch, A. Biomedical applications of functional hydrogels: Innovative developments, relevant clinical trials and advanced products. *Biomaterials* **312**, 122718 (2025).
67. Mehta, P., Sharma, M. & Devi, M. Hydrogels: An overview of its classifications, properties, and applications. *J Mech Behav Biomed Mater* **147**, 106145 (2023).
68. Spang, M. T. & Christman, K. L. Extracellular matrix hydrogel therapies: In vivo applications and development. *Acta Biomater* **68**, 1–14 (2018).
69. Kasai, R. D. *et al.* A review on hydrogels classification and recent developments in biomedical applications. *International Journal of Polymeric Materials and Polymeric Biomaterials* **72**, 1059–1069 (2023).
70. Khan, S., Ullah, A., Ullah, K. & Rehman, N. U. Insight into hydrogels. *Des Monomers Polym* **19**, 456–478 (2016).
71. Bao, Z. *et al.* Natural Polymer-Based Hydrogels with Enhanced Mechanical Performances: Preparation, Structure, and Property. *Adv Healthc Mater* **8**, 1900670 (2019).
72. Catoira, M. C., Fusaro, L., Di Francesco, D., Ramella, M. & Boccafoschi, F. Overview of natural hydrogels for regenerative medicine applications. *J Mater Sci Mater Med* **30**, 1–10 (2019).
73. Wang, Z., Wei, H., Huang, Y., Wei, Y. & Chen, J. Naturally sourced hydrogels: emerging fundamental materials for next-generation healthcare sensing. *Chem Soc Rev* **52**, 2992–3034 (2023).
74. Yang, Q., Peng, J., Xiao, H., Xu, X. & Qian, Z. Polysaccharide hydrogels: Functionalization, construction and served as scaffold for tissue engineering. *Carbohydr Polym* **278**, 118952 (2022).
75. Cao, H., Duan, L., Zhang, Y., Cao, J. & Zhang, K. Current hydrogel advances in physicochemical and biological response-driven biomedical application diversity. *Signal Transduction and Targeted Therapy 2021 6:1* **6**, 1–31 (2021).
76. Jonker, A. M., Löwik, D. W. P. M. & Van Hest, J. C. M. Peptide- and protein-based hydrogels. *Chemistry of Materials* **24**, 759–773 (2012).
77. Wang, Y. *et al.* Recent advances in the fabrication, functionalization, and bioapplications of peptide hydrogels. *Soft Matter* **16**, 10029–10045 (2020).
78. Kopeček, J. & Yang, J. Peptide-directed self-assembly of hydrogels. *Acta Biomater* **5**, 805–816 (2009).

79. Laurent, T. C., Laurent, U. B. G. & Fraser, J. R. E. The structure and function of hyaluronan: An overview. *Immunol Cell Biol* **74**, a1–a7 (1996).
80. Laurent, T. C., Laurent, U. B. G. & Fraser, J. R. Functions of hyaluronan. *Ann Rheum Dis* **54**, 429–432 (1995).
81. He, L. & Theato, P. Collagen and collagen mimetic peptide conjugates in polymer science. *Eur Polym J* **49**, 2986–2997 (2013).
82. Lin, K. *et al.* Advanced Collagen-Based Biomaterials for Regenerative Biomedicine. *Adv Funct Mater* **29**, 1804943 (2019).
83. Peppas, N. A., Keys, K. B., Torres-Lugo, M. & Lowman, A. M. Poly(ethylene glycol)-containing hydrogels in drug delivery. *Journal of Controlled Release* **62**, 81–87 (1999).
84. D'souza, A. A. & Shegokar, R. Polyethylene glycol (PEG): a versatile polymer for pharmaceutical applications. *Expert Opin Drug Deliv* **13**, 1257–1275 (2016).
85. Zhao, W., Jin, X., Cong, Y., Liu, Y. & Fu, J. Degradable natural polymer hydrogels for articular cartilage tissue engineering. *Journal of Chemical Technology & Biotechnology* **88**, 327–339 (2013).
86. Hu, W., Wang, Z., Xiao, Y., Zhang, S. & Wang, J. Advances in crosslinking strategies of biomedical hydrogels. *Biomater Sci* **7**, 843–855 (2019).
87. Rosales, A. M. & Anseth, K. S. The design of reversible hydrogels to capture extracellular matrix dynamics. *Nature Reviews Materials 2016 1:2* **1**, 1–15 (2016).
88. Catoira, M. C., González-Payo, J., Fusaro, L., Ramella, M. & Boccafoschi, F. Natural hydrogels R&D process: technical and regulatory aspects for industrial implementation. *J Mater Sci Mater Med* **31**, 1–16 (2020).
89. Gyles, D. A., Castro, L. D., Silva, J. O. C. & Ribeiro-Costa, R. M. A review of the designs and prominent biomedical advances of natural and synthetic hydrogel formulations. *Eur Polym J* **88**, 373–392 (2017).
90. Madduma-Bandarage, U. S. K. & Madihally, S. V. Synthetic hydrogels: Synthesis, novel trends, and applications. *J Appl Polym Sci* **138**, 50376 (2021).
91. RATNER, B. D. & HOFFMAN, A. S. Synthetic Hydrogels for Biomedical Applications. 1–36 (1976) doi:10.1021/BK-1976-0031.CH001.
92. Unal, A. Z. & West, J. L. Synthetic ECM: Bioactive Synthetic Hydrogels for 3D Tissue Engineering. *Bioconjug Chem* **31**, 2253–2271 (2020).
93. Khan, F. *et al.* Synthesis, classification and properties of hydrogels: their applications in drug delivery and agriculture. *J Mater Chem B* **10**, 170–203 (2022).
94. Hoffman, A. S. Hydrogels for biomedical applications. *Adv Drug Deliv Rev* **64**, 18–23 (2012).
95. Cho, E. *et al.* A novel synthetic route for the preparation of hydrolytically degradable synthetic hydrogels. *J Biomed Mater Res A* **90A**, 1073–1082 (2009).
96. Heyde, M. Ecological considerations on the use and production of biosynthetic and synthetic biodegradable polymers. *Polym Degrad Stab* **59**, 3–6 (1998).
97. Voorhaar, L. & Hoogenboom, R. Supramolecular polymer networks: hydrogels and bulk materials. *Chem Soc Rev* **45**, 4013–4031 (2016).
98. Kuo, C. K. & Ma, P. X. Ionically crosslinked alginate hydrogels as scaffolds for tissue engineering: Part 1. Structure, gelation rate and mechanical properties. *Biomaterials* **22**, 511–521 (2001).
99. Berger, J. *et al.* Structure and interactions in covalently and ionically crosslinked chitosan hydrogels for biomedical applications. *European Journal of Pharmaceutics and Biopharmaceutics* **57**, 19–34 (2004).
100. Bustamante-Torres, M. *et al.* Hydrogels Classification According to the Physical or Chemical Interactions and as Stimuli-Sensitive Materials. *Gels 2021, Vol. 7, Page 182* **7**, 182 (2021).
101. Hennink, W. E. & van Nostrum, C. F. Novel crosslinking methods to design hydrogels. *Adv Drug Deliv Rev* **64**, 223–236 (2012).
102. Xue, X. *et al.* Fabrication of physical and chemical crosslinked hydrogels for bone tissue engineering. *Bioact Mater* **12**, 327–339 (2022).
103. Perera, M. M. & Ayres, N. Dynamic covalent bonds in self-healing, shape memory, and controllable stiffness hydrogels. *Polym Chem* **11**, 1410–1423 (2020).
104. Rizwan, M., Baker, A. E. G. & Shoichet, M. S. Designing Hydrogels for 3D Cell Culture Using Dynamic Covalent Crosslinking. *Adv Healthc Mater* **10**, 2100234 (2021).

105. Lee, K. Y., Bouhadir, K. H. & Mooney, D. J. Controlled degradation of hydrogels using multi-functional cross-linking molecules. *Biomaterials* **25**, 2461–2466 (2004).
106. Gao, Y. *et al.* Covalently Crosslinked Hydrogels via Step-Growth Reactions: Crosslinking Chemistries, Polymers, and Clinical Impact. *Advanced Materials* **33**, 2006362 (2021).
107. Výborný, K. *et al.* Genipin and EDC crosslinking of extracellular matrix hydrogel derived from human umbilical cord for neural tissue repair. *Scientific Reports 2019 9:1* **9**, 1–15 (2019).
108. Tran, D. L., Le Thi, P., Hoang Thi, T. T. & Park, K. D. Novel enzymatically crosslinked chitosan hydrogels with free-radical-scavenging property and promoted cellular behaviors under hyperglycemia. *Progress in Natural Science: Materials International* **30**, 661–668 (2020).
109. Chen, Q., Chen, H., Zhu, L. & Zheng, J. Fundamentals of double network hydrogels. *J Mater Chem B* **3**, 3654–3676 (2015).
110. Gu, Z. *et al.* Double network hydrogel for tissue engineering. *Wiley Interdiscip Rev Nanomed Nanobiotechnol* **10**, e1520 (2018).
111. Xu, X., Jerca, V. V. & Hoogenboom, R. Bioinspired double network hydrogels: from covalent double network hydrogels via hybrid double network hydrogels to physical double network hydrogels. *Mater Horiz* **8**, 1173–1188 (2021).
112. Chen, Q., Chen, H., Zhu, L. & Zheng, J. Engineering of Tough Double Network Hydrogels. *Macromol Chem Phys* **217**, 1022–1036 (2016).
113. Gong, J. P. Why are double network hydrogels so tough? *Soft Matter* **6**, 2583–2590 (2010).
114. Paiva, M. T. P. *et al.* Crosslinking Methods in Polysaccharide-Based Hydrogels for Drug Delivery Systems. *Biomedical Materials & Devices 2023 2:1* **2**, 288–306 (2023).
115. Devaraj, N. K. & Finn, M. G. Introduction: Click Chemistry. *Chem Rev* **121**, 6697–6698 (2021).
116. Xi, W., Scott, T. F., Kloxin, C. J. & Bowman, C. N. Click Chemistry in Materials Science. *Adv Funct Mater* **24**, 2572–2590 (2014).
117. Moses, J. E. & Moorhouse, A. D. The growing applications of click chemistry. *Chem Soc Rev* **36**, 1249–1262 (2007).
118. Hein, C. D., Liu, X. M. & Wang, D. Click Chemistry, A Powerful Tool for Pharmaceutical Sciences. *Pharmaceutical Research 2008 25:10* **25**, 2216–2230 (2008).
119. Binder, W. H. & Sachsenhofer, R. 'Click' Chemistry in Polymer and Material Science: An Update. *Macromol Rapid Commun* **29**, 952–981 (2008).
120. Baskin, J. M. & Bertozzi, C. R. Bioorthogonal Click Chemistry: Covalent Labeling in Living Systems. *QSAR Comb Sci* **26**, 1211–1219 (2007).
121. Best, M. D. Click chemistry and bioorthogonal reactions: Unprecedented selectivity in the labeling of biological molecules. *Biochemistry* **48**, 6571–6584 (2009).
122. Presolski, S. I., Hong, V. P. & Finn, M. G. Copper-Catalyzed Azide–Alkyne Click Chemistry for Bioconjugation. *Curr Protoc Chem Biol* **3**, 153–162 (2011).
123. Singh, M. S., Chowdhury, S. & Koley, S. Advances of azide-alkyne cycloaddition-click chemistry over the recent decade. *Tetrahedron* **72**, 5257–5283 (2016).
124. Rodionov, V. O., Fokin, V. V. & Finn, M. G. Mechanism of the Ligand-Free CuI-Catalyzed Azide–Alkyne Cycloaddition Reaction. *Angewandte Chemie International Edition* **44**, 2210–2215 (2005).
125. Himo, F. *et al.* Copper(I)-catalyzed synthesis of azoles. DFT study predicts unprecedented reactivity and intermediates. *J Am Chem Soc* **127**, 210–216 (2005).
126. Chen, M. M., Kopittke, P. M., Zhao, F. J. & Wang, P. Applications and opportunities of click chemistry in plant science. *Trends Plant Sci* **29**, 167–178 (2024).
127. Sutherland, B. P., Kabra, M. & Kloxin, C. J. Expanding the thiol–X toolbox: photoinitiation and materials application of the acid-catalyzed thiol–ene (ACT) reaction. *Polym Chem* **12**, 1562–1570 (2021).
128. Hong, V., Steinmetz, N. F., Manchester, M. & Finn, M. G. Labeling live cells by copper-catalyzed alkyne-azide click chemistry. *Bioconjug Chem* **21**, 1912–1916 (2010).
129. Abel, G. R., Calabrese, Z. A., Ayco, J., Hein, J. E. & Ye, T. Measuring and Suppressing the Oxidative Damage to DNA during Cu(I)-Catalyzed Azide-Alkyne Cycloaddition. *Bioconjug Chem* **27**, 698–704 (2016).
130. Agard, N. J., Prescher, J. A. & Bertozzi, C. R. A strain-promoted [3 + 2] azide-alkyne cycloaddition for covalent modification of biomolecules in living systems. *J Am Chem Soc* **126**, 15046–15047 (2004).

131. Li, K., Fong, D., Meichsner, E. & Adronov, A. A Survey of Strain-Promoted Azide–Alkyne Cycloaddition in Polymer Chemistry. *Chemistry – A European Journal* **27**, 5057–5073 (2021).
132. Svatunek, D. *et al.* Efficient low-cost preparation of trans-cyclooctenes using a simplified flow setup for photoisomerization. *Monatsh Chem* **147**, 579–585 (2016).
133. Northrop, B. H. & Coffey, R. N. Thiol-ene click chemistry: Computational and kinetic analysis of the influence of alkene functionality. *J Am Chem Soc* **134**, 13804–13817 (2012).
134. Sutherland, B. P., Kabra, M. & Kloxin, C. J. Expanding the thiol–X toolbox: photoinitiation and materials application of the acid-catalyzed thiol–ene (ACT) reaction. *Polym Chem* **12**, 1562–1570 (2021).
135. Hoyle, C. E., Bowman, C. N., Bowman, C. N. & Hoyle, C. E. Thiol–Ene Click Chemistry. *Angewandte Chemie International Edition* **49**, 1540–1573 (2010).
136. Kade, M. J., Burke, D. J. & Hawker, C. J. The power of thiol-ene chemistry. *J Polym Sci A Polym Chem* **48**, 743–750 (2010).
137. Hoyle, C. E., Lowe, A. B. & Bowman, C. N. Thiol-click chemistry: a multifaceted toolbox for small molecule and polymer synthesis. *Chem Soc Rev* **39**, 1355–1387 (2010).
138. Lowe, A. B. Thiol-ene “click” reactions and recent applications in polymer and materials synthesis. *Polym Chem* **1**, 17–36 (2010).
139. Nair, D. P. *et al.* The Thiol-Michael addition click reaction: A powerful and widely used tool in materials chemistry. *Chemistry of Materials* **26**, 724–744 (2014).
140. Sun, Y. *et al.* Thiol Michael addition reaction: a facile tool for introducing peptides into polymer-based gene delivery systems. *Polym Int* **67**, 25–31 (2018).
141. Kölmel, D. K. & Kool, E. T. Oximes and Hydrazones in Bioconjugation: Mechanism and Catalysis. *Chem Rev* **117**, 10358–10376 (2017).
142. Knall, A. C. & Slugovc, C. Inverse electron demand Diels–Alder (iEDDA)-initiated conjugation: a (high) potential click chemistry scheme. *Chem Soc Rev* **42**, 5131–5142 (2013).
143. Oliveira, B. L., Guo, Z. & Bernardes, G. J. L. Inverse electron demand Diels–Alder reactions in chemical biology. *Chem Soc Rev* **46**, 4895–4950 (2017).
144. Knall, A. C. & Slugovc, C. Inverse electron demand Diels–Alder (iEDDA)-initiated conjugation: a (high) potential click chemistry scheme. *Chem Soc Rev* **42**, 5131–5142 (2013).
145. Pagel, M. Inverse electron demand Diels–Alder (IEDDA) reactions in peptide chemistry. *Journal of Peptide Science* **25**, e3141 (2019).
146. Png, Z. M., Zeng, H., Ye, Q. & Xu, J. Inverse-Electron-Demand Diels–Alder Reactions: Principles and Applications. *Chem Asian J* **12**, 2142–2159 (2017).
147. Li, X. & Xiong, Y. Application of ‘Click’ Chemistry in Biomedical Hydrogels. *ACS Omega* **7**, 36918–36928 (2022).
148. Alge, D. L., Azagarsamy, M. A., Donohue, D. F. & Anseth, K. S. Synthetically tractable click hydrogels for three-dimensional cell culture formed using tetrazine-norbornene chemistry. *Biomacromolecules* **14**, 949–953 (2013).
149. Anugrah, D. S. B., Ramesh, K., Kim, M., Hyun, K. & Lim, K. T. Near-infrared light-responsive alginate hydrogels based on diselenide-containing cross-linkage for on demand degradation and drug release. *Carbohydr Polym* **223**, 115070 (2019).
150. Rizwan, A. *et al.* Gelatin-based NIR and reduction-responsive injectable hydrogels cross-linked through IEDDA click chemistry for drug delivery application. *Eur Polym J* **191**, 112019 (2023).
151. Delplace, V. *et al.* Nonswelling, Ultralow Content Inverse Electron-Demand Diels–Alder Hyaluronan Hydrogels with Tunable Gelation Time: Synthesis and In Vitro Evaluation. *Adv Funct Mater* **30**, 1903978 (2020).
152. Malkoch, M. *et al.* Synthesis of well-defined hydrogel networks using Click chemistry. *Chemical Communications* 2774–2776 (2006) doi:10.1039/B603438A.
153. Chen, R. T. *et al.* Photoinitiated alkyne-azide click and radical cross-linking reactions for the patterning of PEG hydrogels. *Biomacromolecules* **13**, 889–895 (2012).
154. Ossipov, D. A. & Hilborn, J. Poly(vinyl alcohol)-based hydrogels formed by ‘click chemistry’. *Macromolecules* **39**, 1709–1718 (2006).
155. Hu, X., Li, D., Zhou, F. & Gao, C. Biological hydrogel synthesized from hyaluronic acid, gelatin and chondroitin sulfate by click chemistry. *Acta Biomater* **7**, 1618–1626 (2011).

156. Crescenzi, V., Cornelio, L., Di Meo, C., Nardecchia, S. & Lamanna, R. Novel hydrogels via click chemistry: Synthesis and potential biomedical applications. *Biomacromolecules* **8**, 1844–1850 (2007).
157. Liu, S. Q., Rachel Ee, P. L., Ke, C. Y., Hedrick, J. L. & Yang, Y. Y. Biodegradable poly(ethylene glycol)–peptide hydrogels with well-defined structure and properties for cell delivery. *Biomaterials* **30**, 1453–1461 (2009).
158. Van Dijk, M., Van Nostrum, C. F., Hennink, W. E., Rijkers, D. T. S. & Liskamp, R. M. J. Synthesis and characterization of enzymatically biodegradable peg and peptide-based hydrogels prepared by click chemistry. *Biomacromolecules* **11**, 1608–1614 (2010).
159. Li, F., He, J., Zhang, M. & Ni, P. A pH-sensitive and biodegradable supramolecular hydrogel constructed from a PEGylated polyphosphoester-doxorubicin prodrug and α-cyclodextrin. *Polym Chem* **6**, 5009–5014 (2015).
160. Zhang, J., Xu, X. D., Wu, D. Q., Zhang, X. Z. & Zhuo, R. X. Synthesis of thermosensitive P(NIPAAm-co-HEMA)/cellulose hydrogels via “click” chemistry. *Carbohydr Polym* **77**, 583–589 (2009).
161. Jiang, H. *et al.* An injectable and fast-degradable poly(ethylene glycol) hydrogel fabricated via bioorthogonal strain-promoted azide–alkyne cycloaddition click chemistry. *Soft Matter* **11**, 6029–6036 (2015).
162. Su, X. *et al.* An injectable PEG-based hydrogel synthesized by strain-promoted alkyne–azide cycloaddition for use as an embolic agent. *RSC Adv* **6**, 2904–2909 (2016).
163. Zheng, J. *et al.* Strain-promoted cross-linking of PEG-based hydrogels via copper- free cycloaddition. *ACS Macro Lett* **1**, 1071–1073 (2012).
164. Fu, S., Dong, H., Deng, X., Zhuo, R. & Zhong, Z. Injectable hyaluronic acid/poly(ethylene glycol) hydrogels crosslinked via strain-promoted azide-alkyne cycloaddition click reaction. *Carbohydr Polym* **169**, 332–340 (2017).
165. Jain, E. *et al.* Copper-Free Azide-Alkyne Cycloaddition for Peptide Modification of Alginate Hydrogels. *ACS Appl Bio Mater* **4**, 1229–1237 (2021).
166. Cui, J. *et al.* Synthetically simple, highly resilient hydrogels. *Biomacromolecules* **13**, 584–588 (2012).
167. Aimetti, A. A., Machen, A. J. & Anseth, K. S. Poly(ethylene glycol) hydrogels formed by thiol-ene photopolymerization for enzyme-responsive protein delivery. *Biomaterials* **30**, 6048–6054 (2009).
168. Stevens, D. M. *et al.* Semibranched polyglycidols as “fillers” in polycarbonate hydrogels to tune hydrophobic drug release. *Polym Chem* **6**, 1096–1102 (2015).
169. Kyburz, K. A. & Anseth, K. S. Three-dimensional hMSC motility within peptide-functionalized PEG-based hydrogels of varying adhesivity and crosslinking density. *Acta Biomater* **9**, 6381–6392 (2013).
170. Fairbanks, B. D. *et al.* A Versatile Synthetic Extracellular Matrix Mimic via Thiol-Norbornene Photopolymerization. *Advanced Materials* **21**, 5005–5010 (2009).
171. Holloway, J. L., Ma, H., Rai, R., Hankenson, K. D. & Burdick, J. A. Synergistic Effects of SDF-1α and BMP-2 Delivery from Proteolytically Degradable Hyaluronic Acid Hydrogels for Bone Repair. *Macromol Biosci* **15**, 1218–1223 (2015).
172. Ziegler, C. E., Graf, M., Nagaoka, M., Lehr, H. & Goepferich, A. M. In Situ Forming iEDDA Hydrogels with Tunable Gelation Time Release High-Molecular Weight Proteins in a Controlled Manner over an Extended Time. *Biomacromolecules* **22**, 3223–3236 (2021).
173. Lueckgen, A. *et al.* Hydrolytically-degradable click-crosslinked alginate hydrogels. *Biomaterials* **181**, 189–198 (2018).
174. Ali, I. *et al.* Reduction-responsive and bioorthogonal carboxymethyl cellulose based soft hydrogels cross-linked via IEDDA click chemistry for cancer therapy application. *Int J Biol Macromol* **219**, 109–120 (2022).
175. Vu, T. T., Gulfam, M., Jo, S. H., Park, S. H. & Lim, K. T. Injectable and biocompatible alginate-derived porous hydrogels cross-linked by IEDDA click chemistry for reduction-responsive drug release application. *Carbohydr Polym* **278**, 118964 (2022).
176. Arkenberg, M. R., Koehler, K. & Lin, C. C. Heparinized Gelatin-Based Hydrogels for Differentiation of Induced Pluripotent Stem Cells. *Biomacromolecules* **23**, 4141–4152 (2022).
177. Khansari, M. M. *et al.* Classification of Hydrogels Based on Their Source: A Review and Application in Stem Cell Regulation. *JOM* **69**, 1340–1347 (2017).

178. Kumar, A. C. & Erothu, H. Synthetic Polymer Hydrogels. *Biomedical Applications of Polymeric Materials and Composites* 141–162 (2016) doi:10.1002/9783527690916.CH6.
179. Van Vlierberghe, S., Dubruel, P. & Schacht, E. Biopolymer-based hydrogels as scaffolds for tissue engineering applications: A review. *Biomacromolecules* **12**, 1387–1408 (2011).
180. Karg, M. *et al.* Nanogels and Microgels: From Model Colloids to Applications, Recent Developments, and Future Trends. *Langmuir* **35**, 6231–6255 (2019).
181. Suzuki, D. Nanogel/Microgel Science and beyond. *Langmuir* **39**, 7525–7529 (2023).
182. Suzuki, D., Horigome, K., Kureha, T., Matsui, S. & Watanabe, T. Polymeric hydrogel microspheres: design, synthesis, characterization, assembly and applications. *Polymer Journal 2017 49:10* **49**, 695–702 (2017).
183. Yu, L. *et al.* Microfluidic formation of core-shell alginate microparticles for protein encapsulation and controlled release. *J Colloid Interface Sci* **539**, 497–503 (2019).
184. Guerzoni, L. P. B. *et al.* Microfluidic fabrication of polyethylene glycol microgel capsules with tailored properties for the delivery of biomolecules. *Biomater Sci* **5**, 1549–1557 (2017).
185. Plamper, F. A. & Richtering, W. Functional Microgels and Microgel Systems. *Acc Chem Res* **50**, 131–140 (2017).
186. Mora-Boza, A. *et al.* Microfluidics generation of chitosan microgels containing glycerylphytate crosslinker for in situ human mesenchymal stem cells encapsulation. *Materials Science and Engineering: C* **120**, 111716 (2021).
187. Gwon, K. *et al.* Bioactive hydrogel microcapsules for guiding stem cell fate decisions by release and reloading of growth factors. *Bioact Mater* **15**, 1–14 (2022).
188. Goh, M. C. & Tae, G. Mesenchymal stem cell-encapsulated cellulose nanofiber microbeads and enhanced biological activities by hyaluronic acid incorporation. *Carbohydr Polym* **280**, 119026 (2022).
189. Qiu, G. *et al.* Human periodontal ligament stem cell encapsulation in alginate-fibrin-platelet lysate microbeads for dental and craniofacial regeneration. *J Dent* **124**, 104219 (2022).
190. Kabanov, A. V, Vinogradov, S. V, Kabanov, A. V & Vinogradov, S. V. Nanogels as Pharmaceutical Carriers: Finite Networks of Infinite Capabilities. *Angewandte Chemie International Edition* **48**, 5418–5429 (2009).
191. Neamtu, I., Rusu, A. G., Diaconu, A., Nita, L. E. & Chiriac, A. P. Basic concepts and recent advances in nanogels as carriers for medical applications. *Drug Deliv* **24**, 539–557 (2017).
192. Sivaram, A. J., Rajitha, P., Maya, S., Jayakumar, R. & Sabitha, M. Nanogels for delivery, imaging and therapy. *Wiley Interdiscip Rev Nanomed Nanobiotechnol* **7**, 509–533 (2015).
193. Li, D., van Nostrum, C. F., Mastrobattista, E., Vermonden, T. & Hennink, W. E. Nanogels for intracellular delivery of biotherapeutics. *Journal of Controlled Release* **259**, 16–28 (2017).
194. Lee, H., Mok, H., Lee, S., Oh, Y. K. & Park, T. G. Target-specific intracellular delivery of siRNA using degradable hyaluronic acid nanogels. *Journal of Controlled Release* **119**, 245–252 (2007).
195. Oh, J. K., Drumright, R., Siegwart, D. J. & Matyjaszewski, K. The development of microgels/nanogels for drug delivery applications. *Prog Polym Sci* **33**, 448–477 (2008).
196. Hamzah, Y. Bin, Hashim, S. & Rahman, W. A. W. A. Synthesis of polymeric nano/microgels: a review. *Journal of Polymer Research 2017 24:9* **24**, 1–19 (2017).
197. Yang, S. *et al.* Fabricated technology of biomedical micro-nano hydrogel. *Biomedical Technology* **2**, 31–48 (2023).
198. Oh, J. K., Lee, D. I. & Park, J. M. Biopolymer-based microgels/nanogels for drug delivery applications. *Prog Polym Sci* **34**, 1261–1282 (2009).
199. Giunchedi, P., Genta, I., Conti, B., Muzzarelli, R. A. A. & Conte, U. Preparation and characterization of ampicillin loaded methylpyrrolidinone chitosan and chitosan microspheres. *Biomaterials* **19**, 157–161 (1998).
200. Shi, X. Y. & Tan, T. W. Preparation of chitosan/ethylcellulose complex microcapsule and its application in controlled release of Vitamin D2. *Biomaterials* **23**, 4469–4473 (2002).
201. He, P., Davis, S. S. & Illum, L. In vitro evaluation of the mucoadhesive properties of chitosan microspheres. *Int J Pharm* **166**, 75–88 (1998).
202. Huang, Y. C., Yeh, M. K. & Chiang, C. H. Formulation factors in preparing BTM–chitosan microspheres by spray drying method. *Int J Pharm* **242**, 239–242 (2002).

203. Shi, X. Y. & Tan, T. W. Preparation of chitosan/ethylcellulose complex microcapsule and its application in controlled release of Vitamin D2. *Biomaterials* **23**, 4469–4473 (2002).
204. Zhao, W. *et al.* In situ cross-linking of stimuli-responsive hemicellulose microgels during spray drying. *ACS Appl Mater Interfaces* **7**, 4202–4215 (2015).
205. Gómez, C., Benito, M., Katime, I., Teijón, J. M. & Blanco, M. D. In vitro transdermal and biological evaluation of ALA-loaded poly(N-isopropylacrylamide) and poly(N-isopropylacrylamide-co-acrylic acid) microgels for photodynamic therapy. *J Microencapsul* **29**, 626–635 (2012).
206. Gansau, J., Kelly, L. & Buckley, C. T. Influence of key processing parameters and seeding density effects of microencapsulated chondrocytes fabricated using electrohydrodynamic spraying. *Biofabrication* **10**, 035011 (2018).
207. Lai, W. F. *et al.* Electrospray-mediated preparation of compositionally homogeneous core–shell hydrogel microspheres for sustained drug release. *RSC Adv* **7**, 44482–44491 (2017).
208. Xu, P. *et al.* Improving the thermostability and activity of Paenibacillus pasadenensis chitinase through semi-rational design. *Int J Biol Macromol* **150**, 9–15 (2020).
209. Vossoughi, A., T Matthew, H. W. & Howard T Matthew, C. W. Encapsulation of mesenchymal stem cells in glycosaminoglycans-chitosan polyelectrolyte microcapsules using electrospraying technique: Investigating capsule morphology and cell viability. *Bioeng Transl Med* **3**, 265–274 (2018).
210. Liu, S., Fang, Z. & Ng, K. Electrospray alginate-Konjac glucomannan microgel as efficient colon-targeted delivery vehicle for quercetin. *Food Biosci* **56**, 103307 (2023).
211. Moroni, L. *et al.* Biofabrication strategies for 3D in vitro models and regenerative medicine. *Nature Reviews Materials 2018 3:5* **3**, 21–37 (2018).
212. Seymour, A. J., Shin, S. & Heilshorn, S. C. 3D Printing of Microgel Scaffolds with Tunable Void Fraction to Promote Cell Infiltration. *Adv Healthc Mater* **10**, 2100644 (2021).
213. Chai, N. *et al.* Construction of 3D printed constructs based on microfluidic microgel for bone regeneration. *Compos B Eng* **223**, 109100 (2021).
214. Mandrycky, C., Wang, Z., Kim, K. & Kim, D. H. 3D bioprinting for engineering complex tissues. *Biotechnol Adv* **34**, 422–434 (2016).
215. Feng, Q. *et al.* Assembling Microgels via Dynamic Cross-Linking Reaction Improves Printability, Microporosity, Tissue-Adhesion, and Self-Healing of Microgel Bioink for Extrusion Bioprinting. *ACS Appl Mater Interfaces* **14**, 15653–15666 (2022).
216. Simakova, A., Averick, S., Jazani, A. M. & Matyjaszewski, K. Controlling Size and Surface Chemistry of Cationic Nanogels by Inverse Microemulsion ATRP. *Macromol Chem Phys* **224**, 2200210 (2023).
217. Peng, Y. *et al.* Nanogels loading curcumin in situ through microemulsion photopolymerization for enhancement of antitumor effects. *J Mater Chem B* **10**, 3293–3302 (2022).
218. Wang, Y., Deng, J., Zhong, W., Kong, L. & Yang, W. Facile Surface Superhydrophilic Modification: NVP/MBA Inverse Microemulsion Surface-Grafting Polymerization Initiated by UV Light. *Macromol Rapid Commun* **26**, 1788–1793 (2005).
219. Xi, J., Zhou, L. & Dai, H. Drug-loaded chondroitin sulfate-based nanogels: Preparation and characterization. *Colloids Surf B Biointerfaces* **100**, 107–115 (2012).
220. Guo, J. *et al.* A novel nanogel delivery of poly-α, β-polyasparthydrazide by reverse microemulsion and its redox-responsive release of 5-Fluorouridine. *Asian J Pharm Sci* **11**, 735–743 (2016).
221. Yu, S., Yao, P., Jiang, M. & Zhang, G. Nanogels prepared by self-assembly of oppositely charged globular proteins. *Biopolymers* **83**, 148–158 (2006).
222. Yu, S., Hu, J., Pan, X., Yao, P. & Jiang, M. Stable and pH-sensitive nanogels prepared by self-assembly of chitosan and ovalbumin. *Langmuir* **22**, 2754–2759 (2006).
223. Shen, W. *et al.* Biocompatible, antifouling, and thermosensitive core-shell nanogels synthesized by RAFT aqueous dispersion polymerization. *Macromolecules* **44**, 2524–2530 (2011).
224. Delaittre, G., Save, M. & Charleux, B. Nitroxide-Mediated Aqueous Dispersion Polymerization: From Water-Soluble Macroalkoxyamine to Thermosensitive Nanogels. *Macromol Rapid Commun* **28**, 1528–1533 (2007).
225. Xu, Y., Li, Y., Cao, X., Chen, Q. & An, Z. Versatile RAFT dispersion polymerization in cononsolvents for the synthesis of thermoresponsive nanogels with controlled composition, functionality and architecture. *Polym Chem* **5**, 6244–6255 (2014).

226. Pandey, T., Sharma, A., Sandhu, A. & Pandey, V. Controlled polymerization in microfluidics: Advancement in nanogel synthesis. *SPE Polymers* **5**, 113–126 (2024).
227. Liu, Z. *et al.* Microfluidics for Production of Particles: Mechanism, Methodology, and Applications. *Small* **16**, 1904673 (2020).
228. Liu, D., Zhang, H., Fontana, F., Hirvonen, J. T. & Santos, H. A. Microfluidic-assisted fabrication of carriers for controlled drug delivery. *Lab Chip* **17**, 1856–1883 (2017).
229. Wei, Z. *et al.* Microfluidics Fabrication of Micrometer-Sized Hydrogels with Precisely Controlled Geometries for Biomedical Applications. *Adv Healthc Mater* **11**, 2200846 (2022).
230. Liu, D., Zhang, H., Fontana, F., Hirvonen, J. T. & Santos, H. A. Current developments and applications of microfluidic technology toward clinical translation of nanomedicines. *Adv Drug Deliv Rev* **128**, 54–83 (2018).
231. Ahadian, S. *et al.* Micro and nanoscale technologies in oral drug delivery. *Adv Drug Deliv Rev* **157**, 37–62 (2020).
232. Sackmann, E. K., Fulton, A. L. & Beebe, D. J. The present and future role of microfluidics in biomedical research. *Nature 2014 507:7491* **507**, 181–189 (2014).
233. Liu, D. *et al.* Core/Shell Nanocomposites Produced by Superfast Sequential Microfluidic Nanoprecipitation. *Nano Lett* **17**, 606–614 (2017).
234. Sanjay, S. T. *et al.* Recent advances of controlled drug delivery using microfluidic platforms. *Adv Drug Deliv Rev* **128**, 3–28 (2018).
235. Fontana, F., Ferreira, M. P. A., Correia, A., Hirvonen, J. & Santos, H. A. Microfluidics as a cutting-edge technique for drug delivery applications. *J Drug Deliv Sci Technol* **34**, 76–87 (2016).
236. Nielsen, J. B. *et al.* Microfluidics: innovations in materials and their fabrication and functionalization. *Anal Chem* **92**, 150–168 (2020).
237. Ren, K., Zhou, J. & Wu, H. Materials for microfluidic chip fabrication. *Acc Chem Res* **46**, 2396–2406 (2013).
238. Aralekallu, S., Boddula, R. & Singh, V. Development of glass-based microfluidic devices: A review on its fabrication and biologic applications. *Mater Des* **225**, 111517 (2023).
239. Yu, Y., Shang, L., Guo, J., Wang, J. & Zhao, Y. Design of capillary microfluidics for spinning cell-laden microfibers. *Nature Protocols 2018 13:11* **13**, 2557–2579 (2018).
240. Liu, D. *et al.* Core/Shell Nanocomposites Produced by Superfast Sequential Microfluidic Nanoprecipitation. *Nano Lett* **17**, 606–614 (2017).
241. Duncanson, W. J. *et al.* Microfluidic synthesis of advanced microparticles for encapsulation and controlled release. *Lab Chip* **12**, 2135–2145 (2012).
242. Nunes, J. K., Tsai, S. S. H., Wan, J. & Stone, H. A. Dripping and jetting in microfluidic multiphase flows applied to particle and fibre synthesis. *J Phys D Appl Phys* **46**, 114002 (2013).
243. Lan, W., Li, S. & Luo, G. Numerical and experimental investigation of dripping and jetting flow in a coaxial micro-channel. *Chem Eng Sci* **134**, 76–85 (2015).
244. Whiteley, Z. *et al.* Microfluidic synthesis of protein-loaded nanogels in a coaxial flow reactor using a design of experiments approach. *Nanoscale Adv* **3**, 2039–2055 (2021).
245. Zhang, C. *et al.* Progress, challenges, and future of nanomedicine. *Nano Today* **35**, 101008 (2020).
246. Caruso, F., Hyeon, T., Rotello, V., Doane, T. L. & Burda, C. The unique role of nanoparticles in nanomedicine: imaging, drug delivery and therapy. *Chem Soc Rev* **41**, 2885–2911 (2012).
247. Martins, J. P. *et al.* The solid progress of nanomedicine. *Drug Deliv Transl Res* **10**, 726–729 (2020).
248. Joudeh, N. & Linke, D. Nanoparticle classification, physicochemical properties, characterization, and applications: a comprehensive review for biologists. *Journal of Nanobiotechnology 2022 20:1* **20**, 1–29 (2022).
249. Joyce, P. *et al.* A translational framework to DELIVER nanomedicines to the clinic. *Nature Nanotechnology 2024* **26**, 1–15 (2024).
250. Anselmo, A. C., Mitragotri, | Samir, Mitragotri, S. & Paulson, J. A. Nanoparticles in the clinic: An update post COVID-19 vaccines. *Bioeng Transl Med* **6**, e10246 (2021).
251. Guerrini, G., Magrì, D., Gioria, S., Medaglini, D. & Calzolai, L. Characterization of nanoparticles-based vaccines for COVID-19. *Nature Nanotechnology 2022 17:6* **17**, 570–576 (2022).

252. Joyce, P. *et al.* A translational framework to DELIVER nanomedicines to the clinic. *Nature Nanotechnology 2024* **26**, 1–15 (2024).
253. Jahromi, L. P., Shahbazi, M. A., Maleki, A., Azadi, A. & Santos, H. A. Chemically Engineered Immune Cell-Derived Microrobots and Biomimetic Nanoparticles: Emerging Biodiagnostic and Therapeutic Tools. *Advanced Science* **8**, 2002499 (2021).
254. Zan, G., Wu, Q., Zan, G. & Wu, Q. Biomimetic and Bioinspired Synthesis of Nanomaterials/Nanostructures. *Advanced Materials* **28**, 2099–2147 (2016).
255. Qin, M., Du, G. & Sun, X. Biomimetic cell-derived nanocarriers for modulating immune responses. *Biomater Sci* **8**, 530–543 (2020).
256. Zhou, J. *et al.* Biomimetic Nanotechnology toward Personalized Vaccines. *Advanced Materials* **32**, 1901255 (2020).
257. Chen, Z., Wang, Z. & Gu, Z. Bioinspired and Biomimetic Nanomedicines. *Acc Chem Res* **52**, 1255–1264 (2019).
258. Tkach, M. & Théry, C. Communication by Extracellular Vesicles: Where We Are and Where We Need to Go. *Cell* **164**, 1226–1232 (2016).
259. El Andaloussi, S., Mäger, I., Breakefield, X. O. & Wood, M. J. A. Extracellular vesicles: biology and emerging therapeutic opportunities. *Nature Reviews Drug Discovery 2013 12:5* **12**, 347–357 (2013).
260. Zaborowski, M. P., Balaj, L., Breakefield, X. O. & Lai, C. P. Extracellular Vesicles: Composition, Biological Relevance, and Methods of Study. *Bioscience* **65**, 783–797 (2015).
261. van der Koog, L., Gandek, T. B. & Nagelkerke, A. Liposomes and Extracellular Vesicles as Drug Delivery Systems: A Comparison of Composition, Pharmacokinetics, and Functionalization. *Adv Healthc Mater* **11**, 2100639 (2022).
262. Petrovčíková, E., Vičíková, K. & Leksa, V. Extracellular vesicles – biogenesis, composition, function, uptake and therapeutic applications. *Biologia 2018 73:4* **73**, 437–448 (2018).
263. Rilla, K. *et al.* Extracellular vesicles are integral and functional components of the extracellular matrix. *Matrix Biology* **75–76**, 201–219 (2019).
264. Raposo, G. & Stahl, P. D. Extracellular vesicles: a new communication paradigm? *Nature Reviews Molecular Cell Biology 2019 20:9* **20**, 509–510 (2019).
265. Yuana, Y., Sturk, A. & Nieuwland, R. Extracellular vesicles in physiological and pathological conditions. *Blood Rev* **27**, 31–39 (2013).
266. Yáñez-Mó, M. *et al.* Biological properties of extracellular vesicles and their physiological functions. *J Extracell Vesicles* **4**, 1–60 (2015).
267. Mulcahy, L. A., Pink, R. C. & Carter, D. R. F. Routes and mechanisms of extracellular vesicle uptake. *J Extracell Vesicles* **3**, (2014).
268. Herrmann, I. K., Wood, M. J. A. & Fuhrmann, G. Extracellular vesicles as a next-generation drug delivery platform. *Nature Nanotechnology 2021 16:7* **16**, 748–759 (2021).
269. Zhang, Y. *et al.* Exosome: A review of its classification, isolation techniques, storage, diagnostic and targeted therapy applications. *Int J Nanomedicine* **15**, 6917–6934 (2020).
270. Hessvik, N. P. & Llorente, A. Current knowledge on exosome biogenesis and release. *Cellular and Molecular Life Sciences 2017 75:2* **75**, 193–208 (2017).
271. Brinton, L. T., Sloane, H. S., Kester, M. & Kelly, K. A. Formation and role of exosomes in cancer. *Cellular and Molecular Life Sciences* **72**, 659–671 (2015).
272. Essandoh, K. & Fan, G. C. Insights into the Mechanism of Exosome Formation and Secretion. *Mesenchymal Stem Cell Derived Exosomes: The Potential for Translational Nanomedicine* 1–19 (2015) doi:10.1016/B978-0-12-800164-6.00001-0.
273. Butler, J. T., Abdelhamed, S. & Kurre, P. Extracellular vesicles in the hematopoietic microenvironment. *Haematologica* **103**, 382–394 (2018).
274. Vader, P., Mol, E. A., Pasterkamp, G. & Schiffelers, R. M. Extracellular vesicles for drug delivery. *Adv Drug Deliv Rev* **106**, 148–156 (2016).
275. Sancho-Albero, M. *et al.* Exosome origin determines cell targeting and the transfer of therapeutic nanoparticles towards target cells. *J Nanobiotechnology* **17**, 1–13 (2019).
276. Gurung, S., Perocheau, D., Touramanidou, L. & Baruteau, J. The exosome journey: from biogenesis to uptake and intracellular signalling. *Cell Communication and Signaling 2021 19:1* **19**, 1–19 (2021).

277. Uddin, M. J. *et al.* Extracellular vesicles: The future of therapeutics and drug delivery systems. *Intelligent Pharmacy* **2**, 312–328 (2024).
278. Mettlen, M., Chen, P. H., Srinivasan, S., Danuser, G. & Schmid, S. L. Regulation of Clathrin-Mediated Endocytosis. *Annu Rev Biochem* **87**, 871–896 (2018).
279. Kiss, A. L. & Botos, E. Endocytosis via caveolae: alternative pathway with distinct cellular compartments to avoid lysosomal degradation? *J Cell Mol Med* **13**, 1228–1237 (2009).
280. Escrevente, C., Keller, S., Altevogt, P. & Costa, J. Interaction and uptake of exosomes by ovarian cancer cells. *BMC Cancer* **11**, 1–10 (2011).
281. Heath, N. *et al.* Endosomal escape enhancing compounds facilitate functional delivery of extracellular vesicle cargo. *Nanomedicine* **14**, 2799–2814 (2019).
282. Parolini, I. *et al.* Microenvironmental pH Is a Key Factor for Exosome Traffic in Tumor Cells. *Journal of Biological Chemistry* **284**, 34211–34222 (2009).
283. Du, S. *et al.* Extracellular vesicles: a rising star for therapeutics and drug delivery. *Journal of Nanobiotechnology 2023 21:1* **21**, 1–51 (2023).
284. Rhim, W.-K. *et al.* Recent advances in extracellular vesicle engineering and its applications to regenerative medicine. *Biomater Res* **27**, 130 (2023).
285. Wang, J., Chen, D. & Ho, E. A. Challenges in the development and establishment of exosome-based drug delivery systems. *Journal of Controlled Release* **329**, 894–906 (2021).
286. Pascucci, L. *et al.* Paclitaxel is incorporated by mesenchymal stromal cells and released in exosomes that inhibit in vitro tumor growth: A new approach for drug delivery. *Journal of Controlled Release* **192**, 262–270 (2014).
287. Sadeghi, S., Tehrani, F. R., Tahmasebi, S., Shafiee, A. & Hashemi, S. M. Exosome engineering in cell therapy and drug delivery. *Inflammopharmacology 2023 31:1* **31**, 145–169 (2023).
288. Damasceno, P. K. F. *et al.* Genetic Engineering as a Strategy to Improve the Therapeutic Efficacy of Mesenchymal Stem/Stromal Cells in Regenerative Medicine. *Front Cell Dev Biol* **8**, 539056 (2020).
289. Jia, X., Tang, J., Yao, C. & Yang, D. Recent Progress of Extracellular Vesicle Engineering. *ACS Biomater Sci Eng* **7**, 4430–4438 (2021).
290. Fu, S., Wang, Y., Xia, X. & Zheng, J. C. Exosome engineering: Current progress in cargo loading and targeted delivery. *NanoImpact* **20**, 100261 (2020).
291. Han, Y. *et al.* Overview and Update on Methods for Cargo Loading into Extracellular Vesicles. *Processes 2021, Vol. 9, Page 356* **9**, 356 (2021).
292. Haney, M. J. *et al.* Exosomes as drug delivery vehicles for Parkinson's disease therapy. *Journal of Controlled Release* **207**, 18–30 (2015).
293. Salarpour, S. *et al.* Paclitaxel incorporated exosomes derived from glioblastoma cells: comparative study of two loading techniques. *DARU, Journal of Pharmaceutical Sciences* **27**, 533–539 (2019).
294. Zeng, H. *et al.* Current Strategies for Exosome Cargo Loading and Targeting Delivery. *Cells 2023, Vol. 12, Page 1416* **12**, 1416 (2023).
295. Rhim, W. K. *et al.* Recent advances in extracellular vesicle engineering and its applications to regenerative medicine. *Biomater Res* **27**, 130 (2023).
296. Ducrot, C. *et al.* Hybrid extracellular vesicles for drug delivery. *Cancer Lett* **558**, 216107 (2023).
297. Sun, M. *et al.* Beyond Extracellular Vesicles: Hybrid Membrane Nanovesicles as Emerging Advanced Tools for Biomedical Applications. *Advanced Science* **10**, 2303617 (2023).
298. Ou, Y. H. *et al.* Extracellular Vesicle (EV) biohybrid systems for cancer therapy: Recent advances and future perspectives. *Semin Cancer Biol* **74**, 45–61 (2021).
299. Rodríguez, D. A. & Vader, P. Extracellular Vesicle-Based Hybrid Systems for Advanced Drug Delivery. *Pharmaceutics 2022, Vol. 14, Page 267* **14**, 267 (2022).
300. Zhang, W., Ngo, L., Tsao, S. C. H., Liu, D. & Wang, Y. Engineered Cancer-Derived Small Extracellular Vesicle-Liposome Hybrid Delivery System for Targeted Treatment of Breast Cancer. *ACS Appl Mater Interfaces* **15**, 16420–16433 (2023).
301. Lentz, B. R. PEG as a tool to gain insight into membrane fusion. *European Biophysics Journal* **36**, 315–326 (2007).
302. Lin, Y. *et al.* Exosome–Liposome Hybrid Nanoparticles Deliver CRISPR/Cas9 System in MSCs. *Advanced Science* **5**, 1700611 (2018).

303. Munagala, R. *et al.* Exosome-mediated delivery of RNA and DNA for gene therapy. *Cancer Lett* **505**, 58–72 (2021).
304. Zhupanyn, P. *et al.* Extracellular vesicle (ECV)-modified polyethylenimine (PEI) complexes for enhanced siRNA delivery in vitro and in vivo. *Journal of Controlled Release* **319**, 63–76 (2020).
305. Evers, M. J. W. *et al.* Functional siRNA Delivery by Extracellular Vesicle–Liposome Hybrid Nanoparticles. *Adv Healthc Mater* **11**, 2101202 (2022).
306. Van Deun, J. *et al.* Feasibility of Mechanical Extrusion to Coat Nanoparticles with Extracellular Vesicle Membranes. *Cells 2020, Vol. 9, Page 1797* **9**, 1797 (2020).
307. Hu, Y. *et al.* Exosome-guided bone targeted delivery of Antagomir-188 as an anabolic therapy for bone loss. *Bioact Mater* **6**, 2905–2913 (2021).
308. Rayamajhi, S., Nguyen, T. D. T., Marasini, R. & Aryal, S. Macrophage-derived exosome-mimetic hybrid vesicles for tumor targeted drug delivery. *Acta Biomater* **94**, 482–494 (2019).
309. Kim, B. *et al.* Hybrid Nanoparticles of Extracellular Vesicles and Gemcitabine Prodrug-Loaded Liposomes with Enhanced Targeting Ability for Effective PDAC Treatment. *ACS Appl Bio Mater* (2024) doi:10.1021/ACSABM.4C00658.
310. Sun, L. *et al.* Clodronate-loaded liposomal and fibroblast-derived exosomal hybrid system for enhanced drug delivery to pulmonary fibrosis. *Biomaterials* **271**, 120761 (2021).
311. Dumontel, B. *et al.* Nanotechnological engineering of extracellular vesicles for the development of actively targeted hybrid nanodevices. *Cell Biosci* **12**, 1–18 (2022).
312. Lv, Q. *et al.* Thermosensitive Exosome–Liposome Hybrid Nanoparticle-Mediated Chemoimmunotherapy for Improved Treatment of Metastatic Peritoneal Cancer. *Advanced Science* **7**, 2000515 (2020).
313. Cheng, L., Zhang, X., Tang, J., Lv, Q. & Liu, J. Gene-engineered exosomes-thermosensitive liposomes hybrid nanovesicles by the blockade of CD47 signal for combined photothermal therapy and cancer immunotherapy. *Biomaterials* **275**, 120964 (2021).
314. Liu, C. *et al.* Microfluidic Sonication To Assemble Exosome Membrane-Coated Nanoparticles for Immune Evasion-Mediated Targeting. *Nano Lett* **19**, 7836–7844 (2019).
315. Han, Z. *et al.* Improving Tumor Targeting of Exosomal Membrane-Coated Polymeric Nanoparticles by Conjugation with Aptamers. *ACS Appl Bio Mater* **3**, 2666–2673 (2020).
316. Mukherjee, D. *et al.* Polyethylene Glycol-Mediated Fusion of Extracellular Vesicles with Cationic Liposomes for the Design of Hybrid Delivery Systems. *ACS Appl Bio Mater* **4**, 8259–8266 (2021).
317. Mathias, N. R. & Hussain, M. A. Non-invasive Systemic Drug Delivery: Developability Considerations for Alternate Routes of Administration. *J Pharm Sci* **99**, 1–20 (2010).
318. Rowland, M. Influence of Route of Administration on Drug Availability. *J Pharm Sci* **61**, 70–74 (1972).
319. Das, S. & Chaudhury, A. Recent advances in lipid nanoparticle formulations with solid matrix for oral drug delivery. *AAPS PharmSciTech* **12**, 62–76 (2011).
320. Morishita, M. & Peppas, N. A. Is the oral route possible for peptide and protein drug delivery? *Drug Discov Today* **11**, 905–910 (2006).
321. Plapied, L., Duhem, N., des Rieux, A. & Préat, V. Fate of polymeric nanocarriers for oral drug delivery. *Curr Opin Colloid Interface Sci* **16**, 228–237 (2011).
322. Kumar, T. R. S., Soppimath, K. & Nachaegari, S. K. Novel Delivery Technologies for Protein and Peptide Therapeutics. *Curr Pharm Biotechnol* **7**, 261–276 (2006).
323. Tan, M. L., Choong, P. F. M. & Dass, C. R. Recent developments in liposomes, microparticles and nanoparticles for protein and peptide drug delivery. *Peptides (N.Y.)* **31**, 184–193 (2010).
324. Ensign, L. M., Cone, R. & Hanes, J. Oral drug delivery with polymeric nanoparticles: The gastrointestinal mucus barriers. *Adv Drug Deliv Rev* **64**, 557–570 (2012).
325. Agrawal, U., Sharma, R., Gupta, M. & Vyas, S. P. Is nanotechnology a boon for oral drug delivery? *Drug Discov Today* **19**, 1530–1546 (2014).
326. Neubert, R. H. H. Potentials of new nanocarriers for dermal and transdermal drug delivery. *European Journal of Pharmaceutics and Biopharmaceutics* **77**, 1–2 (2011).
327. Prow, T. W. *et al.* Nanoparticles and microparticles for skin drug delivery. *Adv Drug Deliv Rev* **63**, 470–491 (2011).

328. Valenzuela, P. & Simon, J. A. Nanoparticle delivery for transdermal HRT. *Nanomedicine* **8**, S83–S89 (2012).
329. Carter, P., Narasimhan, B. & Wang, Q. Biocompatible nanoparticles and vesicular systems in transdermal drug delivery for various skin diseases. *Int J Pharm* **555**, 49–62 (2019).
330. Singhal, M., Lapteva, M. & Kalia, Y. N. Formulation challenges for 21st century topical and transdermal delivery systems. *Expert Opin Drug Deliv* **14**, 705–708 (2017).
331. Hassett, K. J. *et al.* Optimization of Lipid Nanoparticles for Intramuscular Administration of mRNA Vaccines. *Mol Ther Nucleic Acids* **15**, 1–11 (2019).
332. Elbrink, K. *et al.* Application of solid lipid nanoparticles as a long-term drug delivery platform for intramuscular and subcutaneous administration: In vitro and in vivo evaluation. *European Journal of Pharmaceutics and Biopharmaceutics* **163**, 158–170 (2021).
333. Kara, D. & Yapucu Güneş, Ü. The effect on pain of three different methods of intramuscular injection: A randomized controlled trial. *Int J Nurs Pract* **22**, 152–159 (2016).
334. Evans, C. H., Kraus, V. B. & Setton, L. A. Progress in intra-articular therapy. *Nature Reviews Rheumatology 2013 10:1* **10**, 11–22 (2013).
335. Vicentini, F. T. M. D. C. *et al.* Delivery Systems and Local Administration Routes for Therapeutic siRNA. *Pharmaceutical Research 2013 30:4* **30**, 915–931 (2013).
336. Larsen, C. *et al.* Intra-articular depot formulation principles: Role in the management of postoperative pain and arthritic disorders. *J Pharm Sci* **97**, 4622–4654 (2008).
337. Jones, I. A., Togashi, R., Wilson, M. L., Heckmann, N. & Vangsness, C. T. Intra-articular treatment options for knee osteoarthritis. *Nature Reviews Rheumatology 2018 15:2* **15**, 77–90 (2018).
338. Gerwin, N., Hops, C. & Lucke, A. Intraarticular drug delivery in osteoarthritis. *Adv Drug Deliv Rev* **58**, 226–242 (2006).
339. Jeong, M. & Park, J. H. Nanomedicine for the Treatment of Rheumatoid Arthritis. *Mol Pharm* **18**, 539–549 (2021).
340. He, Z., Wang, B., Hu, C. & Zhao, J. An overview of hydrogel-based intra-articular drug delivery for the treatment of osteoarthritis. *Colloids Surf B Biointerfaces* **154**, 33–39 (2017).
341. Li, G. *et al.* An injectable liposome-anchored teriparatide incorporated gallic acid-grafted gelatin hydrogel for osteoarthritis treatment. *Nature Communications 2023 14:1* **14**, 1–18 (2023).
342. Lindsay, R., Krege, J. H., Marin, F., Jin, L. & Stepan, J. J. Teriparatide for osteoporosis: Importance of the full course. *Osteoporosis International* **27**, 2395–2410 (2016).
343. Ha, M. Y., Yang, D. H., You, S. J., Kim, H. J. & Chun, H. J. In-situ forming injectable GFOGER-conjugated BMSCs-laden hydrogels for osteochondral regeneration. *npj Regenerative Medicine 2023 8:1* **8**, 1–13 (2023).
344. Kim, J. *et al.* Long-term anti-inflammatory effects of injectable celecoxib nanoparticle hydrogels for Achilles tendon regeneration. *Acta Biomater* **144**, 183–194 (2022).
345. Lei, Y. *et al.* Injectable hydrogel microspheres with self-renewable hydration layers alleviate osteoarthritis. *Sci Adv* **8**, 6449 (2022).
346. Sebbag, E. *et al.* The world-wide burden of musculoskeletal diseases: a systematic analysis of the World Health Organization Burden of Diseases Database. *Ann Rheum Dis* **78**, 844–848 (2019).
347. Maffulli, N., Wong, J. & Almekinders, L. C. Types and epidemiology of tendinopathy. *Clin Sports Med* **22**, 675–692 (2003).
348. Józsa, L. & Kannus, P. Histopathological findings in spontaneous tendon ruptures. *Scand J Med Sci Sports* **7**, 113–118 (1997).
349. Karousou, E. *et al.* Molecular interactions in extracellular matrix of tendon. *Frontiers in Bioscience - Elite* **2 E**, 1–12 (2010).
350. Ivirico, J. L. E. & Laurencin, C. T. Case Studies for Soft Tissue Regenerative Engineering. *Encyclopedia of Biomedical Engineering* **1–3**, 530–536 (2019).
351. Thorpe, C. T., Birch, H. L., Clegg, P. D. & Screen, H. R. C. Tendon Physiology and Mechanical Behavior: Structure–Function Relationships. *Tendon Regeneration: Understanding Tissue Physiology and Development to Engineer Functional Substitutes* 3–39 (2015) doi:10.1016/B978-0-12-801590-2.00001-6.

352. Obst, S. J. *et al.* Are the Mechanical or Material Properties of the Achilles and Patellar Tendons Altered in Tendinopathy? A Systematic Review with Meta-analysis. *Sports Medicine* **48**, 2179–2198 (2018).
353. Ortega-Castillo, M., Cuesta-Vargas, A., Luque-Teba, A. & Trinidad-Fernández, M. The role of progressive, therapeutic exercise in the management of upper limb tendinopathies: A systematic review and meta-analysis. *Musculoskelet Sci Pract* **62**, 102645 (2022).
354. Millar, N. L. *et al.* Tendinopathy. *Nat Rev Dis Primers* **7**, 1 (2021).
355. Hopkins, C. *et al.* Critical review on the socio-economic impact of tendinopathy. *Asia Pac J Sports Med Arthrosc Rehabil Technol* **4**, 9–20 (2016).
356. September, A., Rahim, M. & Collins, M. Towards an understanding of the genetics of tendinopathy. *Adv Exp Med Biol* **920**, 109–116 (2016).
357. Janssen, I., van der Worp, H., Hensing, S. & Zwerver, J. Investigating Achilles and patellar tendinopathy prevalence in elite athletics. *Research in Sports Medicine* **26**, 1–12 (2018).
358. Wang, Y., Zhou, H., Nie, Z. & Cui, S. Prevalence of Achilles tendinopathy in physical exercise: A systematic review and meta-analysis. *Sports Medicine and Health Science* **4**, 152–159 (2022).
359. Åström, M. Partial rupture in chronic achilles tendinopathy: A retrospective analysis of 342 cases. *Acta Orthop Scand* **69**, 404–407 (1998).
360. Riel, H., Lindstrøm, C. F., Rathleff, M. S., Jensen, M. B. & Olesen, J. L. Prevalence and incidence rate of lower-extremity tendinopathies in a Danish general practice: A registry-based study. *BMC Musculoskelet Disord* **20**, 1–6 (2019).
361. Albers, I. S., Zwerver, J., Diercks, R. L., Dekker, J. H. & Van Den Akker-Scheek, I. Incidence and prevalence of lower extremity tendinopathy in a Dutch general practice population: A cross sectional study. *BMC Musculoskelet Disord* **17**, 1–6 (2016).
362. Cardoso, T. B., Pizzari, T., Kinsella, R., Hope, D. & Cook, J. L. Current trends in tendinopathy management. *Best Pract Res Clin Rheumatol* **33**, 122–140 (2019).
363. Sleeswijk Visser, T. S. O. *et al.* Impact of chronic Achilles tendinopathy on health-related quality of life, work performance, healthcare utilisation and costs. *BMJ Open Sport Exerc Med* **7**, e001023 (2021).
364. Thorpe, C. T. & Screen, H. R. C. Tendon structure and composition. *Adv Exp Med Biol* **920**, 3–10 (2016).
365. Kastelic, J., Galeski, A. & Baer, E. The Multicomposite Structure of Tendon. *Connect Tissue Res* **6**, 11–23 (1978).
366. Barnard, K., Light, N. D., Sims, T. J. & Bailey, A. J. Chemistry of the collagen cross-links. Origin and partial characterization of a putative mature cross-link of collagen. *Biochemical Journal* **244**, 303–309 (1987).
367. Thorpe, C. T., Udeze, C. P., Birch, H. L., Clegg, P. D. & Screen, H. R. C. Specialization of tendon mechanical properties results from interfascicular differences. *J R Soc Interface* **9**, 3108–3117 (2012).
368. Aparecida de Aro, A., de Campos Vidal, B. & Pimentel, E. R. Biochemical and anisotropical properties of tendons. *Micron* **43**, 205–214 (2012).
369. Birch, H. L. Tendon matrix composition and turnover in relation to functional requirements. *Int J Exp Pathol* **88**, 241–248 (2007).
370. Kjær, M. *et al.* From mechanical loading to collagen synthesis, structural changes and function in human tendon. *Scand J Med Sci Sports* **19**, 500–510 (2009).
371. Franchi, M., Trirè, A., Quaranta, M., Orsini, E. & Ottani, V. Collagen Structure of Tendon Relates to Function. *The Scientific World Journal* **7**, 404–420 (2007).
372. Kadler, K. E., Hojima, Y. & Prockop, D. J. Collagen fibrils in vitro grow from pointed tips in the C- to N-terminal direction. *Biochemical Journal* **268**, 339–343 (1990).
373. Riley, G. The pathogenesis of tendinopathy. A molecular perspective. *Rheumatology* **43**, 131–142 (2004).
374. Banos, C. C., Thomas, A. H. & Kuo, C. K. Collagen fibrillogenesis in tendon development: Current models and regulation of fibril assembly. *Birth Defects Res C Embryo Today* **84**, 228–244 (2008).
375. Thorpe, C. T., Birch, H. L., Clegg, P. D. & Screen, H. R. C. The role of the non-collagenous matrix in tendon function. *Int J Exp Pathol* **94**, 248–259 (2013).
376. Li, Y., Wu, T. & Liu, S. Identification and Distinction of Tenocytes and Tendon-Derived Stem Cells. *Front Cell Dev Biol* **9**, 629515 (2021).

377. Hess, G. P., Cappiello, W. L., Poole, R. M. & Hunter, S. C. Prevention and Treatment of Overuse Tendon Injuries. *Sports Medicine* **8**, 371–384 (1989).
378. Kannus, P. Structure of the tendon connective tissue. *Scand J Med Sci Sports* **10**, 312–320 (2000).
379. Luesma, M. J., Cantarero, I., Sánchez-Cano, A. I., Rodellar, C. & Junquera, C. Ultrastructural evidence for telocytes in equine tendon. *J Anat* **238**, 527–535 (2021).
380. Zhang, C., Zhu, J., Zhou, Y., Thampatty, B. P. & Wang, J. H. C. Tendon Stem/Progenitor Cells and Their Interactions with Extracellular Matrix and Mechanical Loading. *Stem Cells Int* **2019**, 3674647 (2019).
381. Bi, Y. *et al.* Identification of tendon stem/progenitor cells and the role of the extracellular matrix in their niche. *Nature Medicine 2007 13:10* **13**, 1219–1227 (2007).
382. Huang, Z. *et al.* Tendon Stem/Progenitor Cell Subpopulations and Their Implications in Tendon Biology. *Front Cell Dev Biol* **9**, 631272 (2021).
383. Lui, P. P. Y. Markers for the identification of tendon-derived stem cells in vitro and tendon stem cells in situ - Update and future development. *Stem Cell Res Ther* **6**, 1–9 (2015).
384. Tempfer, H. *et al.* Perivascular cells of the supraspinatus tendon express both tendon- and stem cell-related markers. *Histochem Cell Biol* **131**, 733–741 (2009).
385. Runesson, E., Ackermann, P., Brisby, H., Karlsson, J. & Eriksson, B. I. Detection of slow-cycling and stem/progenitor cells in different regions of rat Achilles tendon: Response to treadmill exercise. *Knee Surgery, Sports Traumatology, Arthroscopy* **21**, 1694–1703 (2013).
386. Grinstein, M. *et al.* A distinct transition from cell growth to physiological homeostasis in the tendon. *Elife* **8**, (2019).
387. Zhang, J. & Wang, J. H. C. Mechanobiological response of tendon stem cells: Implications of tendon homeostasis and pathogenesis of tendinopathy. *Journal of Orthopaedic Research* **28**, 639–643 (2010).
388. Interleukin-10 promotes proliferation and migration, and inhibits tendon differentiation via the JAK/Stat3 pathway in tendon-derived stem cells in vitro. https://www.spandidos-publications.com/mmr/18/6/5044.
389. Tarafder, S. *et al.* Tendon stem/progenitor cells regulate inflammation in tendon healing via JNK and STAT3 signaling. *The FASEB Journal* **31**, 3991–3998 (2017).
390. Zhang, M. *et al.* Tendon stem cell-derived exosomes regulate inflammation and promote the high-quality healing of injured tendon. *Stem Cell Res Ther* **11**, 1–15 (2020).
391. Lu, J. *et al.* The Functions and Mechanisms of Basic Fibroblast Growth Factor in Tendon Repair. *Front Physiol* **13**, 852795 (2022).
392. Holladay, C., Abbah, S. A., O'Dowd, C., Pandit, A. & Zeugolis, D. I. Preferential tendon stem cell response to growth factor supplementation. *J Tissue Eng Regen Med* **10**, 783–798 (2016).
393. Xu, K. *et al.* Synergistic promoting effects of bone morphogenetic protein 12/connective tissue growth factor on functional differentiation of tendon derived stem cells and patellar tendon window defect regeneration. *J Biomech* **66**, 95–102 (2018).
394. Lui, P. P. Y., Wong, O. T. & Lee, Y. W. Transplantation of tendon-derived stem cells pre-treated with connective tissue growth factor and ascorbic acid in vitro promoted better tendon repair in a patellar tendon window injury rat model. *Cytotherapy* **18**, 99–112 (2016).
395. Komatsu, I., Wang, J. H. C., Iwasaki, K., Shimizu, T. & Okano, T. The effect of tendon stem/progenitor cell (TSC) sheet on the early tendon healing in a rat Achilles tendon injury model. *Acta Biomater* **42**, 136–146 (2016).
396. Yin, H. *et al.* Tenomodulin regulates matrix remodeling of mouse tendon stem/progenitor cells in an ex vivo collagen I gel model. *Biochem Biophys Res Commun* **512**, 691–697 (2019).
397. Riggin, C. N., Morris, T. R. & Soslowsky, L. J. Tendinopathy II: Etiology, Pathology, and Healing of Tendon Injury and Disease. *Tendon Regeneration: Understanding Tissue Physiology and Development to Engineer Functional Substitutes* 149–183 (2015) doi:10.1016/B978-0-12-801590-2.00005-3.
398. Abate, M. *et al.* Pathogenesis of tendinopathies: inflammation or degeneration? *Arthritis Res Ther* **11**, 235 (2009).
399. KRAUSHAAR, B. S. & NIRSCHL, R. P. Current Concepts Review - Tendinosis of the Elbow (Tennis Elbow). Clinical Features and Findings of Histological, Immunohistochemical, and Electron Microscopy Studies*. *JBJS* **81**, (1999).

400. Rees, J. D., Wilson, A. M. & Wolman, R. L. Current concepts in the management of tendon disorders. *Rheumatology* **45**, 508–521 (2006).
401. Aicale, R., Tarantino, D. & Maffulli, N. Basic science of tendons. *Bio-orthopaedics: A New Approach* 249–273 (2017) doi:10.1007/978-3-662-54181-4_21/TABLES/6.
402. Uhthoff, H. K. Calcifying tendinitis, an active cell-mediated calcification. *Virchows Arch A Pathol Anat Histol* **366**, 51–58 (1975).
403. Selvanetti, A., Cipolla, M. & Puddu, G. Overuse tendon injuries: Basic science and classification. *Oper Tech Sports Med* **5**, 110–117 (1997).
404. Khan, K. M., Cook, J. L., Taunton, J. E. & Bonar, F. Overuse Tendinosis, Not Tendinitis. *Phys Sportsmed* **28**, 38–48 (2000).
405. Sharma, P. & Maffulli, N. Tendon injury and tendinopathy: Healing and repair. *Journal of Bone and Joint Surgery* **87**, 187–202 (2005).
406. Lin, T. W., Cardenas, L. & Soslowsky, L. J. Biomechanics of tendon injury and repair. *J Biomech* **37**, 865–877 (2004).
407. Docheva, D., Müller, S. A., Majewski, M. & Evans, C. H. Biologics for tendon repair. *Adv Drug Deliv Rev* **84**, 222–239 (2015).
408. D'Addona, A., Maffulli, N., Formisano, S. & Rosa, D. Inflammation in tendinopathy. *The Surgeon* **15**, 297–302 (2017).
409. Fenwick, S. A., Hazleman, B. L. & Riley, G. P. The vasculature and its role in the damaged and healing tendon. *Arthritis Res* **4**, 252–260 (2002).
410. Sunwoo, J. Y., Eliasberg, C. D., Carballo, C. B. & Rodeo, S. A. The role of the macrophage in tendinopathy and tendon healing. *Journal of Orthopaedic Research®* **38**, 1666–1675 (2020).
411. Chisari, E., Rehak, L., Khan, W. S. & Maffulli, N. The role of the immune system in tendon healing: a systematic review. *Br Med Bull* **133**, 49–64 (2020).
412. Vinhas, A., Rodrigues, M. T. & Gomes, M. E. Exploring stem cells and inflammation in Tendon repair and regeneration. *Adv Exp Med Biol* **1089**, 37–46 (2018).
413. Visnes, H. & Bahr, R. The evolution of eccentric training as treatment for patellar tendinopathy (jumper's knee): a critical review of exercise programmes. *Br J Sports Med* **41**, 217–223 (2007).
414. Lim, H. Y. & Wong, S. H. Effects of isometric, eccentric, or heavy slow resistance exercises on pain and function in individuals with patellar tendinopathy: A systematic review. *Physiotherapy Research International* **23**, e1721 (2018).
415. Murtaugh, B. & Ihm, J. M. Eccentric training for the treatment of tendinopathies. *Curr Sports Med Rep* **12**, 175–182 (2013).
416. Gravare Silbernagel, K., Vicenzino, B. T., Rathleff, M. S. & Thorborg, K. Isometric exercise for acute pain relief: is it relevant in tendinopathy management? *Br J Sports Med* **53**, 1330–1331 (2019).
417. Andres, B. M. & Murrell, G. A. C. Treatment of tendinopathy: What works, what does not, and what is on the horizon. *Clin Orthop Relat Res* **466**, 1539–1554 (2008).
418. Coombes, B. K., Bisset, L., Brooks, P., Khan, A. & Vicenzino, B. Effect of Corticosteroid Injection, Physiotherapy, or Both on Clinical Outcomes in Patients With Unilateral Lateral Epicondylalgia: A Randomized Controlled Trial. *JAMA* **309**, 461–469 (2013).
419. Dean, B. J. F. *et al.* The risks and benefits of glucocorticoid treatment for tendinopathy: A systematic review of the effects of local glucocorticoid on tendon. *Semin Arthritis Rheum* **43**, 570–576 (2014).
420. van den Boom, N. A. C., Winters, M., Haisma, H. J. & Moen, M. H. Efficacy of Stem Cell Therapy for Tendon Disorders: A Systematic Review. *Orthop J Sports Med* **8**, (2020).
421. Chen, Z. *et al.* Challenges and perspectives of tendon-derived cell therapy for tendinopathy: from bench to bedside. *Stem Cell Research & Therapy 2022 13:1* **13**, 1–21 (2022).
422. Le, A. D. K., Enweze, L., DeBaun, M. R. & Dragoo, J. L. Current Clinical Recommendations for Use of Platelet-Rich Plasma. *Curr Rev Musculoskelet Med* **11**, 624–634 (2018).
423. Zhou, Y. & Wang, J. H. C. PRP Treatment Efficacy for Tendinopathy: A Review of Basic Science Studies. *Biomed Res Int* **2016**, 9103792 (2016).
424. De Vos, R. J., Windt, J. & Weir, A. Strong evidence against platelet-rich plasma injections for chronic lateral epicondylar tendinopathy: A systematic review. *Br J Sports Med* **48**, 952–956 (2014).

425. Franchini, M. *et al.* Efficacy of platelet-rich plasma as conservative treatment in orthopaedics: a systematic review and meta-analysis. *Blood Transfusion* **16**, 502–513 (2018).
426. Maffulli, N., Oliva, F., Maffulli, G. D., Buono, A. Del & Gougoulias, N. Surgical management of chronic Achilles tendon ruptures using less invasive techniques. *Foot and Ankle Surgery* **24**, 164–170 (2018).
427. Quintero, D. *et al.* The roles and therapeutic potentialof mesenchymal stem/stromal cells and their extracellular vesicles in tendinopathies. *Front Bioeng Biotechnol* **11**, 1040762 (2023).
428. Ragni, E. *et al.* Amniotic membrane-mesenchymal stromal cells secreted factors and extracellular vesicle-miRNAs: Anti-inflammatory and regenerative features for musculoskeletal tissues. *Stem Cells Transl Med* **10**, 1044–1062 (2021).
429. Smith, R. K. W. *et al.* Beneficial Effects of Autologous Bone Marrow-Derived Mesenchymal Stem Cells in Naturally Occurring Tendinopathy. *PLoS One* **8**, e75697 (2013).
430. Goldberg, A. J. *et al.* Autologous bone marrow derived mesenchymal stem cells are safe for the treatment of Achilles tendinopathy. *Scientific Reports 2024 14:1* **14**, 1–10 (2024).
431. Rodas, G. *et al.* Effect of Autologous Expanded Bone Marrow Mesenchymal Stem Cells or Leukocyte-Poor Platelet-Rich Plasma in Chronic Patellar Tendinopathy (With Gap >3 mm): Preliminary Outcomes After 6 Months of a Double-Blind, Randomized, Prospective Study. *American Journal of Sports Medicine* **49**, 1492–1504 (2021).
432. Zhang, Y. *et al.* Mechanisms and therapeutic prospects of mesenchymal stem cells-derived exosomes for tendinopathy. *Stem Cell Res Ther* **14**, 1–10 (2023).
433. Wang, Y. *et al.* Exosomes from tendon stem cells promote injury tendon healing through balancing synthesis and degradation of the tendon extracellular matrix. *J Cell Mol Med* **23**, 5475–5485 (2019).
434. Liu, H. *et al.* Adipose-derived mesenchymal stromal cell-derived exosomes promote tendon healing by activating both SMAD1/5/9 and SMAD2/3. *Stem Cell Res Ther* **12**, 1–13 (2021).
435. Li, Z. *et al.* BMSC-derived exosomes promote tendon-bone healing after anterior cruciate ligament reconstruction by regulating M1/M2 macrophage polarization in rats. *Stem Cell Res Ther* **13**, 1–20 (2022).
436. Yu, H. *et al.* Bone marrow mesenchymal stem cell-derived exosomes promote tendon regeneration by facilitating the proliferation and migration of endogenous tendon stem/progenitor cells. *Acta Biomater* **106**, 328–341 (2020).
437. Fu, G., Lu, L., Pan, Z., Fan, A. & Yin, F. Adipose-Derived Stem Cell Exosomes Facilitate Rotator Cuff Repair by Mediating Tendon-Derived Stem Cells. *Regenerative Med* **16**, 359–372 (2021).
438. Zhang, Q. & Lai, D. Application of human amniotic epithelial cells in regenerative medicine: a systematic review. *Stem Cell Res Ther* **11**, 439 (2020).
439. Miki, T. Stem cell characteristics and the therapeutic potential of amniotic epithelial cells. *American Journal of Reproductive Immunology* **80**, e13003 (2018).
440. Fathi, I. & Miki, T. Human Amniotic Epithelial Cells Secretome: Components, Bioactivity, and Challenges. *Front Med (Lausanne)* **8**, (2022).
441. Russo, V. *et al.* Assessing the functional potential of conditioned media derived from amniotic epithelial stem cells engineered on 3D biomimetic scaffolds: An in vitro model for tendon regeneration. *Mater Today Bio* **25**, 101001 (2024).
442. Tan, J. L. *et al.* Amnion Epithelial Cell-Derived Exosomes Restrict Lung Injury and Enhance Endogenous Lung Repair. *Stem Cells Transl Med* **7**, 180–196 (2018).
443. López-Cerdá, S. *et al.* Antifibrotic and Pro-regenerative Effects of SMAD3 siRNA and Collagen I mRNA-Loaded Lipid Nanoparticles in Human Tenocytes. *ACS Appl Nano Mater* (2024) doi:10.1021/ACSANM.4C02996.
444. Chen, W. *et al.* Lipid nanoparticle-assisted miR29a delivery based on core-shell nanofibers improves tendon healing by cross-regulation of the immune response and matrix remodeling. *Biomaterials* **291**, 121888 (2022).
445. Choi, H. J. *et al.* Enhanced tendon restoration effects of anti-inflammatory, lactoferrin-immobilized, heparin-polymeric nanoparticles in an Achilles tendinitis rat model. *Carbohydr Polym* **241**, 116284 (2020).

446. Zhou, Y. L., Yang, Q. Q., Zhang, L. & Tang, J. B. Nanoparticle-coated sutures providing sustained growth factor delivery to improve the healing strength of injured tendons. *Acta Biomater* **124**, 301–314 (2021).
447. Jie Li, Z. *et al.* Metformin suppressed tendon injury-induced adhesion via hydrogel-nanoparticle sustained-release system. *Int J Pharm* **642**, 123190 (2023).
448. Jin, S. *et al.* Young Exosome Bio-Nanoparticles Restore Aging-Impaired Tendon Stem/Progenitor Cell Function and Reparative Capacity. *Advanced Materials* **35**, 2211602 (2023).
449. Han, Q. *et al.* Antioxidant and anti-inflammatory injectable hydrogel microspheres for in situ treatment of tendinopathy. *Regen Biomater* **11**, (2024).
450. Cai, C. *et al.* Self-Healing Hydrogel Embodied with Macrophage-Regulation and Responsive-Gene-Silencing Properties for Synergistic Prevention of Peritendinous Adhesion. *Advanced Materials* **34**, 2106564 (2022).
451. Alge, D. L., Azagarsamy, M. A., Donohue, D. F. & Anseth, K. S. Synthetically Tractable Click Hydrogels for Three-Dimensional Cell Culture Formed Using Tetrazine–Norbornene Chemistry. *Biomacromolecules* **14**, 949–953 (2013).
452. Holt, S. E., Rakoski, A., Jivan, F., Pérez, L. M. & Alge, D. L. Hydrogel Synthesis and Stabilization via Tetrazine Click-Induced Secondary Interactions. *Macromol Rapid Commun* **41**, 2000287 (2020).
453. Freudenberg, U. *et al.* A star-PEG–heparin hydrogel platform to aid cell replacement therapies for neurodegenerative diseases. *Biomaterials* **30**, 5049–5060 (2009).
454. Xiao, X. *et al.* Facile synthesize of norbornene-hyaluronic acid to form hydrogel via thiol-norbornene reaction for biomedical application. *Polymer (Guildf)* **245**, 124696 (2022).
455. Piffoux, M., Silva, A. K. A., Wilhelm, C., Gazeau, F. & Tareste, D. Modification of Extracellular Vesicles by Fusion with Liposomes for the Design of Personalized Biogenic Drug Delivery Systems. *ACS Nano* **12**, 6830–6842 (2018).
456. Scott, B. L. *et al.* Liposome Fusion Assay to Monitor Intracellular Membrane Fusion Machines. in *Liposomes, Part B* vol. 372 274–300 (Academic Press, 2003).
457. Holt, S. E. *et al.* Hydrogel Synthesis and Stabilization via Tetrazine Click-Induced Secondary Interactions. *Macromol Rapid Commun* **41**, 2000287 (2020).
458. Joshi, S., Raj, K. A., Rao, M. R. & Ghosh, R. An electronic biosensor based on semiconducting tetrazine polymer immobilizing matrix coated on rGO for carcinoembryonic antigen. *Scientific Reports 2022 12:1* **12**, 1–14 (2022).
459. Browning, M. B., Wilems, T., Hahn, M. & Cosgriff-Hernandez, E. Compositional control of poly(ethylene glycol) hydrogel modulus independent of mesh size. *J Biomed Mater Res A* **98A**, 268–273 (2011).
460. Hoang, H. T. *et al.* Dual pH-/thermo-responsive chitosan-based hydrogels prepared using 'click' chemistry for colon-targeted drug delivery applications. *Carbohydr Polym* **260**, 117812 (2021).
461. Li, S. *et al.* Injectable Click Chemistry-based Bioadhesives for Accelerated Wound Closure. *Acta Biomater* **110**, 95–104 (2020).
462. Joo, S. Bin *et al.* Fast Absorbent and Highly Bioorthogonal Hydrogels Developed by IEDDA Click Reaction for Drug Delivery Application. *Materials* **15**, 7128 (2022).
463. Gulfam, M. *et al.* Highly porous and injectable hydrogels derived from cartilage acellularized matrix exhibit reduction and NIR light dual-responsive drug release properties for application in antitumor therapy. *NPG Asia Materials 2022 14:1* **14**, 1–17 (2022).
464. Qiao, Y. *et al.* Gelatin Templated Polypeptide Co-Cross-Linked Hydrogel for Bone Regeneration. *Adv Healthc Mater* **9**, 1901239 (2020).
465. Yang, N., Wang, Y., Zhang, Q., Chen, L. & Zhao, Y. In situ formation of poly (thiolated chitosan-co-alkylated β-cyclodextrin) hydrogels using click cross-linking for sustained drug release. *J Mater Sci* **54**, 1677–1691 (2019).
466. Dimmitt, N. H., Arkenberg, M. R., de Lima Perini, M. M., Li, J. & Lin, C.-C. Hydrolytically Degradable PEG-Based Inverse Electron Demand Diels–Alder Click Hydrogels. *ACS Biomater Sci Eng* **8**, 4262–4273 (2022).
467. Darling, N. J. *et al.* Click by Click Microporous Annealed Particle (MAP) Scaffolds. *Adv Healthc Mater* **9**, 1901391 (2020).

468. Ghosh, K. *et al.* Rheological characterization of in situ cross-linkable hysluronan hydrogels. *Biomacromolecules* **6**, 2857–2865 (2005).
469. Frith, J. E. *et al.* Effects of bound versus soluble pentosan polysulphate in PEG/HA-based hydrogels tailored for intervertebral disc regeneration. *Biomaterials* **35**, 1150–1162 (2014).
470. Ilochonwu, B. C. *et al.* Hyaluronic Acid-PEG-Based Diels-Alder in Situ Forming Hydrogels for Sustained Intraocular Delivery of Bevacizumab. *Biomacromolecules* **23**, 2914–2929 (2022).
471. Jo, Y. J. *et al.* Multi-stimuli responsive hydrogels derived from hyaluronic acid for cancer therapy application. *Carbohydr Polym* **286**, 119303 (2022).
472. Shih, H. & Lin, C. C. Cross-linking and degradation of step-growth hydrogels formed by thiol-ene photoclick chemistry. *Biomacromolecules* **13**, 2003–2012 (2012).
473. Hori, K. *et al.* Theoretical study on the reaction mechanism for the hydrolysis of esters and amides under acidic conditions. *Tetrahedron* **63**, 1264–1269 (2007).
474. Zhou, D. *et al.* Dopamine-Modified Hyaluronic Acid Hydrogel Adhesives with Fast-Forming and High Tissue Adhesion. *ACS Appl Mater Interfaces* **12**, 18225–18234 (2020).
475. Yabuuchi, K. *et al.* Variable swelling behavior of and drug encapsulation in a maleimide-modified hyaluronic acid nanogel-based hydrogel. *Polymer Journal 2024 56:5* **56**, 505–515 (2024).
476. Liaqat, H. *et al.* pH-Sensitive Hydrogels Fabricated with Hyaluronic Acid as a Polymer for Site-Specific Delivery of Mesalamine. *ACS Omega* **9**, 28827–28840 (2024).
477. Feng, W. & Wang, Z. Tailoring the Swelling-Shrinkable Behavior of Hydrogels for Biomedical Applications. *Advanced Science* **10**, 2303326 (2023).
478. Yabuuchi, K. *et al.* Variable swelling behavior of and drug encapsulation in a maleimide-modified hyaluronic acid nanogel-based hydrogel. *Polymer Journal 2024 56:5* **56**, 505–515 (2024).
479. Carducci, F., Yoneda, J. S., Itri, R. & Mariani, P. On the structural stability of guanosine-based supramolecular hydrogels. *Soft Matter* **14**, 2938–2948 (2018).
480. Kulkarni, J. A. *et al.* On the Formation and Morphology of Lipid Nanoparticles Containing Ionizable Cationic Lipids and siRNA. *ACS Nano* **12**, 4787–4795 (2018).
481. Eygeris, Y., Patel, S., Jozic, A. & Sahay, G. Deconvoluting Lipid Nanoparticle Structure for Messenger RNA Delivery. *Nano Lett* **20**, 4543–4549 (2020).
482. Scott, B. L. *et al.* Liposome Fusion Assay to Monitor Intracellular Membrane Fusion Machines. in *Liposomes, Part B* vol. 372 274–300 (Academic Press, 2003).
483. Sato, Y. T. *et al.* Engineering hybrid exosomes by membrane fusion with liposomes. *Sci Rep* **6**, 21933 (2016).
484. Ding, Z. *et al.* Understanding molecular characteristics of extracellular vesicles derived from different types of mesenchymal stem cells for therapeutic translation. *Extracellular Vesicle* **3**, 100034 (2024).
485. Zhao, H. *et al.* Exosomes From Adipose-Derived Stem Cells Attenuate Adipose Inflammation and Obesity Through Polarizing M2 Macrophages and Beiging in White Adipose Tissue. *Diabetes* **67**, 235–247 (2017).
486. Pogozhykh, O. *et al.* Molecular and cellular characteristics of human and non-human primate multipotent stromal cells from the amnion and bone marrow during long term culture. *Stem Cell Res Ther* **6**, 150 (2015).
487. Kou, M. *et al.* Mesenchymal stem cell-derived extracellular vesicles for immunomodulation and regeneration: a next generation therapeutic tool? *Cell Death Dis* **13**, 580 (2022).
488. Jiang, Y., Chen, J., Deng, C., Suuronen, E. J. & Zhong, Z. Click hydrogels, microgels and nanogels: Emerging platforms for drug delivery and tissue engineering. *Biomaterials* **35**, 4969–4985 (2014).
489. Gayet, J. C. & Fortier, G. High water content BSA-PEG hydrogel for controlled release device: Evaluation of the drug release properties. *Journal of Controlled Release* **38**, 177–184 (1996).
490. Leach, J. B. & Schmidt, C. E. Characterization of protein release from photocrosslinkable hyaluronic acid-polyethylene glycol hydrogel tissue engineering scaffolds. *Biomaterials* **26**, 125–135 (2005).
491. Prencipe, G. *et al.* Amphiregulin orchestrates the paracrine immune-suppressive function of amniotic-derived cells through its interplay with COX-2/PGE2/EP4 axis. *iScience* **27**, 110508 (2024).
492. Di Mattia, M. *et al.* Hypoxia-Mimetic CoCl2 Agent Enhances Pro-Angiogenic Activities in Ovine Amniotic Epithelial Cells-Derived Conditioned Medium. *Cells 2022, Vol. 11, Page 461* **11**, 461 (2022).

493. Chen, K., Chen, X., Han, X. & Fu, Y. A comparison study on the release kinetics and mechanism of bovine serum albumin and nanoencapsulated albumin from hydrogel networks. *Int J Biol Macromol* **163**, 1291–1300 (2020).
494. Ma, X. *et al.* Injectable hydrogels based on the hyaluronic acid and poly (γ-glutamic acid) for controlled protein delivery. *Carbohydr Polym* **179**, 100–109 (2018).
495. Cao, W. *et al.* The preparation and biocompatible evaluation of injectable dual crosslinking hyaluronic acid hydrogels as cytoprotective agents. *J Mater Chem B* **7**, 4413–4423 (2019).
496. Liang, Y. & Kiick, K. L. Heparin-functionalized polymeric biomaterials in tissue engineering and drug delivery applications. *Acta Biomater* **10**, 1588–1600 (2014).
497. Zustiak, S. P. & Leach, J. B. Hydrolytically Degradable Poly(Ethylene Glycol) Hydrogel Scaffolds with Tunable Degradation and Mechanical Properties. *Biomacromolecules* **11**, 1348–1357 (2010).
498. Barboni, B. *et al.* Therapeutic potential of hAECs for early Achilles tendon defect repair through regeneration. *J Tissue Eng Regen Med* **12**, e1594–e1608 (2018).
499. Sousa, A. R. *et al.* Encapsulated Mesenchymal Stromal Cells as Cyclic Providers of Immunomodulatory Secretomes: A Living on-Demand Delivery System. *Adv Healthc Mater* **13**, 2304012 (2024).
500. Doshi, R. B. *et al.* Mesenchymal stem cell-secretome laden photopolymerizable hydrogels for wound healing. *J Biomed Mater Res A* **112**, 1484–1493 (2024).
501. Kim, I. S. *et al.* Effects of triethylene glycol dimethacrylate and hydroxyethyl methacrylate on macrophage polarization. *Int Endod J* **52**, 987–998 (2019).
502. He, H., Zhang, S., Tighe, S., Son, J. & Tseng, S. C. G. Immobilized heavy chain-hyaluronic acid polarizes lipopolysaccharide- activated macrophages toward m2 phenotype. *Journal of Biological Chemistry* **288**, 25792–25803 (2013).
503. Kim, H., Cha, J., Jang, M. & Kim, P. Hyaluronic acid-based extracellular matrix triggers spontaneous M2-like polarity of monocyte/macrophage. *Biomater Sci* **7**, 2264–2271 (2019).
504. Yan, T. *et al.* Suppression of the hyaluronic acid pathway induces M1 macrophages polarization via STAT1 in glioblastoma. *Cell Death Discovery 2022 8:1* **8**, 1–13 (2022).
505. Wechsler, M. E., Rao, V. V., Borelli, A. N. & Anseth, K. S. Engineering the MSC Secretome: A Hydrogel Focused Approach. *Adv Healthc Mater* **10**, 2001948 (2021).
506. Lu, J. *et al.* The Functions and Mechanisms of Tendon Stem/Progenitor Cells in Tendon Healing. *Stem Cells Int* **2023**, 1258024 (2023).
507. Walia, B. & Huang, A. H. Tendon stem progenitor cells: Understanding the biology to inform therapeutic strategies for tendon repair. *Journal of Orthopaedic Research®* **37**, 1270–1280 (2019).
508. Huisman, E., Lu, A., McCormack, R. G. & Scott, A. Enhanced collagen type i synthesis by human tenocytes subjected to periodic in vitro mechanical stimulation. *BMC Musculoskelet Disord* **15**, 1–8 (2014).
509. Wang, Y. *et al.* Exosomes from tendon stem cells promote injury tendon healing through balancing synthesis and degradation of the tendon extracellular matrix. *J Cell Mol Med* **23**, 5475–5485 (2019).
510. Gomez-Florit, M., Labrador-Rached, C. J., Domingues, R. M. A. & Gomes, M. E. The tendon microenvironment: Engineered in vitro models to study cellular crosstalk. *Adv Drug Deliv Rev* **185**, 114299 (2022).
511. Herchenhan, A., Bayer, M. L., Eliasson, P., Magnusson, S. P. & Kjaer, M. Insulin-like growth factor I enhances collagen synthesis in engineered human tendon tissue. *Growth Hormone & IGF Research* **25**, 13–19 (2015).
512. Xia, W., Szomor, Z., Wang, Y. & Murrell, G. A. C. Nitric oxide enhances collagen synthesis in cultured human tendon cells. *Journal of Orthopaedic Research* **24**, 159–172 (2006).
513. Barnes, A. M. *et al.* COL1A1 C-propeptide mutations cause ER mislocalization of procollagen and impair C-terminal procollagen processing. *Biochimica et Biophysica Acta (BBA) - Molecular Basis of Disease* **1865**, 2210–2223 (2019).
514. Fratzl, P. Collagen: Structure and Mechanics, an Introduction. *Collagen: Structure and Mechanics* 1–13 (2008) doi:10.1007/978-0-387-73906-9_1.
515. Mienaltowski, M. J., Birk, • D E, Mienaltowski, M. J. & Birk, D. E. Structure, Physiology, and Biochemistry of Collagens. *Adv Exp Med Biol* **802**, 5–29 (2014).

516. Saggese, G., Bertelloni, S., Baroncelli, G. I. & Di Nero, G. Serum levels of carboxyterminal propeptide of type I procollagen in healthy children from 1 st year of life to adulthood and in metabolic bone diseases. *Eur J Pediatr* **151**, 764–768 (1992).
517. Parfitt, A. M., Simon, L. S., Villanueva, A. R. & Krane, S. M. Procollagen type I carboxy-terminal extension peptide in serum as a marker of collagen biosynthesis in bone. Correlation with iliac bone formation rates and comparison with total alkaline phosphatase. *Journal of Bone and Mineral Research* **2**, 427–436 (1987).
518. Seo, W. Y. *et al.* Production of recombinant human procollagen type I C-terminal propeptide and establishment of a sandwich ELISA for quantification. *Scientific Reports 2017 7:1* **7**, 1–13 (2017).
519. Luo, L.-F., Shi, Y., Zhou, Q., Xu, S.-Z. & Lei, T.-C. Insufficient expression of the melanocortin-1 receptor by human dermal fibroblasts contributes to excess collagen synthesis in keloid scars. *Exp Dermatol* **22**, 764–766 (2013).
520. Chamberlain, C. S. *et al.* Exosome-educated macrophages and exosomes differentially improve ligament healing. *Stem Cells* **39**, 55–61 (2021).
521. Costa-Almeida, R., Calejo, I., Reis, R. L. & Gomes, M. E. Crosstalk between adipose stem cells and tendon cells reveals a temporal regulation of tenogenesis by matrix deposition and remodeling. *J Cell Physiol* **233**, 5383–5395 (2018).